

University of Alberta

**Tuning the Surface Composition, Spatial Arrangement,
and Thermal Release Behavior of DNA-Gold
Nanomaterials**

by

Julian Diaz

A thesis submitted to the Faculty of Graduate Studies and Research
in partial fulfillment of the requirements for the degree of

Doctor of Philosophy

Department of Chemistry

©Julian Diaz
Fall 2013
Edmonton, Alberta

Permission is hereby granted to the University of Alberta Libraries to reproduce single copies of this thesis and to lend or sell such copies for private, scholarly or scientific research purposes only. Where the thesis is converted to, or otherwise made available in digital form, the University of Alberta will advise potential users of the thesis of these terms.

The author reserves all other publication and other rights in association with the copyright in the thesis and, except as herein before provided, neither the thesis nor any substantial portion thereof may be printed or otherwise reproduced in any material form whatsoever without the author's prior written permission.

Abstract

Combining multiple functions and controlling their relative organization on the surface, as well as controlling the release of payloads will be essential properties of nanomaterials for future medical applications. In this thesis we studied these properties using as a model DNA-gold nanoparticles, one of the most promising nanomaterials for medical purposes.

First, we studied strategies to control the density and the ratio of combinations of labeled DNA on gold nanoparticles. Using two approaches, thiol self-assembly and DNA-directed assembly (hybridization) we found that thiol self-assembly leads to a higher density of labeled DNA per particle, but poor ratio control, while DNA-directed assembly is better at controlling the proportions of labeled DNA on the particle but the number of strands is lower than the thiol self-assembly approach. Second, to control the relative position of the labels on the particle we used DNA-doublers and Y-shaped DNA complexes to tune the distance between tags. Off particle experiments indicated that the spacing between labels can be controlled in the Angstrom-nanometer scale. On particle experiments showed the apparent formation of these constructs; however more experiments are needed to attain quantitative results

The aim of the last investigation was to achieve thermal stepwise release of DNA from DNA-gold nanoparticles. To do so, it is necessary to obtain sharp thermal dissociation, or melting, transitions as well as control over the melting temperature. Taking advantage of the cooperative properties of DNA, we found that sharpened melting can be achieved using branched DNA-doublers hybridized with complementary DNA bound to the nanoparticle. Tuning the melting temperature can be achieved by modifying the branches of the hybridized doublers with abasic groups. Using these two findings, we sequentially released two DNA-doublers from the same nanoparticle, in a very narrow temperature window, and with minimal overlapping. Current experiments suggest even four strands can be liberated over a narrow temperature interval using a combination of destabilizing abasic groups and different branch lengths and numbers.

Acknowledgements

I would like to thank my supervisor, Professor Julianne Gibbs-Davis, for giving me an opportunity in her group and also for her suggestions, support, and advice over these years. Also, I want to thank Professor Robert Campbell and Professor Hicham Fenniri for their invaluable advise.

I would like to express my appreciation to my supervisory and examining committee: Professor Robert Campbell, Professor Mark T McDermott, Professor Ratmir Derda, Professor Frank Wuest from the Department of Oncology, as well as Professor Hanadi Sleiman from McGill University for agreeing to review this thesis.

I would also like to thank all the members of the Gibbs-Davis group. Particularly, Dr. Champika Weeraman and Delwar Sikder, last months have been unexpectedly entertaining. Also, Rachel Beingessner, Ross Johnson and Gabor Borzsonyi from the Fenniri's group. My appreciation also goes to Gareth Lambkin, Wayne Moffat, and Hayley Wan of the Chemistry Department for their generous favors.

Last, I want to thank my parents and brother. Not too many words here you guys know what you mean to me. *"Ahí vamos pa'lante...!"*

Table of contents

Chapter 1 Introduction	1
1.1 Overview and premise	2
1.2 Nanotechnology in medicine.....	5
1.3 Nucleic acids in nanotechnology	10
1.4 Nanoparticles.....	13
1.4.1 Gold nanoparticles	15
1.5 Hybrid materials.....	20
1.5.1 Biomolecules conjugated to GNP.....	21
1.6 DNA-gold nanoparticles.....	23
1.7 Multifunctional materials	30
1.8 Controlled release.....	31
1.9 Research objectives	32
Chapter 2 Multifunctional DNA-GNPs	36
2.1 Introduction	37
2.2 Results and discussion.....	38
2.2.1 Self-assembly of labeled DNA.....	38
2.2.2 DNA-directed assembly of labeled DNA	43
2.2.3 Combined strategy	46
2.3 Conclusion	48
2.4 Materials and methods	49
2.4.1 Quenching of fluorescein by Cy5	49
2.4.2 Preparation of DNA strands and gold nanoparticles	49
2.4.3 Loading of thiolated DNA on GNPs.....	50
2.4.4 Hybridization of ssDNA on DNA-GNPs.....	51
2.4.5 Quantification of labeled DNA strand on GNPs.....	51
2.4.6 Fluorescence measurements	53
2.4.7 Sequences	54
Chapter 3 Supramolecular spacing control using DNA as scaffold..	55
3.1 Introduction	56
3.2 Results and discussion.....	56
3.2.1 Spacing control using Y-shaped DNA clamps.....	56

3.2.2	Spacing control using DNA-doublers clamps	64
3.2.3	Supramolecular spacing control on GNPs	67
3.3	Conclusions	70
3.4	Materials and methods	70
3.4.1	FRET experiments	70
3.4.2	PAGE experiments	73
3.4.3	Aggregation experiments	75
3.4.4	Sequences	76
Chapter 4 Sharpening the thermal release of DNA from GNPs: Towards a sequential release strategy		77
4.1	Introduction	78
4.2	Results and discussion	82
4.2.1	System design	82
4.2.2	Melting behavior	84
4.2.3	Controlling melting temperature while maintaining sharpness 89	
4.2.4	Off-particles experiments: sharp melting of DNA-doublers and modified DNA-doublers	92
4.2.5	Sequential release	94
4.3	Conclusions	97
4.4	Materials and methods	99
4.4.1	Sequences	99
4.4.2	Preparation of DNA strands and gold nanoparticles	99
4.4.3	DNA loading and hybridization	99
4.4.4	Excitation and emission spectra as a function of temperature 102	
4.4.5	Fluorescence intensity dependence on temperature and DNA length of Au-S bounded strands to GNPs	104
4.4.6	Aggregation experiments	105
4.4.7	PAGE experiments	106
4.4.8	Melting analysis	107
Chapter 5 Tuning the thermal release of branched DNA from GNPs by varying the extent of destabilization, DNA length, and the number of branches		110

5.1	Introduction	111
5.2	Results and discussion	114
5.2.1	Effect of abasic groups on the melting behavior	114
5.2.2	Effect of the length of the arms on the melting behavior ...	118
5.2.3	Effect of branching in the melting behavior	121
5.2.4	Release of multiple strands	123
5.3	Conclusions	126
5.4	Materials and methods	127
5.4.1	DNA sequences	127
5.4.2	Preparation of DNA strands and gold nanoparticles	127
5.4.3	DNA loading and hybridization	127
5.4.4	Melting experiments	128
	Chapter 6 Epilogue	129
6.1	General conclusions	130
6.2	Perspectives and future research	132
	Appendix Synthesis of a β-glycoside functionalized G\wedgeC motif for self-assembly into rosette nanotubes with predefined length.....	136
A.1	Introduction	137
A.2	Result and discussion	139
A.2.1	Protecting group strategies to access the free amide	139
A.2.2	Deprotection of the G \wedge C base amide	141
A.2.3	Glycosylation	143
A.3	Conclusion	144
A.4	Materials and methods.....	145
	Bibliography	163

List of tables

Table 2.1 DNA sequences corresponding to DNA structures described in Figures 2.1–7	54
Table 3.1 Intra-complex spacing with varying adjuster bridging Nucleotides (x) for a Series of Y-shaped Clamps	60
Table 3.2 Melting temperatures of the hybridized adjuster	62
Table 3.3 Intra-complex spacing with varying adjuster bridging nucleotides for a Series of DNA-doublers clamps	65
Table 3.4 DNA sequences corresponding to DNA structures described in Figures 3.1, 3.3, 3.4, 3.5, 3.7 and 3.8	76
Table A.1 Deprotection of 16 in the presence of primary amines	143

List of figures

Figure 1.1 Representation of a "magic bullet".....	4
Figure 1.3 Optical properties of gold nanoparticles with distinct shapes.	16
Figure 1.4 Artistic representation of a DNA-gold nanoparticle (DNA-GNP)	24
Figure 1.5 Sharp melting of DNA-GNPs aggregates	26
Figure 1.6 Proposed surface control of DNA-GNPs	33
Figure 1.7 Spacing control	34
Figure 1.8 Thermally controlled sequential release strategy of different agents	35
Figure 2.1 Schematic representation of the approaches for synthesizing bifunctional labeled DNA-GNPs	38
Figure 2.2 The number of fluorophore labels per particle for bifunctional DNA-GNPs prepared by self-assembly on citrate-stabilized GNPs ...	39
Figure 2.3 Loading of labeled DNA on GNPs using 100% fluorescein or Cy5 (<i>self-assembly</i>)	40
Figure 2.4 Observed GNPs aggregation.....	42
Figure 2.5 Bifunctional DNA-GNPs prepared by DNA-directed assembly	43
Figure 2.6 Loading of labeled DNA on GNPs using 100% fluorescein or Cy5 (<i>DNA-directed assembly</i>).....	44
Figure 2.7 Bifunctional DNA-GNPs (<i>self-assembled Fln-DNA-GNPs hybridized to partially complementary Cy5-labeled strands</i>).....	47
Figure 2.8 Emission spectrum of a Fln- and Cy5-modified bifunctional DNA-doubler	49
Figure 2.9 Fluorescent emission spectra of a DNA-GNP after DTT treatment (<i>difference in cleavage after 1 and 15 hours</i>)	52
Figure 3.1 Y-shaped clamp formation.....	58
Figure 3.2 Typical FRET titrations for Y-shaped clamps	59
Figure 3.3 Long Y-clamp (20-base arm) hybridized with three different adjuster sequences (<i>Upper, Lower, and Full</i>)	61
Figure 3.4 Non-denaturing PAGE fluorescent image tracking the Y clamp formation	63
Figure 3.5 Adjustable DNA-doubler clamp design.	64
Figure 3.6 Example of a titration for DNA-doubler clamp	65

Figure 3.7 Non-denaturing PAGE fluorescent image tracking the doubler clamp formation.....	67
Figure 3.8 Y-clamp and DNA-doubler clamp complexes hybridized to DNA-GNPs.....	69
Figure 3.9 Non-denaturing polyacrylamide gel electrophoresis experiment tracking the formation percentages of the Y-clamp.....	74
Figure 3.10 UV-vis absorbance spectra for Clamp-GNP complexes (<i>aggregation experiments</i>)	75
Figure 4.1 Schematic representations of hybridization combinations.....	84
Figure 4.2 Melting profiles of ssDNA and DNA-doublers hybridized to DNA-GNPs.....	85
Figure 4.3 Melting profiles comparing DNA-doublers hybridized to GNPs and DNA-doubler hybridized to ssDNA.....	88
Figure 4.4 Melting profiles of short and abasic modified DNA–doublers hybridized to DNA-GNPs	89
Figure 4.5 The formation and melting behavior of solution-phase caged dimers made from complementary DT ₄ constructs	92
Figure 4.6 Schematic representation of the sequential thermal release of DNA.....	94
Figure 4.7 Sequential release of DNA in tri-component mixtures	95
Figure 4.8 Sequential release of tri-component mixture (<i>each DNA half the concentration of GNPs</i>).....	97
Figure 4.9 Commercially available DNA modifications and sequences used	99
Figure 4.10 Excitation spectra, emission spectra, and emission versus temperature.....	102
Figure 4.11 Changes in fluorescence of an FIn-DT ₄ strand solution in PBS buffer as the temperature increases	103
Figure 4.12 Changes in fluorescence intensity as the temperature increases for FIn-modified single strands of different lengths covalently linked to GNPs via S-Au bond.....	104
Figure 4.13 Aggregation control experiments showing the absorbance of GNPs as the temperature is increased	105
Figure 4.14 The same aggregation control experiments shown in Figure 4.13 following the absorbance at the surface plasmon resonant frequency of DNA-modified 13-nm GNPs (525 nm) versus temperature.....	106

Figure 4.15 PAGE of titration of a fluorescein-labeled DT ₂ with a complementary DT ₂ strand and the same experiment using DT ₄ doublers	107
Figure 5.1 Branch DNA structures explored in this chapter.....	112
Figure 5.2 Melting profiles of DNA-doublers with abasic groups based on the change in fluorescent intensity with temperature.....	115
Figure 5.3 The normalized first derivatives of the melting profiles shown in Figure 5.2.....	117
Figure 5.4 Melting properties of doublers with different lengths	119
Figure 5.5 Melting properties of branched DNA with different number of arms.	121
Figure 5.6 The normalized first derivatives of three DNA doublers of varying stability hybridized independently with GNP-DNA.....	123
Figure 5.7 Combination of strands that could allow us to release four different strands in a temperature window from 14 to 84 °C with minimal overlapping	125
Figure 5.8 DNA sequences and structures used in this chapter.....	127
Figure A.1 G _Λ C motif. “D” and “A” refer to hydrogen bond donors and acceptors, respectively.....	137
Figure A.2 Reagents and conditions scheme.....	138
Figure A.3 Reagents and conditions for the synthesis of 13 from 2	140
Figure A.4 Proposed mechanism for the deprotection of 16	141
Figure A.5 Reagents and conditions for the synthesis of 5 or 18 from 2	142
Figure A.6 Glycosylation and deprotection reaction of 5.	144

Chapter 1 Introduction

1.1 Overview and premise

In 1908 Paul Ehrlich shared the Nobel Prize in Physiology or Medicine for his insights in immunology. His work comprised the study of dyes and their specific interaction with cells and their organelles, as well as the study of toxins and anti-toxins, and natural and acquired immunity.¹ All these investigations led to groundbreaking results, such as novel treatments like chemotherapy and development of revolutionary ideas such as the “side-chain theory of immunity”.¹ The concept of the side-chain theory later evolved into what is known today as the receptor theory. From these experiences Paul Ehrlich also coined the concept of “magic bullet”: In his idea, drugs go directly to the diseased cells, making the therapeutic agents harmless to the healthy ones: the concept of targeted drug delivery was born.¹

The challenge of efficient drug administration however, is greater than merely the targeting strategies, and variables such as solubility, circulating times, and controlled release of therapeutics have an equal role in the expected performance of the administration strategy. To alleviate these issues, drug delivery vehicles in the micro-nano scale have emerged with the promise to include all these desirable properties in only one entity. However, the lack of success of many of these platforms *in vivo* and in clinical trials, has called researchers in academia and the pharmaceutical industry to improve their performance.² The question is now how to circumvent the new challenges presented by the increased complexity of multifunctional platforms. To answer this question it is necessary to achieve a better understanding of the nano-biointerface,³ and the interactions at the surface of these vehicles with the biological milieu, as well as better control of the composition of these devices.

Delivery systems consist of several types of materials: As of May of 2008, among the nano/microparticle-based vehicles approved for clinical use are: liposomes, polymer-drug conjugates, and other macromolecule-

drug conjugates or adducts.⁴ Nanoparticle platforms in clinical trials include complex liposome-based systems in which polymers have been added as a protective shell to increase circulation times and targeting ligands have been attached to increase the accumulation of these agents in the desired cells. Also, polymer-drug conjugates using PEGylated (polyethylene glycol PEG) therapeutics to increase solubility are common at this stage. Furthermore, examples of dendrimers, inorganic particles, and nanoemulsions have reached this point, too. The promising capabilities of these agents have increased the community efforts to make more effective vehicles. Currently, many other platforms are in preclinical trials, the most popular are metallic nanoparticles, polymeric nanoparticles, micelles, nanoshells, dendrimers, modified viral particles, albumin based particles and polysaccharide based nanoparticles.⁴

Today's efforts are not only devoted to the search of new materials, but also to achieve dual to multifunctional platforms that perform several tasks to increase the efficacy of these vehicles, that is, to achieve the proposed "magic bullet" that Paul Ehrlich once imagined. To do this, several functionalities should be attached to the delivery vehicle depending on the specific objective of the therapy; for example, targeting ligands for membrane receptors, targeting ligands for organelle receptors, stability enhancers, drugs, tags, etc. (Figure 1.1) But, the progress towards multifunctional platforms has been slow, and most of these studies are in a proof-of-concept stage, which does not directly reflect the *in vivo* performance for the treatment of diseases.⁵

In spite of the slow progress in the development of effective devices, the field of nanotechnology in drug delivery systems has had a very rapid market growth. This is mainly due to the advantages that delivery systems offer to the already existing drugs, compared to the high risk and cost of development of new therapeutic compounds. As an alternative, delivery systems provide opportunities for delivering existing therapeutics in a

novel manner, improving treatments, and extending patents, as well as diversifying the approaches for new therapies. Predictions estimate that the total market size for nanotechnology in drug delivery systems in 2021 will be approximately US \$136 billion. For 2010 the total addressable market (TAM) was 1.35 billion, split into the following technologies: drug nanocrystals (US \$596 million), total nanocarriers (US \$434 million), targeted delivery (US \$178 million), solubility and bioavailability (US \$139 million). In 2021 the nanocarrier market share for the top five nanocarrier technologies is expected to be in USD: \$118 million for liposomes (28%), \$84 million for dendrimers (19%), \$63 million for micelles (15%), \$56 million for gold nanocarriers (13%), \$56 million for carbon nanotubes (13%).⁶ All these numbers and more importantly, the advantages that drug delivery systems may offer to current and new therapies to improve life quality and expectancy, make them a critical research topic that deserves close attention.

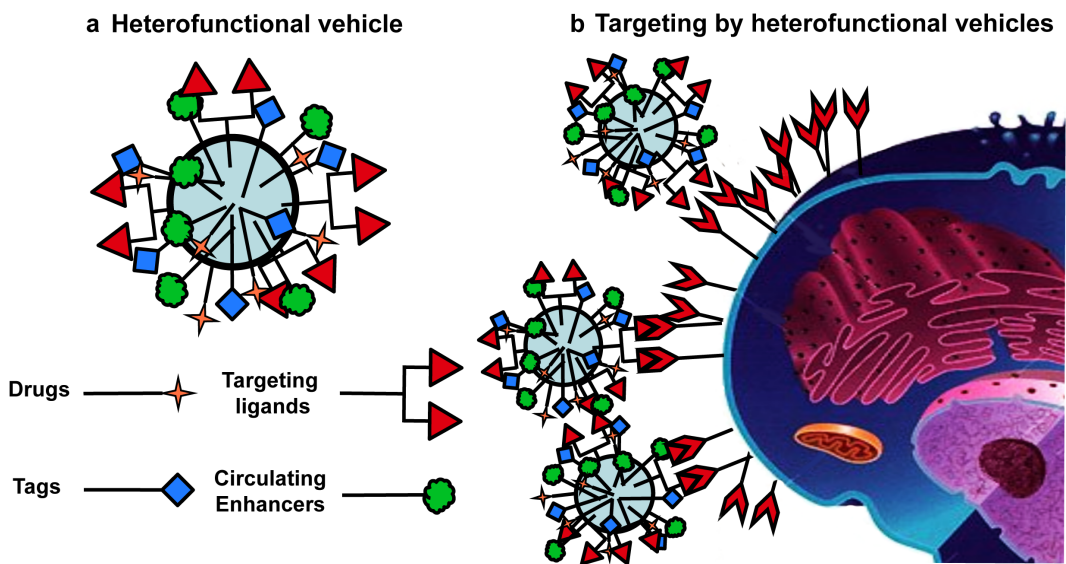


Figure 1.1 Representation of a "magic bullet" (a)"magic bullet" or heterofunctional particle loaded with different functionalities of interest for drug delivery. (b) Representation of a magic bullet in action by targeting a diseased cell while taking cargo to it.

In this thesis, we will describe our efforts to address some of the challenges key to improve drug delivery systems performance. We will

use DNA-gold nanoparticle (DNA-GNP) hybrids as a model for controlling the surface composition and release. However, many of the concepts studied here may be applicable to other types of DNA-nanostructure devices. In the next sections I described the role of nanotechnology in medicine, the current status of DNA nanotechnology and hybrid materials with medical applications, and an introduction to advances and properties of DNA-GNP conjugates.

1.2 Nanotechnology in medicine

Richard Feynman in his famous lecture “There is Plenty of Room at the Bottom” at Caltech in 1959 promulgated the idea of manipulating matter at the atomic level. This lecture set the stage for what is known today as nanotechnology, defined as the manipulation of matter at the molecular and atomic level, usually in the range from 1 to 100 nm where quantum mechanics still reigns, at the frontier of the molecular and the macroscopic world.^{7,8} In medicine, nanotechnology has a broader scale interval usually from 1 nm to 1,000 nm. And the definition is focused mainly in the medical effect that the nanostructured device could cause; therefore, is not surprising to find structures like liposomes, which are normally between 100 nm to 1,000 nm, categorized as nanodevices.⁹ The early vision of nanotechnology applications in medicine—or nanomedicine—was the idea of small robots that could be introduced in the body that would be able to perform medical procedures at the cellular level.¹⁰ This general concept in which molecular machines perform complicated procedures at the nanoscale was further expanded by Drexler in writings such as “Engines of Creation: The Coming Era of Nanotechnology” causing debate in the community and opening a new vision in the field.^{8, 10} Currently, nanomedicine comprises a number of branches or research fields that overlap with each other; for example, raw materials (nanocrystals), nanostructured materials, drug delivery, tools for diagnostics, DNA manipulation, BioMEMS, nanorobotics, among others. This plethora of

opportunities for the health sector will inevitably revolutionize the way of how medicine will be practiced in the future.¹⁰

For the purpose of this Thesis, it is important to emphasize technologies such as drug delivery systems, nanostructured materials, and tools for diagnostics since it is in these types of approaches in which the results of our investigations may find immediate application for the real world. As mentioned earlier, the nanocarrier market share for 2021 is expected to be around \$377 million, making the area of drug delivery among the most promising fields economically and medically speaking.⁶ But to achieve that ideal delivery vehicle (the magic bullet), there are still many challenges to overcome. Among those variables influencing the performance of nanocarriers are: size and shape of the nanoparticle, surface characteristics, and release of therapeutics. All these variables should be finely controlled in order to obtain the best therapeutic to toxicity ratio.¹¹

Depending on the application, a delivery vehicle will face several biological barriers before reaching the targeted site. The first obstacle—at the system level—is the mode of administration i.e., oral, inhalation, intravenous or intraperitoneal (in the body cavity) injection, each mode demanding specific considerations on delivery vehicle design. Avoidance of clearance by the reticuloendothelial system or fenestration in the spleen becomes important at the organ level thus again, size, shape, and surface features of the vehicle should be considered in order to trespass these barriers. The same characteristics are important at cellular and organelle level where the corresponding membranes should be penetrated. In these last cases, the surface composition is critical since targeting ligands, charge, and stability enhancers can dramatically influence the mechanism and amount of particle internalization.¹¹

In summary, size, shape, and surface characteristics determine the design of drug delivery vehicles. Also, tuning of these features is essential

depending on the specific application or intended action site. Yet, one more characteristic is necessary to complement the aforementioned, and that is the controlled release of therapeutics. This feature provides opportunities to release drugs in the time and place where they are need it, as a consequence reducing toxicity and improving treatment efficacy. Therefore, responsive materials allowing for the modulated liberation of payloads should be included in the original design.¹¹

Other field related to nanomedicine is biomedical diagnosis, this area has evolved significantly over the past years, and enormous part of the rapid progress is due to nanotechnology contributions. For example, the miniaturization of structures has led to the development of technologies such as lab-on-a-chip. Nanomaterials bring many advantages compared to current tools; for instance, the outstanding optical properties of some nanostructures allow ultra-trace detection in a rapid and cost effective fashion, and using only tiny amounts of sample. But the analysis of samples *in situ* and *in vitro* is not the only application of nanomaterials in diagnosis, just as in targeted drug delivery, nanostructures can be functionalized to reach specific locations inside the body for imaging and diagnosis at early stages of diseases.^{12, 13}

The most common nanomaterials for diagnostic applications are nanoparticles, quantum dots, nanotubes and dendrimers. Also, nanostructures such as nanopores, nanopillars, nanogaps and nanowires are essential in the construction of diagnostic devices. The proper functioning of this constructs depends again on the size, shape, and composition of the nanostructure and these properties must be tailored and modified for any specific application.¹²

The outlook for diagnostic technologies is very promising. From the “*in site* diagnostic” point of view, the applications (i.e. diagnostic targets), range from analysis of metabolites, small molecules and ionic blood chemicals to proteins and nucleic acids to even human cells, microbes,

and pathogens.¹³ Others areas of interest, as a targets include the analysis of food, waters and drugs (illegal substances). Among the most targeted metabolites today are creatinine, lactate, glucose, cholesterol, triglycerides, ammonia, and urea. The protein repertoire, include enzymes, hormones, and antibodies, which could be specific to certain diseases such as influenza, HIV or cardio vascular disease among others. Nucleic acids analysis measures DNA and RNAs, these essays can give clues of genetic or genomic illness as well as tracking unique sequences of pathogens.¹³ Human and animals cells can also be detected by point of care diagnostics. These cell-based assays can also find applications in cancers, prognosis of infectious diseases, analysis of inflammatory responses, and analysis of hematological parameters. In terms of pathogens detection, such as microbes, parasites, and viruses, the advantages of a fast identification of a severe infection can produce profound impact in the survival rates and the cost of treatments. Regarding drug and food analysis, the focus is on testing metabolites of these substances in saliva, sweat, and other fluids. Detection techniques are also useful in the food industry, to test deliberate contamination, nonedible or toxic substances and adulterants.¹³ The important thing to bear in mind is that nanostructures and their specific composition and surface manipulation are behind most of the principles allowing such a broad spectrum of applications in point of care diagnostics.

The other common diagnostic approach is the *in vivo* detection of diseases. For doing so, several imaging techniques have been developed; for example, single emission computed tomography (SPECT), positron emission tomography (PET), magnetic resonance imaging (MRI), ultra sound, fluorescence microscopy and computed tomography. In all of these procedures nanomaterials are expected to substantially improve the current outcomes. Common materials used for this purpose are radiopharmaceuticals, contrast agents, and dyes. The proposed role of

nanomaterials in this field extends from encapsulation of the existing imaging agents to the replacement of the current chemical with a nanostructure (for instance, replacement of dyes by quantum dots). Some of the most versatile approaches in the imaging area are: liposomes for encapsulation of contrast agents such as ^{99m}Tc or paramagnetic liposomes loaded with gadolinium (Gd). Quantum dots (QD) and their unique optical and electronic properties offer an excellent alternative for fluorescence imaging. Magnetic nanoparticles made of iron oxide can be used as MRI contrast agents, but ways to reduce their toxicity are still under investigation. Other materials like dendrimers and fullerenes have also been developed to improve MRI imaging using Gd.¹⁴

Very recently Funkhouser introduced the term “theranostic”¹⁵ a portmanteau of therapeutics and diagnostics. As its name indicates, this new area, combining imaging and therapy, is ligated to the drug delivery systems mentioned before. As a whole, it promises to take medicine to the level of a personalized approach; and nanomaterials, and more specifically, nanoparticles are at the heart of theranostics. In the previous section we discussed some of the approaches for the diagnosis of diseases *in vivo*, in theranostics the aim is to include therapeutic and imaging agents in only one entity, instead of developing separate materials. The major advantage of theranostics is the capability to monitor and treat the affected tissue at the same time; this allows tuning the required therapeutic dose according to the particular evolution of the disease. Theranostic strategies for cancer treatment include nucleic acid therapy, chemotherapy, hyperthermia treatments (e.g. photothermal therapy), photodynamic therapy, and radiation therapy. These are combined with imaging agents for one or more diagnostic technique such as MRI, PET, SPECT, CT, and fluorescence.¹⁶

Importantly enough, and it should be emphasized again, to build these complex materials, it is primordial to control their composition and surface

characteristics. The introduction of different types of ligands, stability enhancers, and drugs as well as different kinds of imaging agents, demands precise manipulation of nanoparticles' multi- and heterovalency (number and type of ligands attached to the nanoparticle). We will come back to analyze this specific challenge in a later section.

1.3 Nucleic acids in nanotechnology

Nucleic acids' recognition properties make them an excellent candidate as a template to pattern materials on the nanoscale. The origins of the field were established in 1982 when Nadrian Seeman postulated that sequences of oligomeric nucleic acids might associate in different ways rather than linear duplexes.¹⁷ Since then, from one to three dimensional structures have used DNA and RNA¹⁸ sequences to generate all type of arrangements, with potential applications in very diverse fields such as photonics, diagnostics, drug delivery, and biomimetic systems.^{19, 20}

Several strategies for the construction of these structures are common in the field. For example, structural DNA nanotechnology is the basic approach of using the pairing rules to generate two- and three-dimensional assemblies, normally employing relatively short strands. In DNA origami a long continuous strand is folded using smaller DNA segments (stapling strands) to make different 2D patterns with high precision. Another strategy is "the supramolecular DNA assembly", here not only the traditional bases are used, but different types of organic and inorganic modifiers are included in the nucleic acid strand as building blocks to help form the desired construct. These strategies diversify the types of nanostructures that can be achieved using nucleic acids as scaffold. Furthermore, modifiers also allow the introduction of other elements such as nanoparticles or fluorescent labels, as well as strand attachment to other structures or surfaces.¹⁹

Present and future applications of nucleic acids in nanomaterials have expanded beyond the original idea proposed by Seeman to hold proteins inside DNA crystals to obtain their detailed structure by X-ray diffraction. Now DNA nanomaterials are widely used as well as biochemistry in the field of biophysics. For example, membrane proteins have been studied using NMR with the aid of liquid crystal DNA nanotubes.²¹ Biomimetics is an important area because its role as a simple model of complex biological systems. One objective of DNA nanomaterials in this field is to make DNA-based artificial cells in which DNA interactions control their behavior.²⁰ Another field of very active research in which DNA nanotechnology can contribute due its capacity to precisely organize objects is in photonics and energy transfer. For these kinds of processes it is fundamental that the molecular entities are exactly positioned a task that nucleic acids can perform. Also, the charge transport properties of DNA make it appealing for these purposes, thus light harvesting and artificial photosynthetic devices can benefit from the remarkable properties of DNA.²² Just as in drug delivery systems, careful DNA functionalization of the devices components and accurate control of the number of functionalities is essential.

Diagnostics and therapeutics are perhaps the areas with more expectations regarding the use of nucleic acid nanotechnology. Drug delivery/theranostics and *in situ* diagnostics such as point of care devices can all benefit from the advance in DNA/RNA nanotechnology. Nanoparticles functionalized with nucleic acids are very promising to combat disease as well; These DNA and RNA strands can be used directly as a therapeutic agent (genetic therapy) as well as active components for the controlled release of drugs.²³ Also nucleic acid aptamers and molecular beacons are common to recognize an analyte and generate a signal that can be easily interpreted for the reader.²⁰

Some of the current challenges in nucleic acids nanotechnology like DNA origami are related with the high cost of synthesizing long sequences and technical issues involving their handling. Also, fine structure control still represents a major challenge that requires better understanding of the thermodynamics and kinetics of self-assembly. Related to the previous point and relevant to the work presented in this thesis are the challenges associated with the precise positioning of functionalities (e.g. proteins and nanoparticles). Since some of the promises of nucleic acid nanotechnology are its ability to pattern, organize objects, and obtain multi- and heterofunctional devices, it is mandatory to dedicate big efforts in order to solve the current issues regarding this point. Other areas that still need further development are mechanism for active self-assembly, that is, DNA assemblies that continually rearrange and reconfigure like in molecular motors and *In vivo* expression and assembly, that is, that the nucleic acid nanostructure accomplish the expected function at *in vivo* settings.²⁰

But the relevance of nucleic acids in nanomedicine is not only limited as a building block in the construction of complex nanostructures, they can also have a more active role specially concerning drug delivery and theranostics systems. For example, due to their intrinsic nature (they control the genetic information), treatment of inherited or acquired diseases is possible with nucleic acid therapies such as gene therapy.¹⁶ Today other ways to employ DNA or RNA as a therapeutic agent are gaining acceptance and are providing alternative routes to fight against diseases. Antisense oligonucleotides, small interfering RNA (siRNA), DNAzymes, ribozymes, aptamers, and plasmids, are all examples of the wide spectrum of opportunities that nucleic acids offer in this field.¹⁶ Furthermore, introducing modifiers like drugs into DNA's backbone, enhances this therapeutic power, allowing nucleic acids strands to become into "warheads" that can attack diseased cells.²⁴

1.4 Nanoparticles

Most delivery systems and theranostics technologies are based on micro and nanoparticles. Therefore, in this section we will give an overview of the most common nanoparticle systems focusing on their biomedical applications. Later in this section and the next one, we will emphasize on the specifics of gold nanoparticles.

Although evidence of synthesis, use, and manipulation of nanoparticles comes from ancient times, it was not only until Faraday studies of light on gold and other metals that they received scientific treatment.²⁵ Since then, the major advances in nanoparticle science have occurred in the past 40 years, first in combustion related investigations, in which they were referred to as ultrafine particles, and later, with the advent of nanotechnology.

Nanoparticles can be prepared from different sources such as metals, polymers, ceramics, and assemblies of small molecules. They have unusual properties that differ from the original “raw” material. Normally, they are divided into categories like “soft” and “hard”. Fullerenes, metal and semiconductor particles, carbon nanotubes, and other inorganic particles, can be considered as “hard”. On the other hand, particles made of polymers, small molecules, and dendrimers are often referred to as “soft”.²⁶

Virtually any field can benefit from the extraordinary properties of these constructs, their power has been demonstrated from solar cells²⁷ to the improved synthesis of organic molecules,²⁸ and medicine is not the exception to this trend. As mentioned earlier, the term “nano” for medical applications is usually extended from the most common definition of a size ≤ 100 nm. This broader terminology is specially found in nanoparticles for drug delivery, which can have dimensions of 1000 nm and beyond. Attractive properties of nanoparticles in biomedical applications are their high surface to mass ratio, which facilitates adsorption and transport of

other compounds. Also, their size allows them to easily trespass biological barriers and reach diseased cells. Depending on the material, hollow nanoparticles such as liposomes that have the ability to encapsulate compounds of interest can also be fabricated. Metallic or semiconductor particles can be used as diagnostic agents due to their fluorescence properties, others are able to act as the therapeutic agent by themselves, thanks to their SPR properties that enables them for example to directly ablate tumors.²⁹

A general objective of delivery systems is to reduce the toxicity that many therapeutics cause when they act alone. Thus, a major concern in this area is the relative toxicity introduced by the delivery vehicle itself. Nanoparticles have shown different levels of toxicity, from highly toxic to non-toxic. Toxicity may also vary considerably from *in vitro* to *in vivo* studies. The question that always should be addressed is if the unique properties that make them so appealing for certain treatments are as well harmful enough to cause unexpected damage. For example, it has been known that in some cases, more particle surface area equals more toxicity.²⁹ In general, a conscious analysis of particle toxicity takes into account separately the effect of the bare particles and the functionalized ones, since often the toxic effects comes only from the stabilizer/functionalities or particle degradation/accumulation.

Toxicity ranges based on the structure of the nanoparticle for carbon nanotubes *in vitro* investigations have shown their presence in cells increases the reactive oxygen species (ROS), lipid peroxidation, oxidative stress, mitochondrial dysfunction, and changes in cell morphology. Lung granulomas were also observed *in vivo*. Fullerenes have shown antimicrobial activity, but this also raised concern about their ecological impact when released to the environment. They also showed lipid peroxidation in the brain and glutathione depletion in the gill of fish. For quantum dots (QDs) the toxicity of several types of these nanostructures is

due to the surface coating. However, some bare Qds have shown cytotoxicity by producing reactive oxygen species that destroy membranes, mitochondria, and the nucleus. Also, cadmium/telluride Qds were found to release Cd^{2+} ions rendering them highly toxic. Silica nanoparticles have shown dose and time exposure dependent toxicity *in vitro*. Some of the effects were ROS, reduced glutathione, and oxidative stress. (Toxicity of Gold Nanoparticles will be briefly discussed in the next section).²⁹ This short overview is an “aliquot” of the diverse causes of toxicity and the effect of nanoparticles, composition and coatings. Therefore, control of composition is necessary to find the right balance between risk and benefit.

1.4.1 Gold nanoparticles

Among all types of nanoparticles, noble metal particles hold great promise in diagnosis and therapeutics. This is due to their unique characteristics such as high surface-to-volume ratio, rich and easily tunable optical properties, known surface chemistry, and relatively easy synthesis.³⁰ Particularly, gold nanoparticles have been investigated intensively and we will review here some of their history, types, properties synthesis and current applications. Later, in the next section, we will address a special kind of gold nanoparticle hybrid material: DNA-GNPs, which we used as materials in our studies.

Gold (Au) atomic number 79, electronic configuration $[\text{Xe}] 4f^{14} 5d^{10} 6s^1$, is a yellow, malleable, shiny, and ductile metal. “Bulk” gold has been always regarded because of its unusual properties, for example its very low reactivity or nobility (e.g. resistance to oxidation). These properties are attributed to relativistic effects at the valence shells, where electrons move close to the speed of light, contracting (direct relativistic effect), expanding (indirect relativistic effect), and screening the outer orbitals.^{31, 32} The

nobility and other properties (e.g. color) resulting from these effects have rendered gold their common use in jewelry, coinage, and electronics.³³

SPR of gold nanospheres and nanorods

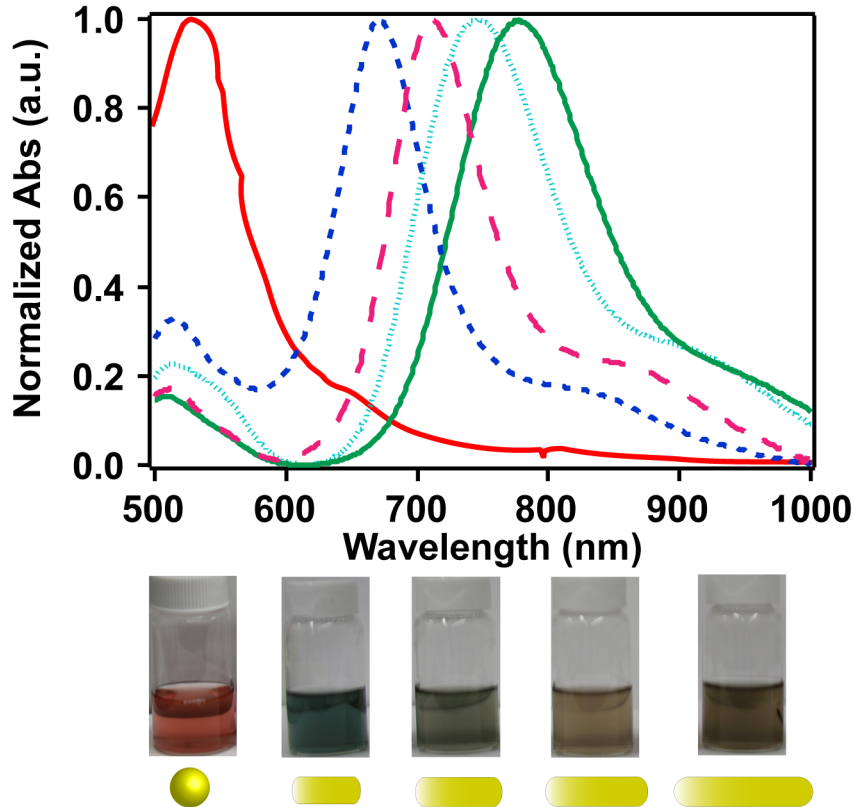


Figure 1.2 Optical properties of gold nanoparticles with distinct shapes. Spheres and rods of different aspect ratio. Top, absorption bands due to surface plasmon resonance (SPR) of the particles, spheres 525 nm (red solid line); transverse SPR of rods, 520 to 530 nm; longitudinal SPR of rods, from 650 to 795 nm.

As striking as the properties of bulk gold, are the properties of gold nanostructures. These nanostructures have unique photophysical characteristics that can be tunable by controlling their size and shape. A well-known feature of these materials is the range of colors observed when the size and shape are changed. The color is a consequence of the oscillating electrons in the conduction band of the nanostructure interacting with light. More specifically, d electrons move freely through the material. Since the mean free path of gold is around 50 nm, no scattering

should be observed in constructs smaller than this size; therefore, all interactions with light should arise from the surface of the material. Light of greater wavelength than the particles size resonates with the electrons on the surface causing them to oscillate. The frequencies of these oscillations are usually in the visible region causing the typical strong absorption observed in these materials, this phenomenon is called surface plasmon resonance or simply SPR (Figure 1.2).³⁴

Surface plasmon resonance is sensitive to the anisotropy of the particle, thus nanostructures with different geometries display different plasmon resonances. For example, gold nanorods have two plasmon bands: the transverse resonance, which is originated at the tips of the rod, and the longitudinal resonance, which is due to the long axis of the rod. In this type of nanostructure, the longitudinal band absorption shifts to the red as the particle becomes longer; in contrast, the transverse band barely shifts when the aspect ratio is changed (Figure 1.2). Since, synthetically it is possible to control the shape of the nanorods, it is possible to modulate the plasmon properties as well. But the consequences of surface plasmon resonance are not limited to the absorption of light. These electron interactions also create enhanced local electromagnetic fields enhance Raman signals and other properties such as fluorescence of molecules attached to the particle.³⁴

Different “top-down” and “bottom-up” methods to make gold nanoparticles have been proposed; herein, we will deal mainly with the bottom-up or chemical transformation approach. This method is quite similar for all types of nanostructures, and consists of: first, dissolving a gold salt, then adding metal ions and reducing agents and lastly seeding with particles protected with ionic groups, to trigger the formation of the nanostructure.^{33, 35}

Citrate and related methods to synthesize gold nanoparticles are among the most popular, and the Turkevich method, developed in 1951, is still the

most common way to prepare spherical nanostructures. In this strategy, hydrated HAuCl_4 is dissolved in water, and then citric acid is added. Citric acid has a dual role; it acts as the capping agent and the reducing agent at the same time. Later, G. Frens following the same method found that by varying the gold to citrate ratio, the size of the nanoparticle could be controlled. A complementary approach that allows for functionalized GNPs is the Brust–Schiffrin method that yields thiol protected spherical nanostructures. In this phase transfer approach HAuCl_4 , sodium borohydride (reducing agent), tetraoctylammonium bromide (phase transfer surfactant), and an alkane thiol (the capping agent), are present in a water-toluene mixture. The tuning of particle size can be afforded by varying the gold:thiol ratio and the temperature.³⁵

Gold nanostructures with shapes other than spherical have also been prepared using a bottom-up approach closely related to the protocols described above. Murphy and El-Sayed have pioneered the synthesis of gold nanorods using a seeded growth technique, in which a seed dispersion is prepared by reducing HAuCl_4 with NaBH_4 in the presence of cetyltrimethylammonium bromide (CTAB). An aliquot of this seeding dispersion is then added to a growth solution made of HAuCl_4 , silver ions, CTAB, and ascorbic acid as the reducing agent. Nanorods from 10 to 20 nm in diameter and up to 300 nm long can be prepared this way after variation of the ratio of silver and/or seeding.^{36, 37} Other shapes can be prepared similarly; for example, Yang and colleagues, synthesized tetrahedra, cubes, octahedra, and icosahedra in a modified version of the polyol process (using diols or polyols as a reducing agent). In their method, they used ethylene glycol as a reducing agent/solvent, and poly(vinylpyrrolidone) as the stabilizer. They found that the morphology of the particles was dependent on the concentration of gold in the reaction mixture.³⁸ Murphy and coworkers also prepared rectangular, hexagonal, cubic, triangular and star-shaped nanoparticles, using similar conditions

as the nanorods synthesis but varying the proportion of reactants.³⁹ Mirkin and colleagues also used Murphy's seeding strategy for nanorods but this time to obtain nanocubes by substituting CTAB with its chloride analogue CTAC.⁴⁰ From tetragons, nanocages, and nanoframes to nanoprisms and truncated octahedral have been synthesized using analogous methods. All of these gold nanostructures have shown remarkable optical properties and have promising applications in nanomedicine and diagnostics.³³

To include the remarkable properties of gold nanoparticles into biological or other systems (e.g. electronic circuits), specific surface functionalities are required to make them compatible or to achieve a precise goal like biodetection or targeting. After the preparation of nanoparticles however, the surface is covered with the stabilizing agents selected for the synthesis; thus, it becomes necessary to find strategies to replace the original ligands by the ones required. The process of switching functionalities is often referred to as the ligand exchange reaction or place exchange method and has its origins in the chemistries developed by Nuzzo and Whitesides, and their work on self-assembled monolayers (SAMs) on planar gold.⁴¹ Later, Murray took those ideas and introduced the concept to gold nanoparticles by substituting thiol ligands with other thiol ligands. Briefly, the exchange reaction normally consists of exposing a dispersion of the ligand₁-thiol functionalized nanoparticle with an excess of free ligand₂-thiol. Currently, similar processes can be performed using several gold-binding groups; for example, amines, carboxylates, selenides, phosphines, and many others sulfur based functional groups. The functional group selected normally depends on the final application and how labile/stable the gold ligand bond needs to be. Utilizing this approach it is possible to prepare mixed monolayers—a combination of ligands in different proportions—, which opens up interesting opportunities when ligands have to interact synergistically in the same material.^{33, 35} We

will come back to this topic more deeply in our second chapter since the obtention of well-controlled mixed monolayer is the central discussion.

Regarding toxicity, gold nanoparticles have shown different results that vary with size, shape, and functionalization. Usually smaller particles (~1.5 nm) tend to be more toxic than particles of ~15 nm. Shape has shown less influence in toxicity. Most of the studies suggest that the particle functionalization or passivation agent can change dramatically the toxic effects. CTAB for example has shown to be toxic, meanwhile DNA-GNPs have not exhibited cytotoxic effects.⁴²

1.5 Hybrid materials

Materials interfacing components from several facets of chemistry have emerged to solve the more intricate engineering challenges encountered recently. Therefore, it is not surprising to find inorganic-organic, inorganic-biomolecule, and/or organic-biomolecule structures in today's more advanced materials. The combination of structures usually results in improved and also new remarkable properties. Common constituents of hybrid materials are: polymers, clay, metal nanoparticles, metal oxides, biomolecules, carbon nanostructures, and so on. The tendency is that any molecule, polymer nanoparticle or nanostructure, will have to evolve in a type of hybrid material so that it can be included as functional part of a device.^{43, 44} A closer look in the development of drug delivery/theranostic systems shows exactly this tendency of how a drug, a nanoparticle, a dye, and targeting ligands come together to form a hybrid material with enhanced and new properties, properties that it could not be achieved using its components separately.

Before moving onto the specifics of the hybrid material used as a model in our work, we would like to set the stage with a broader overview of the current status of biomolecule-GNP hybrids.

1.5.1 Biomolecules conjugated to GNP

Peptides are a group of biomolecules that functionalized to GNPs results in a material with great interest in biomedical applications; this is because of the potential as targeting ligands such as tumor-homing peptides with RGD and NGR motifs,⁴⁵ and as transfection agents such as cell-penetrating peptides.^{46, 47} But functionalization of GNPs with peptides has proven challenging; for instance, immobilization via thiol self-assembly has been possible only for certain amino acid sequences.^{48, 49} Other methods to functionalize GNPs with peptides consist of conjugating them to proteins such as bovine serum albumin (BSA)⁵⁰ or streptavidin⁵¹ and then stabilizing the particles with the resulting protein-peptide motif. Mixed monolayers have also been prepared by combining PEG derivatives and peptides,⁵² and something similar was achieved functionalizing the nanoparticles with suitable linkers and then coupling peptides using standard conjugation chemistries.⁴⁷ In a somewhat different approach, peptides can be used as a reducing and capping agent at the same time, during nanoparticle formation, avoiding posterior ligand exchange reactions.⁵³

Understanding the binding of proteins to gold nanoparticles is another area of interest. First, the introduction of antibodies and targeting factors onto GNPs is useful in therapeutic strategies.⁵⁴ Second, proteins are indicative of certain health threatening conditions (e.g. hepatopathy markers),⁵⁵ and gold nanoparticles may improve the essays to evaluate these conditions. Third, proteins bind to the surface of therapeutics vehicles forming the so-called protein corona, affecting their *in vivo* response.^{56, 57}

The direct binding of proteins to gold nanoparticles can be afforded by a ligand exchange reaction in which stabilizing molecules such as citrates can be substituted by thiol-containing proteins (e.g. cysteine residues). Immunoglobulins (IgG) and albumins, which contain cysteines, have been

functionalized utilizing this approach. Also, thiol groups can be introduced into the protein chemically or can be genetically engineered.⁵⁸ Electrostatic interactions are very efficient to passivate proteins on gold nanoparticles as well,⁵⁹ citrate capped nanoparticles, for example, can be functionalized with positively charged proteins. It should be mentioned that electrostatic interactions are the main cause for the formation of what is known as the protein corona. Other noncovalent interactions, such as streptavidin-biotin binding, are frequently used as a functionalization strategy.⁵⁸ As with peptides, proteins are also attached to nanoparticles via amidation or esterification using carbodiimide chemistry;⁵⁸ couplings like cycloadditions are also popular under this functionalization category.⁵⁵

Carbohydrates are another group of molecules with essential biological properties that make them important to be functionalized to gold nanoparticles. Complex carbohydrates and carbohydrate conjugates like glycoproteins, glycolipids or proteoglycans (glycans) make up a vital part of cell membranes and intervene in many cell interactions with the surrounding media (e.g. recognition, trafficking, signal transduction and cell adhesion).⁶⁰ These biological roles make carbohydrates relevant for targeting strategies and early detection of abnormalities in cells. Since binding affinities are weak for a single oligosaccharide chain, multivalency becomes the strategy of choice to enhance this effect. In this context, the carbohydrate-nanoparticle hybrid is especially important because it allows several ligands (carbohydrate chains) to interact together with the targeted receptors at the same time.⁶⁰ Kamerling and colleagues examined glyco-GNPs and their multivalent binding to a carbohydrate-binding protein. They prepared gold nanoparticles functionalized with a series of sugars and tested their binding affinities with concanavalin A.⁶¹ Glyco-GNPs can also mimic the glycocalyx on the cell surface helping them to carry carbohydrates to easily target cells.⁶² In another example mannose modified gold nanoparticles (m-GNPs) selectively bound to bacterial type

1 pili, demonstrating another method to specifically bind and visualize proteins.⁶³ Other applications of glycan-GNPs are the detection of ions, for example Ca^{2+} cations have been detected in serum using thiohexyl β -D-lactopyranoside as chelating agent.⁶⁴ The typical functionalization strategy is the passivation with a thiol linker and then modification/coupling of the linker with a carbohydrate.⁶⁰

Phospholipid-stabilized gold nanoparticles have also been prepared. Using 1,2-dipalmitoyl-*sn*-glycero-3-phosphothio-ethanol 1 nm particles were functionalized via thiol chemistry. These bifunctional lipids bind the nanoparticle by a S-Au bond at one end while the other hydrophobic ends interact with themselves forming a bilayer that surrounds the nanostructure.⁶⁵ Zheng prepared encapsulated dye-GNPs for surface enhanced Raman scattering (SERS) in a nonthiol phospholipid coating held by electrostatic interactions between the positively charged lipid and the remaining citrate on the particle.⁶⁶ Nanorods have also been passivated by exchanging the cationic (CTAB) with the zwitterionic 1-palmitoyl-2-oleoyl-*sn*-glycero-3-phosphocholine (POPC), resulting in a lipid bilayer encapsulating the nanorods.⁶⁷ One recent extension of the phospholipid approach was demonstrated when a high-density lipoprotein (HDL) was formed on the nanoparticle. Multifunctionality was achieved by embedding not only the ApoA-I protein in the bilayer, but also inserting fluorescence and MRI contrast agents.⁶⁸ One of the major interests on this type of functionalization is the compatibility expected from the phospholipids on the particle's surface and the phospholipids in the cell's membrane.

1.6 DNA-gold nanoparticles

On August 15th of 1996, in its volume 382, *Nature* published two seminal contributions in the field of DNA-goldnanoparticles. In page 607 Mirkin and coworkers assembled DNA functionalized gold nanoparticles using a third

strand as a linker and showed that this arrangement forms thermally reversible aggregates.⁶⁹ In the same issue Alivisatos, Schultz, and colleagues reported a similar approach, in which DNA functionalized gold nanocrystals were assembled into dimers and trimers on addition of a template strand. These two examples demonstrated the power of DNA to control nanomaterials in a bottom-up approach. In the next pages we will discuss the synthesis, properties, developments and potential application of these materials.

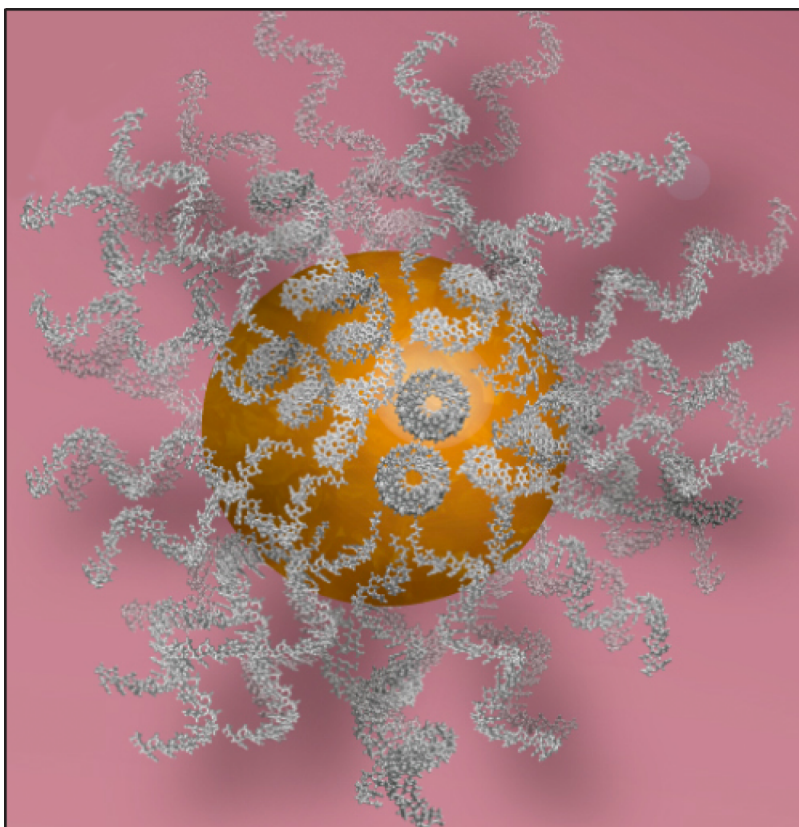


Figure 1.3 Artistic representation of a DNA-gold nanoparticle (DNA-GNP).

Synthesis of DNA-gold nanoparticles follows similar approaches such as those mentioned for others GNP hybrid materials. First, particles are prepared via the Turkevich method or any of its modifications, then the DNA strands are usually attached to the gold surface using thiol ligand exchange reaction. Since sodium chloride is necessary to screen the

negative charges on the DNA strands, its concentration has to be carefully addressed over the exchange reaction to avoid precipitation of the nanoparticles. The number of DNA strands functionalized varies depending on the sequence, modifiers, length of the strand, and size of the particles.⁷⁰

The resulting material is a DNA-polyvalent nanoparticle (Figure 1.3) with remarkable new properties. For example, the dense packing of strands causes a high local counterion concentration, creating a shared-ion screening effect that enhances the binding constants to complementary DNA by two orders of magnitude, when compared to analogous “off-particle” sequences. Also, the aggregates formed by hybridizing together DNA-GNPs exhibit very sharp thermal dissociation or melting transitions (Figure 1.4), again as a consequence of the tight DNA packing, the local ion concentration, and the multiple links generated among the particles. Since sharp transitions are one of the most outstanding characteristics of these materials, and it will also be part of the discussion in Chapter 4, it is worthwhile to introduce some concepts regarding this property.

Mirkin, Schatz, and colleagues have studied deeply the melting properties of DNA-linked gold nanoparticle aggregates. They found that two main factors govern the extraordinary sharp melting transition of these assemblies. First, the presence of multiple strands linking particles and second, a reduction of melting temperature, associated with a decrease in local dielectric. Several variables affect these factors, and we will briefly discuss what Mirkin and coworkers found.⁷¹

They examined the effect of probe oligonucleotide density on the nanoparticle’s surface, that is, they varied the number of strands attached to each nanoparticle. To assemble these GNPs, they added a third complementary strand that led to duplex-linked aggregates. After melting these assemblies they found that denser particles have sharper transitions

and higher melting temperatures, suggesting a direct relationship between the proximity of the strands and the enhanced properties.⁷¹

Varying the particle size showed that bigger particles have remarkable sharper transitions. The melting temperatures trends, however, were more difficult to compare directly, since this property depends on variables such as surface DNA coverage and local dielectric environment, which were not constant for each size GNP.⁷¹

Salt concentration showed a marked effect, supporting the hypothesis of the dielectric environment influence in melting. First, an increase in salt concentration provoked a substantial increase in T_m . Second, the higher salt content triggered the formation of bigger nanoparticle aggregates. Last, these aggregates assemble/disassemble over a very narrow salt concentration range.⁷¹

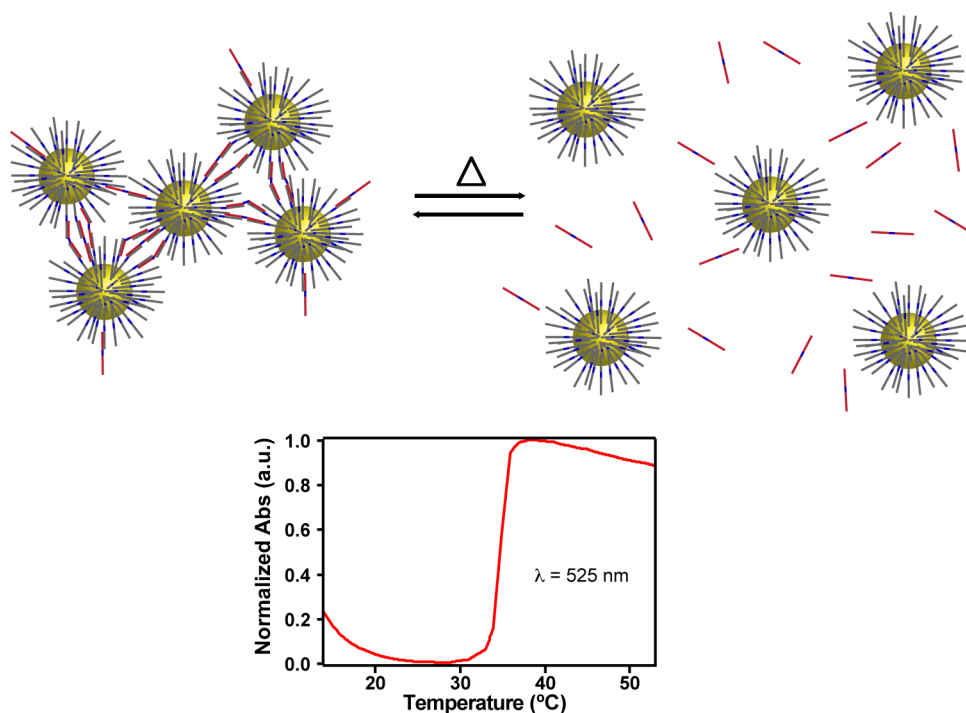


Figure 1.4 Sharp melting of DNA-GNPs aggregates.

One more variable that could influence the melting behavior of the aggregates is the interparticle distance. By changing the length of the DNA duplex formed between the strands on the particles and the target

strand, Mirkin and collaborators found that the general trend was an increase of melting temperature as the interparticle distance increased. They attributed this effect to the particle-particle repulsion due to electrostatic interactions.⁷¹

The particular melting behavior of DNA-gold nanoparticle aggregates has been explained in terms of the cooperative interactions among the DNA strands linking the assemblies. Cooperativity arises from the proximity of the hybridizing strands and their ion cloud overlap, which stabilizes the duplexes causing them to melt as a unit.^{71, 72} This effect is not exclusive of gold nanoparticles aggregates and has been observed in DNA-polymer hybrids and DNA-small molecule assemblies.^{72, 73}

The intrinsic DNA-GNPs features just discussed, generates interesting properties for applications in other fields. For example, the particle's densely DNA-populated surface creates a shield that prevents enzymatic degradation of the loaded oligonucleotides. This stabilizing effect makes these systems ideal to deliver nucleic acids into cells, and avoids, one of the complications with nucleic acid therapies, which is the short life time of DNA/RNA strands in the biological milieu.⁴²

Moreover, even though it is counterintuitive due to the negative charged surface of DNA-GNPs, these nanostructures can still penetrate cell membranes. Experiments demonstrated that more than 30 cell lines internalize GNPs and the amount taken up varies depending on the cell type.⁴² The exact mechanism of internalization is still under debate, but it has been observed that increasing the density of oligonucleotides increases the up-take.⁷⁴ Proteins adsorbed to the nanoparticles appear to facilitate their internalization. Other data suggests the involvement of scavenger receptors in this process.⁷⁵ No matter the mechanism involved, the remarkable property of entering cells gives gold-DNA nanoconjugates its relevance in fields such as *in vitro* diagnostics and drug delivery/theranostics.

Because of the nucleic acid component of DNA-GNPs, one obvious application involves controlling gene expression. Small interfering RNA (siRNA) and antisense oligonucleotides are ways to achieve this goal. Although the idea of gene therapy is not recent—and indeed literature has plenty of examples—most of them suffer from serious drawbacks such as toxicity and degradation of the nucleic acid payload. Gold nanoparticles conjugates offer alternatives to the standard approaches (e.g. lipid, peptide, polymer, and virus mediated delivery)⁷⁶ and promise overcome many of the current challenges.⁴²

Mirkin and colleagues already demonstrated how gene control can be achieved using “antisense nanoparticles”. In their first example, they silenced up to 75% of the expression of enhanced green fluorescence protein (eGFP) in mouse endothelial cells.⁷⁷ In a similar study, they also showed that locked nucleic acids (LNA)—a DNA analog with bridged sugars—, conjugated to GNPs, knocked down survivin protein in lung carcinoma cell line A549.⁷⁸

Based on the color change (from red to purple) observed when DNA-GNPs aggregate, several colorimetric detection systems have also been designed. For example, Hg²⁺ detection methods take advantage of the thymidine affinity for these cations. When GNPs are functionalized with sequences that coordinate Hg²⁺, assemblies are formed causing a change in color.⁷⁹ In an inverse approach, that is, disassembling the aggregates, Lu and co-workers have been able to detect small molecules, such as adenosine and cocaine, using DNA-aptamers linked to GNPs.⁸⁰ Later, Yang and colleagues reported the detection of Ochratoxin A in a similar strategy.⁸¹ Nucleic acid detection is another intrinsic application of these constructs. The first example of DNA-GNPs assembly, given by Mirkin, can be understood as a demonstration of the colorimetric detection oligonucleotides.⁶⁹ The same group has also demonstrated colorimetric detection of DNA triplex structures. Colorimetric sensing, however, is not

the only way to detect nucleic acids, DNA-GNPs molecular beacons,⁸² electrical detection based on “sandwich” hybridization of DNA-GNPs,⁸³ and SPR enhanced DNA detection assays,⁸⁴ are some of the techniques developed for this purposes.

Intracellular detection is desirable to quantify biological activity, and some of the techniques mentioned so far, such as DNA-GNPs based molecular beacons have that purpose. Nanoflares are a method that is worth mentioning in live-cell nucleic acid detection. The approach consists of short fluorescently labeled sequences hybridized to DNA-GNPs, these constructs enter cells and the target mRNA, which is more complementary than the hybridized strand, displaces the short sequence making it fluoresce.⁸⁵ The technology was recently acquired, in a partnership, by Millipore™ and launched as a SmartFlare™ for RNA detection.⁸⁶ Furthermore, due to the fast degradation of RNA by RNases, nucleic acid-GNPs and its dense surface, offers an opportunity to deliver RNA interference strands (RNAi) to cells without decomposition.

Modern nucleic acid synthesis allows for the design of strands with bases other than the conventional; conjugation chemistries enrich even more the type of groups that can be included in a determined strand. The broad scope of DNA synthetic chemistry makes nucleic acids a very versatile building block, since not only the intrinsic nature of DNA/RNA can be exploited but also properties from other molecular entities can be used. We have already seen fluorescently labeled DNA in action, and in the same way that dyes can be attached to oligonucleotides, other molecules such as small peptides, carbohydrates, PEG, and inorganic complexes can be linked to the DNA/RNA backbone as well. As a consequence, the therapeutics and sensing opportunities of nucleic acids are exponentially increased. As already highlighted, Mirkin and Lippard demonstrated a powerful proof-of-concept of DNA-GNPs adaptability by illustrating how DNA can be doubly functionalized with a thiol group at one end and a

Pt(IV) prodrug on the other, to target different types of cancer cell lines.²⁴ From the therapeutic point of view, this means that DNA-GNPs can potentially become a type of those “magic bullets” that Paul Ehrlich once proposed, in which multiple functionalities and the rich properties of gold nanoconstructs, create a device that performs complex task such as the ones needed in drug delivery.

In this thesis we have aimed to answer some of the basic questions that arise in order to build those complex vehicles. For example, how to introduce controlled combinations of functional group, how to control the relative position of those groups at the particle surface so that they interact better with the biological milieu, and how to control the release of the payload. In the next section, we will give a short introduction to the relevance of properties such as multifunctionality/heterofunctionality and controlled release, in therapeutic systems.

1.7 Multifunctional materials

The surface of nanoparticles offers the opportunity to attach many copies of one functional group or a combination of different functional groups, thus, allowing the design of multipurpose vehicles that detect and treat illnesses at the same time.⁵ The main characteristics desired on a nanocarrier are: drugs, targeting agents, imaging moieties, stability enhancers, stimuli response components, and transfection agents. But including all of them in one vehicle is not straightforward,⁸⁷ and the complexity increases even more if for example, two or more imaging agents were required for techniques such as, MRI and PET. Along the same lines, if targeting of cell's nuclei were necessary, then two types of targeting ligands would be required, one for the cell membrane and the second one for the nuclear membrane.¹¹ A similar need would result if two drugs that act synergistically were needed—for example, to sensitize and then kill the diseased cell—. Therefore, attachment of all the required

ligands demands very specific chemistries. Another complication comes from the fact that linking all the desired functionalities is not enough to achieve the expected results, and in most cases, it becomes necessary to control the number of the groups or the ratio with respect the other. For instance, reports indicate that excess of PEG (a stability enhancer) on the surface substantially decreases the targeting properties of delivery vehicles; So to maintain the specificity, control over the PEG/Targeting ligands ratio should be assured.² Tuning is also necessary when a specific effect on the delivery systems is required, that is the case for long vs. short circulating times.⁴⁵ For the former, more stability enhancer groups should be functionalized; conversely, for the latter fewer groups should be attached.

In terms of targeting ligands, not only the number but also, the position with respect to each other may have a marked effect on the ligand-receptor affinities.^{45, 88} It has been demonstrated that multivalent interactions can increase significantly the association constants of otherwise weakly binding carbohydrates. Is also expected that finely tuning the spacing among ligands should lead to stronger interactions.⁸⁹ We will discuss more about this in chapter 3, when we deal with “tuning supramolecular spacing” using DNA as the tunable coating on GNP.

1.8 Controlled release

Another property of interest in drug delivery systems is the controlled release of therapeutics. The promise of this approach is to reduce toxicity by liberating therapeutic agents at the desired location avoiding their presence where they are not required.⁹⁰ Usually, a responsive material releases the payload when exposed to an exclusive stimulus of the targeted site, such as a decrease of pH. A more convenient strategy is to trigger the release remotely; this would avoid the necessity of an intrinsic stimulus in the action site. The use of heat is a common way to activate

the liberation of agents and can be induced in different ways, for example, with the introduction of ultrasound, magnetic field, and laser irradiation. In our work we investigated a strategy that could be suitable for any of these thermal techniques.⁹¹

We are also interested in an even more sophisticated approach, in which more than one agent is liberated stepwise, in a temporal and localized manner. This type of strategy can have potential applications in combination and gene therapies where several drugs/probes need to work together, but independent control of each agent is necessary.⁹⁰

In this brief general introduction, we aimed to give some historical background of the field of smart therapeutics and diagnostics, we stated the crucial role of nanotechnology in the development of these technologies and then we focused on the current status and applications of the materials we used in our work. We also defined some terms and highlighted some visions of the future of the field. Throughout the introduction the words, surface, composition, control, tuning, functionalities and multifunctional, were repeated several times. This was purposely done to emphasize the challenges that our findings may help to solve. We certainly think nucleic acids are a unique and multifaceted building block, with enormous potential in this field that combined with gold nanostructures become a strong candidate for the magic bullet.

1.9 Research objectives

Our aim with this work is to contribute to the development of better drug delivery/theranostic systems. We focus our ideas on two fundamental challenges in the design of delivery nanocarriers: 1) surface modulation (ligand functionalization Figure 1.5 and spacing control Figure 1.6) and 2) controlled release Figure 1.7.

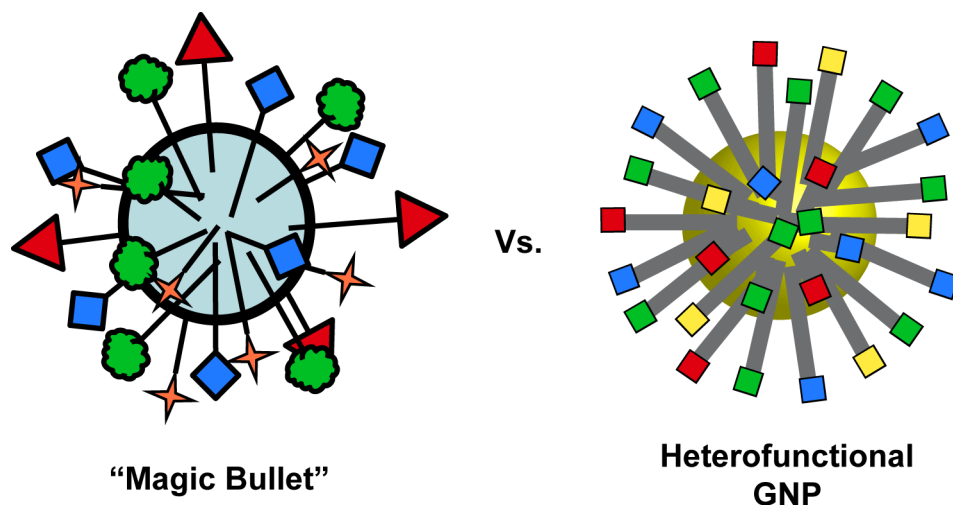


Figure 1.5 Proposed surface control of DNA-GNPs. Just as in the “magic bullet” our objective is to functionalize GNPs with different DNA strands represent here with labels of different colors.

In this thesis we will use GNPs as a model of our drug delivery vehicle, DNA as a linker, and fluorophores as model small molecules that represent drugs or targeting ligands. In Chapter 2, we will attach fluorophore-labeled DNA to the surface of the GNP directly using thiol chemistry and indirectly by hybridization with strands attached to the particles. Our objective is to control the number of labeled DNA strands on the nanoparticle and, at the same time, control the proportions of the attached strands. These experiments will allow us to identify the best strategies for the functionalization of GNPs with DNA modified with small molecules that can act as drugs, targeting agents, tags, and stabilizers.

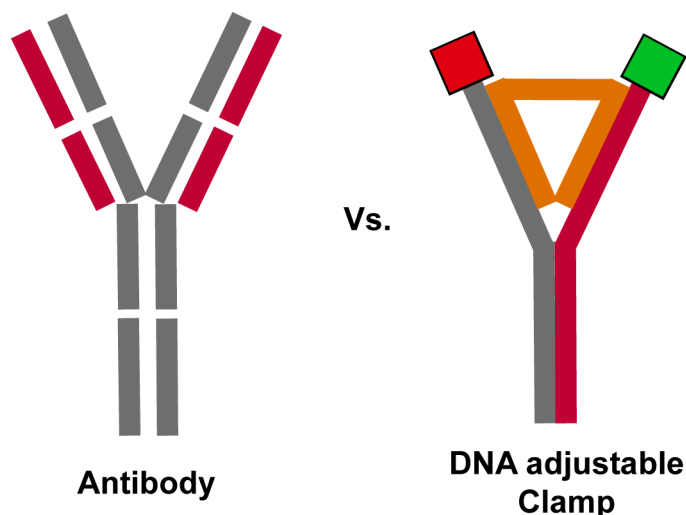


Figure 1.6 Spacing control. Proposed DNA adjustable clamp for spacing control inspired by the antibody structure. Green and red boxes represent the small molecule targeting groups.

Another way to modulate the targeting ability of the vehicles is by controlling the spacing between targeting ligands on the surface. Therefore, in Chapter 3 we will use DNA to modulate the spacing between small molecule end groups of different DNA constructs. We will also test if these architectures could be installed on the surface of gold nanoparticles.

Our last objective regards the stepwise release of nucleic acids from gold nanoparticles, which has potential applications in controlled release in drug delivery and gene control. As discussed in Chapters 4 and 5, we will utilize different branched DNA constructs that can be thermally dissociated over a narrow temperature range due to cooperative interactions between the branches. After evaluating the melting behavior of these strands, we will identify ways to control their melting temperature. We anticipate that using our approach for tuning the thermal properties of DNA, several strands can be released from the same nanoconstruct in a stepwise fashion with no overlapping or cross contamination during the release process.

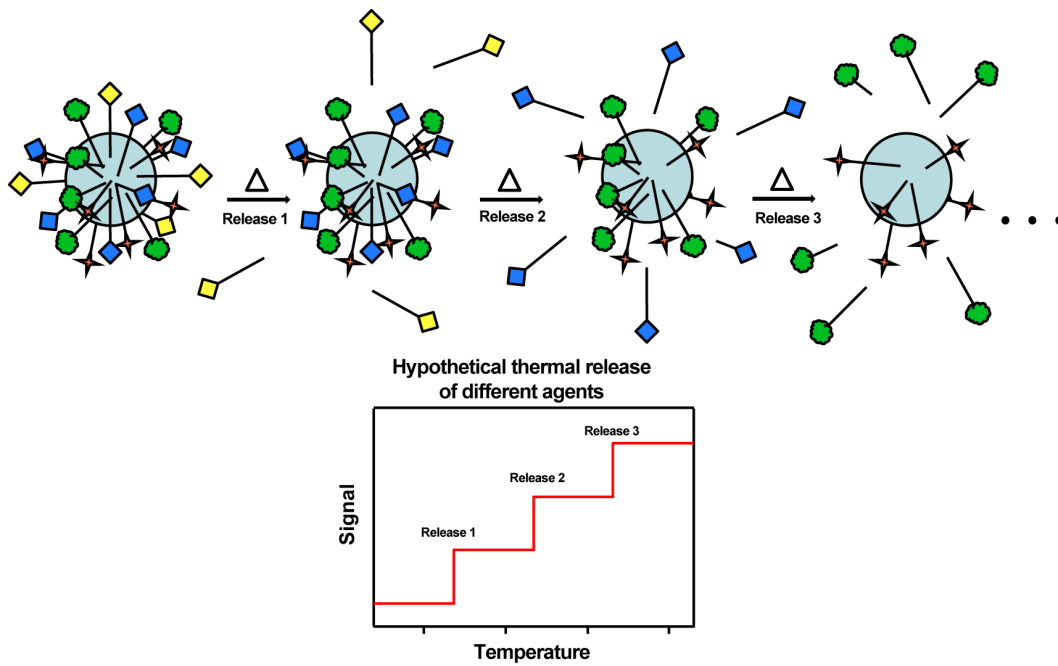


Figure 1.7 Thermally controlled sequential release strategy of different agents.

Chapter 2 Multifunctional DNA-GNPs ¹

¹The research involving tuning ratios and densities in bifunctional DNA-modified gold nanoparticles described in this chapter was published in J.A. Díaz, D.M. Grewer and J.M. Gibbs-Davis, *Small*, 2012, **8**, 873–883

²The research involving the supramolecular spacing control using DNA as

2.1 Introduction

To interface DNA nanotechnology with other real-world applications like information storage and drug delivery, the next generation of DNA hybrid materials including DNA-GNPs will need to incorporate multiple functions in a selective manner.⁹² Indeed, the fields of nanomedicine and smart materials have an urgent need for strategies to systematically tune composition and functional groups arrangement in nanomaterials.^{4, 42, 87, 93-97} Consequently, much current work is aimed at identifying methods to combine targeting ligands, drug, immune-suppressing groups, and imaging moieties in to one material, which should vastly improve the efficacy of drug treatment while limiting toxicity.⁹⁸ However, despite several examples of multifunctional nanomaterials, controlling the ratio and number of each functional group has proven to be challenging.⁹⁹⁻¹⁰²

Among DNA-based materials, DNA-modified gold nanoparticles (DNA-GNPs) are promising candidates for multicomponent drug delivery owing to their ease of synthesis and functionalization as well as their photothermal properties.^{42, 99} In one recent example, Mirkin, Lippard and co-workers demonstrated that a DNA sequence containing two functional end groups, one that reacts with the nanoparticle surface and the other modifiable with drugs, can be used to generate cis-platin-DNA-gold nanoparticles with enhanced toxicity towards multiple types of cancer cells.²⁴ Increasing the functionality of materials such as these requires the development of methods for controlling the composition of monolayers on gold.⁹² As a result we have focused on identifying methods for incorporating multiple functions into DNA-GNPs as a first step towards making well-defined multifunctional therapeutic materials. Utilizing fluorophore-labeled DNA we compared three general ways of introducing combinations of non-nucleotide based functional groups in DNA-GNPs: 1) the *self-assembly* of labeled DNA mixtures bearing GNP-reactive thiols (Figure 2.1a-b); 2) the *DNA-directed assembly* of labeled DNA mixtures

through hybridization of complementary sequences (Figure 2.1c-e); and 3) a *combined strategy* based on both self-assembly and DNA hybridization of labeled DNA (Figure 2.1f). We also explored introducing multiple functional groups with bifunctional branched DNA that contained two unique arms (*DNA-doublers*, Figure 2.1). From our experiments, DNA-directed assembly rather than the self-assembly of thiol mixtures emerges as the best method for controlling functional group ratios and densities.

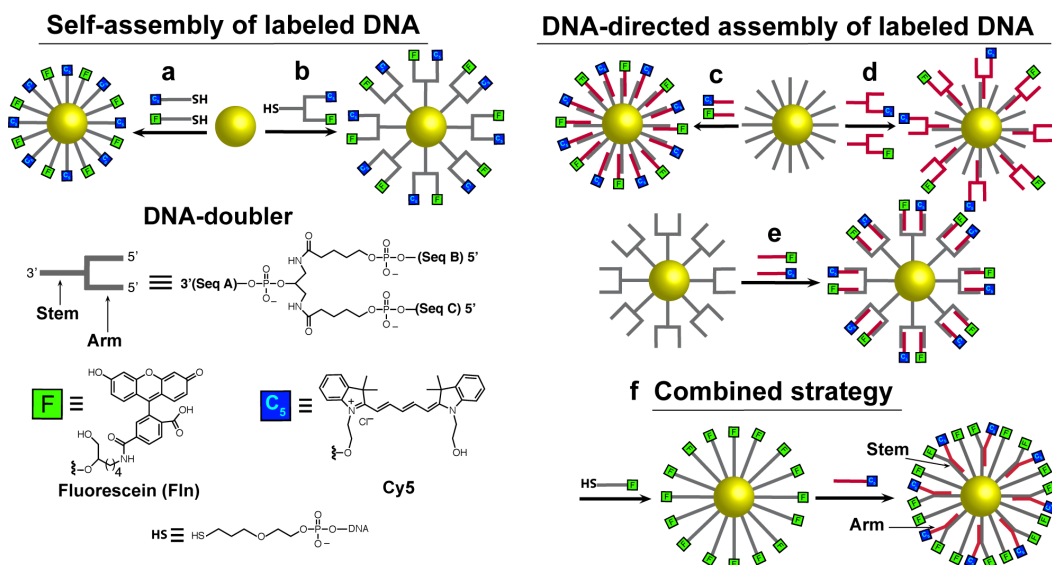


Figure 2.1 Schematic representation of the approaches for synthesizing bifunctional labeled DNA-GNPs. *Self-assembly* on gold nanoparticles of labeled thiolated (a) DNA mixtures or (b) bifunctional DNA-doublers. *DNA-directed assembly* onto DNA-GNPs of labeled complementary (c) DNA mixtures or (d) DNA-doubler mixtures. (e) *DNA-directed assembly* onto a DNA-doubler-GNP of a complementary labeled DNA mixture. (f) *Combined strategy* using one labeled DNA attached via thiol self-assembly and the other by DNA-directed assembly.

2.2 Results and discussion

2.2.1 Self-assembly of labeled DNA

The first strategy involved self-assembly of a mixture of 3'-thiolated strands modified with two fluorophores onto gold nanoparticles (Figure 2.1a). Following a similar self-assembly strategy, a bifunctional Fln and

Cy5-modified DNA-doubler containing a 3'-thiol group was also self-assembled on GNPs (Figure 2.1b).

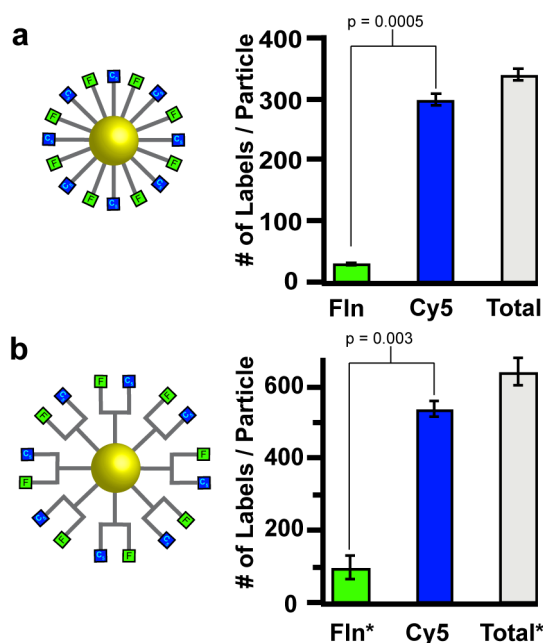


Figure 2.2 The number of fluorophore labels per particle for bifunctional DNA-GNPs prepared by self-assembly on citrate-stabilized GNPs of: a) a 1:1 molar mixture of Cy5 and Fln-labeled thiolated DNA, and b) a solution of Cy5 and Fln-modified thiolated DNA-doubler. (**The amount of Fln appears to be less than Cy5 because Fln is quenched by the latter.*)

The ability of thiols to self-assemble onto noble metal surfaces has been critical to the development of nanomaterials, including DNA-modified gold nanoparticles.⁴² To determine if self-assembly could be used to control the ratio of functionalized DNA, citrate-stabilized GNPs were exposed to a 1:1 molar mixture of 5'-modified DNA bearing a fluorescein (Fln) or a cyanine dye (Cy5) and also a 3' thiol modification (Figure 2.2a). Previously Niemeyer and co-workers demonstrated DNA-GNPs prepared from thiolated oligonucleotide mixtures containing a fluorescent-labeled strand and an unlabeled strand showed a systematic increase in fluorescence as the proportion of labeled strand increased in solution. From the linear relationship between the fluorescence and the solution fraction of labeled DNA, the authors inferred that the ratio of the different DNA on the nanoparticle surface was equal to the ratio of the DNA mixture in

solution.¹⁰³ Indeed, this approach to generate multifunctional gold nanoparticles by controlling the stoichiometry of the thiol mixture during self-assembly is the most common approach in the literature.^{47, 92, 99, 101-104} However, using labeled DNA as a model for ligand or drug-functionalized DNA, we found that Cy5-modified strands were preferentially incorporated on the GNPs over Fln-modified strands, leading to a Fln: Cy5 ratio of 0.109 ± 0.002 , despite the 1:1 ratio in solution (Figure 2.2a, 300 ± 10 Cy5 per GNP versus 33 ± 1 Fln per GNP). Moreover, the amount of Cy5 strands per particle was unusually high, which was also observed when GNPs were decorated with only Cy5 strands (390 ± 40 strands per GNP) Figure 2.3.

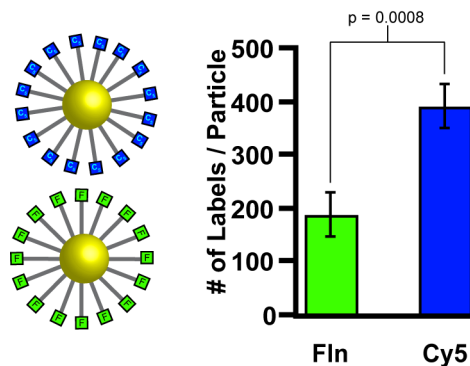


Figure 2.3 Loading of labeled DNA on GNPs using 100% fluorescein or Cy5 (no mixtures). *Self-assembly* of thiolated Fln- or Cy5-DNA on citrate-stabilized GNPs (experiment 2.1a).

On the other hand, when only fluorescein-labeled DNA was reacted with the citrate-stabilized GNPs, 190 ± 40 strands were observed per particle, which is in the range of previously reported examples using this fluorophore (see Figure 2.3).⁷⁰ It is likely that the overwhelming attachment of Cy5-modified DNA comes from interactions other than gold-thiol bonding, and that the charge on Cy5 or its specific structure is leading to nonspecific interactions with the nanoparticles. Regardless of the molecular origin of the effect, the difficulty in controlling the incorporation of Cy5 relative to Fln suggests that self-assembly of functional DNA does not lead to simple control of the surface composition.

Our results are not surprising considering previous work on self assembled monolayers, where drastic differences between solution ratios and surface ratios are often observed as a result of different surface reactivity or adsorption behavior.¹⁰⁵⁻¹⁰⁷ Moreover, the difficulty in tuning surface ratios using self-assembly highlights the need to identify reliable functionalization strategies for multifunctional DNA-GNP materials.

We next explored gold nanoparticles prepared via self-assembly of a thiolated DNA-doubler that contained a different fluorophore on each arm (Figure 2.1b). For these materials, the ratio of Fln and Cy5 is dictated by the structure of the doubler. From the fluorescent results, however, the amount of Fln appeared less than Cy5 despite their 1:1 ratio on the doubler strand (Figure 2.2b), which can be attributed to quenching of the Fln by the Cy5 (Figure 2.8). In terms of DNA density, these DNA-doubler-GNP conjugates behaved similarly to the previous example, showing an even higher degree of functionalization (Figure 2.2b, 640 ± 40 observable labels per GNP). From the high loading, we infer that nonspecific interactions with the Cy5 are also occurring in these DNA-GNP materials. Once again, these results support that self-assembly using modified thiols can be very sensitive to the structure of the modifier despite its remoteness from the thiol reactive end.

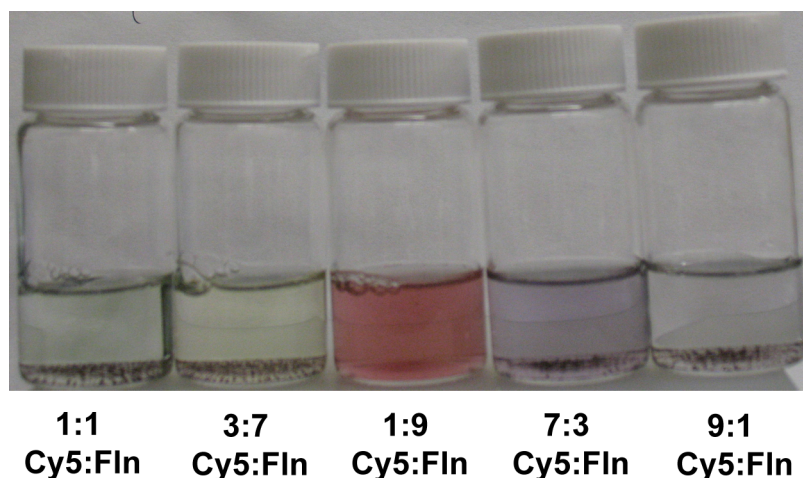


Figure 2.4 Observed GNPs aggregation when Cy5 labeled strands are used and solution is salted up to 0.7 M NaCl. When ratios are varied it is noted that the experiment with highest concentration of Fln labeled strands has lower aggregation.

We also noted that during the preparation of the DNA-GNPs made from thiolated Cy5-modified DNA (both systems shown in Figure 2.2) exhibited a tendency to aggregate in the salt aging process. As observed, Cy5 even at this stage has an effect on the properties of the particles when compared with the Fln-functionalized system. Only when the salting solution had 90% Fln-DNA, the particles did not aggregate as expected for these types of ligand exchange reactions (Figure 2.4). Consequently, the Cy5-modified DNA-GNPs could only be salted to 0.6 M NaCl rather than 0.7 M NaCl. Additionally, it was essential to remove the excess thiolated DNA using 10 mM PBS buffer without NaCl. Similar purification requirements were found to be necessary to prepare larger DNA-GNP conjugates (150-nm diameter particles).⁷⁰ This sensitivity to the preparation process represents another potential challenge of the self-assembly method for introducing labeled DNA.

2.2.2 DNA-directed assembly of labeled DNA

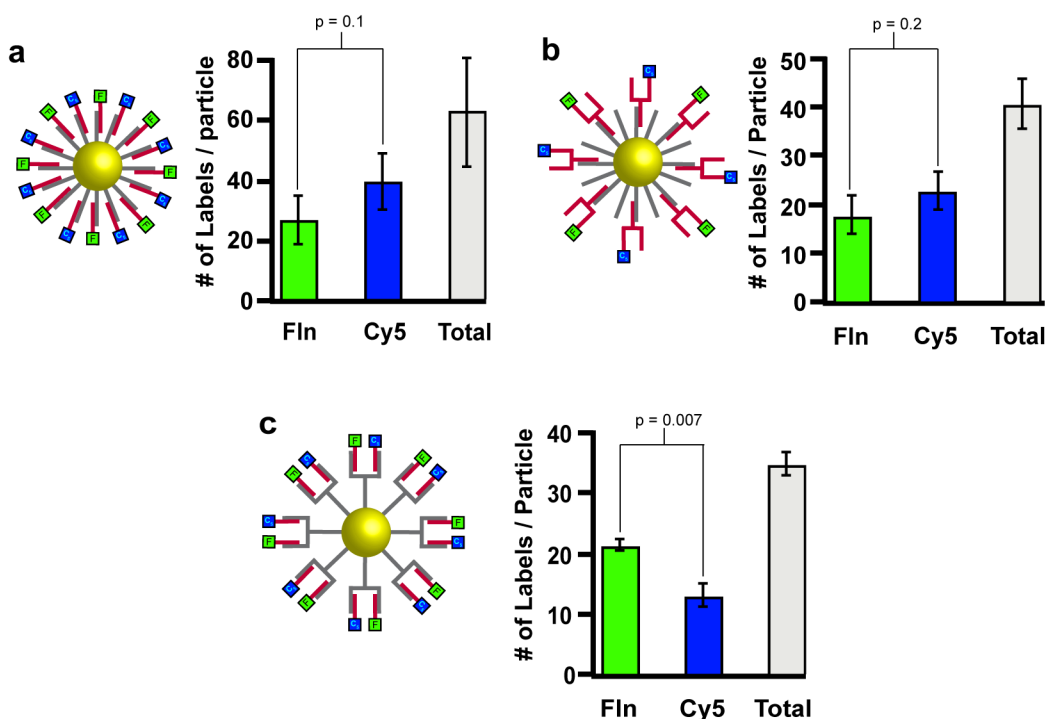


Figure 2.5 Bifunctional DNA-GNPs prepared by DNA-directed assembly of DNA-GNPs hybridized with a labeled complementary solution of a) a 1:1 molar mixture of Cy5 and Fln-modified DNA, b) a 1:1 molar mixture of Cy5 and Fln-modified DNA-doublers and c) NA-GNPs prepared from a 1:1 molar mixture of Fln and Cy5 labeled strands hybridized to a DNA-doubler-GNP conjugate

After establishing that self-assembly on GNP surfaces was not the ideal strategy for controlling the composition of functionalized DNA-GNPs, we turned to DNA-directed assembly as another way to tune label ratios on nanoparticles (Figure 2.1c). When equimolar amounts of Cy5 and fluorescein strands bearing the same sequence were added to complementary DNA-GNPs, we found that the solution ratio was nearly conserved on the DNA-GNP surface (Fln:Cy5 = 0.74 ± 0.07 , Figure 2.5a). The extent of functionalization of the hybridized strands was determined to be around 60 labeled strands per particle, which corresponds to a hybridization percentage of $\sim 50\%$, within ranges previously observed for DNA-GNPs.¹⁰⁸ It is interesting to note that when only Cy5 or Fln strands were hybridized to the DNA-GNP, the final hybridization percentage

remained unchanged (Figure 2.6a) The control over functional group ratio and the consistent hybridization efficiency, independent of the structure of the fluorophore, indicates that using DNA-directed assembly for introducing functional group combination should prove quite general and avoid the issues that plagued the self-assembly method.

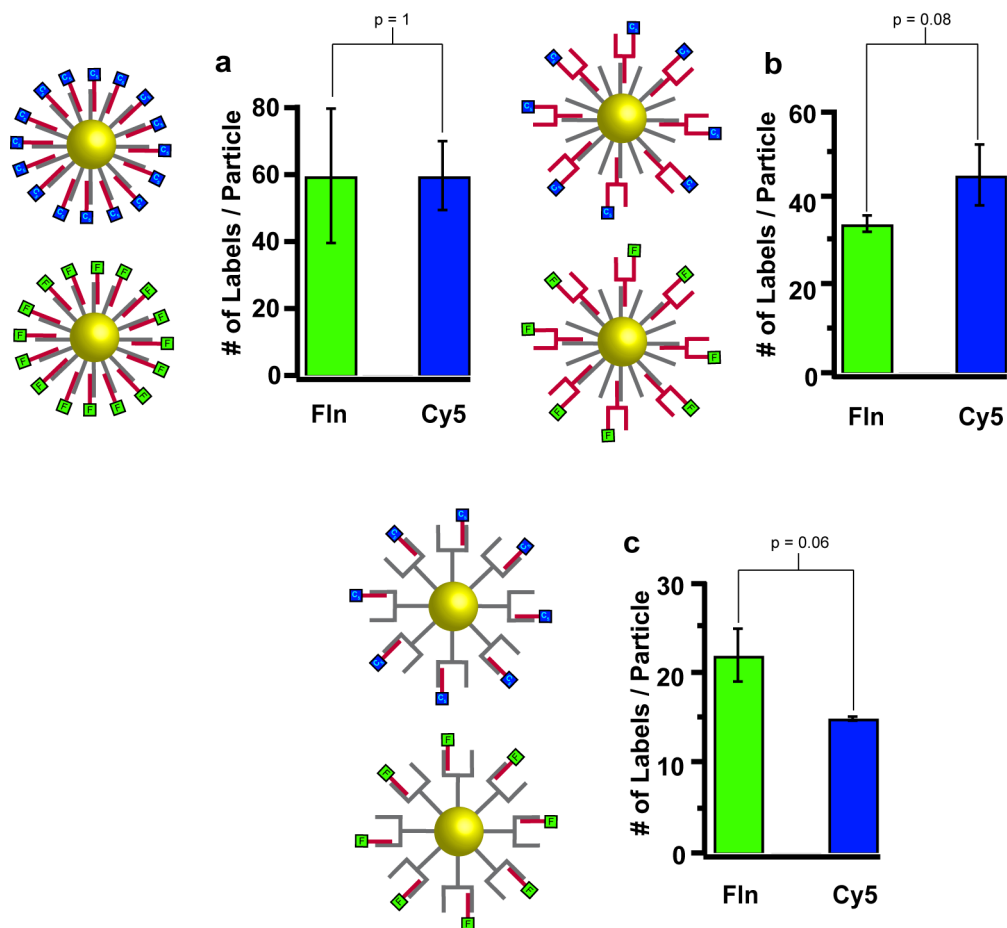


Figure 2.6 Loading of labeled DNA on GNPs using 100% fluorescein or Cy5 (no mixtures). *DNA-directed assembly* of: a) Fln- or Cy5-DNA with DNA-GNPs (experiment 2.5a), b) Fln- or Cy5-DNA-doubler with DNA-GNPs (experiment 2.4b), c) Fln- or Cy5-DNA with DNA-Doubler-GNPs (experiment 2.4c).

A strategy for introducing even more functional groups onto each DNA-GNP involves hybridizing DNA-doublers to DNA-GNP conjugates (Figure 2.1d). When an equimolar mixture of two DNA-doublers labeled with either fluorescein or Cy5 was hybridized to DNA-GNPs complementary to the stem of the DNA-doubler, we measured a Fln: Cy5 ratio of 0.8 ± 0.2

(Figure 2.5b). Not only were the solution and surface ratios similar, but we also found that the loading of the DNA-doubler was efficient. Specifically ~40 doublers hybridized to each DNA-GNP, which corresponds to a higher density of DNA termini at the nanoparticle periphery compared with the analogous linear DNA system (Figure 2.5a). This hybridization efficiency of DNA-doublers was consistent when DNA-GNPs were prepared from either the Cy5-modified DNA-doubler or the Fln-modified DNA-doubler, rather than a mixture. These results support the previous observation that DNA-directed assembly leads to control over surface composition. Additionally, the DNA-doubler strategy enables more functionally complex structures to be accessed by hybridizing layer-upon-layer of DNA-doublers to generate DNA-dendrimers¹⁰⁹ with a GNP core.

Other bifunctional materials with potential in heterovalent targeting are those based on DNA-doublers, where each arm of the doubler can be separately addressed. Unfortunately, we found that self-assembly with Cy5- and Fln-labeled thiolated DNA-doublers on GNPs yielded abnormally high DNA loading (Figure 2.2b), suggesting that they were not forming well-defined monolayers. To link the position of the functional groups to the presence of the different arm sequences, asymmetric DNA-doublers without labels were self-assembled on GNPs and then hybridized to a mixture of the complementary Cy5 and Fln-modified strands (Figure 2.1e, Figure 2.5c). Each arm contained a different sequence with comparable stabilities based on computed melting temperatures, so we expected that the ratio of Fln and Cy5 would be one. From the fluorescent data, the Fln: Cy5 ratio of the two labels was found to be 1.6 ± 0.2 (Figure 2.5c). The overall loading of Cy5 and Fln including the lower loading of the Cy5 strand was consistent with control experiments when only one labeled strand was hybridized (Figure 2.6c). This similarity for the monofunctional and bifunctional systems indicated that the amount of each labeled strand was primarily due to its affinity for the complementary arm and not the

hybridization state of the neighboring arm. Although, we expected the binding constants to be similar for both arm sequences, the lower loading of Cy5-DNA is attributed to a lower binding constant than that of the DNA duplex made with the FIn strand. Despite the deviation from the expected ratio of one, the structure of the DNA-doubler ensures that most of the Cy5 are near a FIn strand indicating that this strategy could find use in heterovalent targeting.

2.2.3 Combined strategy

In nanomedicine, controlling the ratio of the two functional groups will be critical because the therapeutic properties of multifunctional therapeutic agents should depend on the ratio of the different therapeutic components.⁸⁷ However, for heterovalent targeting strategies based on synergistic combinations of ligands, the relative position of the two functional groups must also be controlled.^{88 110} To introduce control over label spacing, we combined self-assembly and a DNA-directed functionalization strategy. First, FIn-labeled DNA-GNPs were prepared by self-assembly followed by subsequent functionalization through hybridization of a Cy5-labeled strand (Figure 2.1f). The resulting FIn: Cy5 ratio was found to be 1.55 ± 0.05 , which corresponded to a hybridization efficiency of 60% (Figure 2.7). As each Cy5 neighbors a FIn group, synergistic interactions for ligand-substituted DNA should be possible, which should allow tuning of biological affinity for future targeting applications.

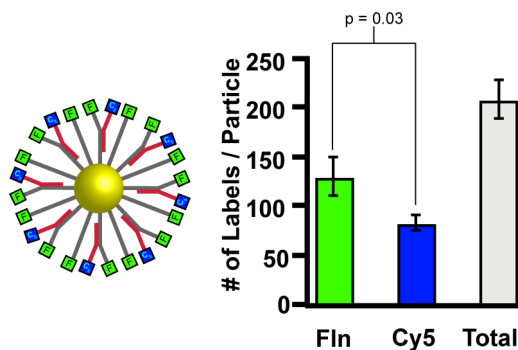


Figure 2.7 Bifunctional DNA-GNPs prepared by a) self-assembled Fln-DNA-GNPs hybridized to partially complementary Cy5-labeled strands.

Overall DNA-directed assembly and combination strategies yielded functionalized DNA-GNPs with the most control over the surface ratio of the two labels. Regarding label density, an inspection of the results also indicates that the different strategies can be used to vary the amount of label per particle. To achieve the highest density of labeling groups, labeled, thiolated DNA can be self-assembled on GNPs (190 ± 40 Fln/GNP and 390 ± 40 Cy5/GNP, see Figure 2.3). The strong dependence of loading on the nature of the label, however, suggests that nonspecific interactions might be at work for certain labels like the positively charged Cy5. Consequently, when well-defined monolayers are desired, then self-assembly with unlabeled DNA or “well-behaved” labeled DNA like Fln-DNA is preferred, followed by DNA-directed assembly. For example the combination strategy illustrated in Figure 3a using a Fln-modified DNA-GNP hybridized to Cy5-labeled strands resulted in a total of 210 ± 20 labeled strands per GNP. Hybridizing labeled DNA to unmodified DNA-GNPs led to 60 ± 20 labels per particle (Figure 4.2a). Similarly, hybridizing DNA-doublers that contained only one label led to a label density of 41 ± 5 labels per GNP (Figure 4.2b), but this number should easily be doubled if both arms contained a modification. Finally, first attaching a thiolated DNA-doubler to the surface and then hybridizing the arms with labeled DNA led to similar loading of labels (35 ± 2 labels per GNP, Figure 2.5c) as for the previous doubler system.

2.3 Conclusion

We have studied several strategies for making Cy5 and Fln modified DNA-GNPs and have found that functionalization by DNA-directed assembly provides the best route to control the ratio of functional groups on the gold nanoparticles. In contrast, the self-assembly of thiolated Cy5 and Fln mixtures led to very little control over the surface composition, which suggests that DNA-directed assembly is a more general route to bifunctional materials. We also illustrated how DNA-doublers can be used to increase complexity; once again the best route involved hybridizing functionalized DNA-doublers to the DNA-GNP rather than introducing doublers via thiol-gold self-assembly. The success of DNA-directed assembly strategies is of particular importance since the structure of any nanoparticle or micro particle, to which DNA can be attached, including those not made from gold, should be tunable with these approaches.¹¹¹⁻¹¹⁴

2.4 Materials and methods

2.4.1 Quenching of fluorescein by Cy5

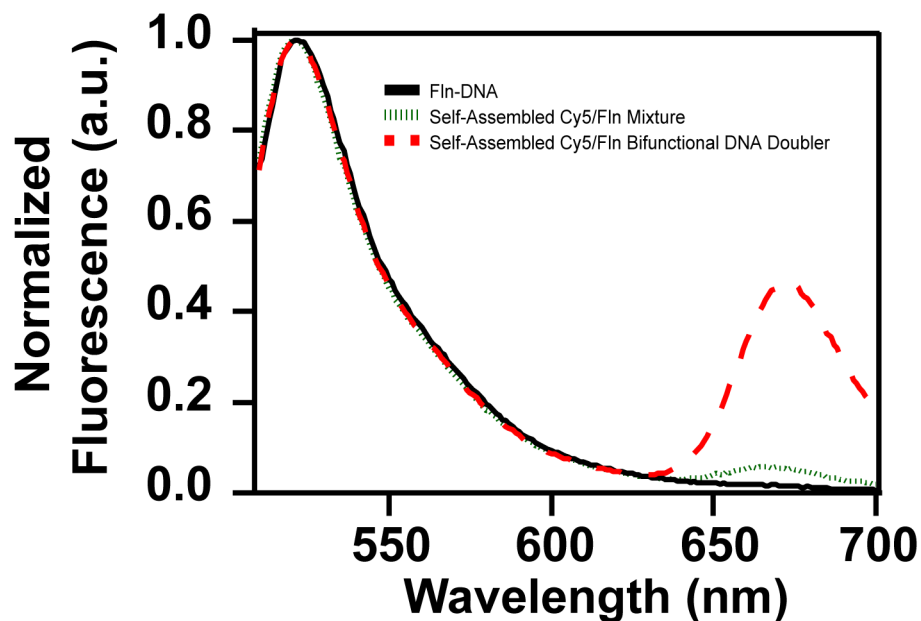


Figure 2.8 Emission spectrum of a Fln- and Cy5-modified bifunctional DNA-doubler excited at 495 nm, which correspond to the excitation of fluorescein (Fln). FRET is observed between Fln and Cy5, which leads to a lower estimate of Fln per GNP (see Figure 2.2b).

The amount of Fln appeared less than Cy5 despite their 1:1 ratio on the doubler strand as shown in Figure 2.2b. Figure 2.8 illustrates that energy transfer occurs from Fln to Cy5 in the DNA-doublers, as consequence determining the actual amount of Fln is not possible.

2.4.2 Preparation of DNA strands and gold nanoparticles

The DNA sequences were synthesized on an Applied Biosystems model 392 DNA/RNA synthesizer, using Glen Research reagents, Glen-Pak purification cartridges and following their protocols. Deprotection of the Fmoc group on the doublers was afforded by attaching two 1-mL syringes to the column and rinsing it back and forth with DBU (1 M) in acetonitrile (1 mL) for 10-12 minutes. The coupling time for the upcoming base, after Fmoc removal, was increased by one minute. Strand purification and

DMT deprotection using Glen-Pak cartridges (Glen Research, cat. 60-5200-01) were done according to the DMT-On protocol. The DNA-doublers used for experiments 2.2b, 2.5b, 2.5c, 2.6b and 2.6c were further purified by non-denaturing PAGE (15% 1 x TBE running buffer). In addition to the standard nucleotide phosphoramidites, the following compounds were used: 6-Fluorescein Phosphoramidite (cat. 10-1964-95), Cy5 Phosphoramidite (cat. 10-5915-95), Cy3 Phosphoramidite (cat. 10-5913-95), Fluorescein-dT Phosphoramidite (cat. 10-1056-95), Thiol-Modifier C6 (cat. 10-1936-90), 3' Phosphate CPG (cat. 20-2900-41), 3' Thiol-Modifier 6 CPG (cat. 20-2938-41), dA-5'-CE Phosphoramidite (cat. 10-0001-02), dC-5'-CE Phosphoramidite (cat. 10-0101-02), dmf-dG-5'-CE Phosphoramidite (cat. 10-9201-02) and dT-5'-CE Phosphoramidite (cat. 10-0301-02). GNPs of 13-nm diameter were synthesized following the procedure reported by Grabar *et al.*¹¹⁵ The concentration of GNPs was determined from UV-vis absorbance spectroscopy based on its reported extinction coefficient of $2.7 \times 10^8 \text{ M}^{-1} \text{ cm}^{-1}$ at $\lambda_{\text{max}} = 520 \text{ nm}$.¹¹⁶

2.4.3 Loading of thiolated DNA on GNPs

Thiolated DNA was covalently attached to the GNPs following the procedure outlined by Hurst *et al.*⁷⁰ The freshly reduced thiolated oligonucleotides were purified either in a NAP 10-Column (cat. 17085401 GE Health Care) for larger scale synthesis or 0.2 Gel-Pak column (cat. 61-5002-05 Glen Research) for smaller scale synthesis. The DNA concentration of the eluted fractions was determined from their absorbance at 260 nm and corresponding extinction coefficients calculated using OligoCalc. The final concentration of NaCl was 0.7 M for all of the samples prepared, except for experiment 2.2a, which was salted up to only 0.6 M NaCl to prevent GNP aggregation. The samples were purified according to the reference in LoBind DNA Eppendorf tubes (cat. 022431048). After purification, the DNA-GNP's were suspended in PBS (10 mM, 0.3 M NaCl). To avoid GNP aggregation, for samples 2.2a, 2.2b

and 2.3 the same washing procedure was used but buffer without NaCl (0.10 M PBS, 0.01% SDS pH = 7.01) replaced the NaCl containing buffer.

2.4.4 Hybridization of ssDNA on DNA-GNPs

DNA-modified gold nanoparticles and the corresponding complementary strand were combined in buffer (0.3 M NaCl 0.10 M PBS 0.01% SDS) to reach final concentrations of 10 nM and 3 μ M, respectively. The hybridization mixtures were then vortexed, sonicated for ~ 10 seconds and heated up to 70 °C for 3 minutes. Next, the mixtures were allowed to cool to room temperature overnight in the dark. The next day, purification was conducted as described in Demers *et al.*¹⁰⁸ by centrifuging the mixture at 4 °C and resuspending the DNA-GNP pellet in cold buffer (500 μ L, 0.3 M NaCl, 0.10 M PBS, 0.01% SDS).

2.4.5 Quantification of labeled DNA strand on GNPs

Because of the quenching properties of gold nanoparticles, the fluorescently labeled DNA had to be cleaved from the purified DNA-GNPs using aqueous DTT as described in previously reported procedures.⁷⁰ For DNA-GNPs prepared in buffer with no added NaCl, the suspensions took longer to aggregate in DTT, requiring 6 hours. The concentration of fluorescent DNA was determined with a calibration curve acquired with fluorescent DNA in a 1:1 buffer:DTT mixture on the same fluorescent plate reader from (0 to 2.5 mM). Our fluorescence data suggested that DTT cleavage required only one hour although we allowed it to react longer (Figure 2.9).

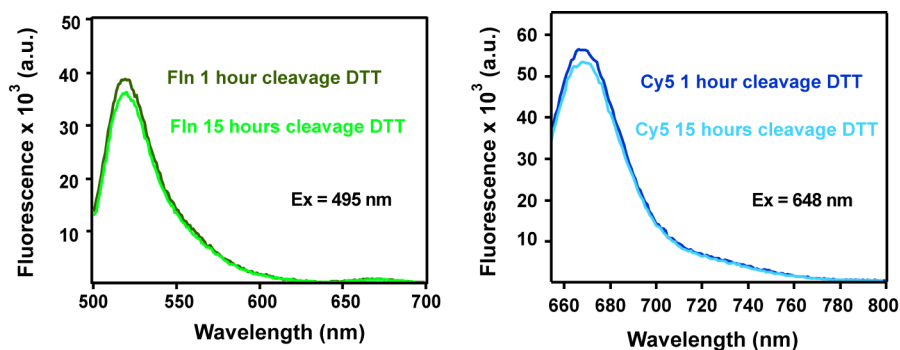


Figure 2.9 Fluorescent emission spectra of a DNA-GNP suspension containing (a) fluorescein (Flu) or (b) Cy5 labeled DNA after 1 hour and 15 hours treatments with 0.5 M DTT. The suspension of the DNA-GNP conjugate was prepared by the self-assembling of a mixture of a 2 μM solution of Flu labeled DNA and a 2 μM solution of Cy5 labeled DNA. These results support that DTT-cleavage of DNA occurs within an hour.

For comparison purposes, curves made with solutions having both dyes in 1:1 proportions were also obtained, using the same range of concentrations, and the presence of both dyes was shown to have no effect on the other's fluorescence. Two calibration curves were acquired for each fluorophore: one for 5'-fluorescently modified DNA and the other for 3'-fluorescently modified DNA.

For sample **2.7** containing a thiolated Flu-DNA bound to the GNP and Cy5-DNA hybridized to the Flu strand, the analysis was slightly different. After determining the GNP concentration in a known volume of the sample, the amount of hybridized Cy5-DNA was determined. Specifically, the bifunctional DNA-GNPs (typically 30 μL) were introduced to an excess of an unlabeled strand completely complementary to the Flu-DNA bound to the GNP (2.7-III, final concentration $\sim 5 \mu\text{M}$) and washed following the *Hybridization of oligonucleotides on GNPs* section described above. The fluorescence was monitored from the combined washes, and from the volume we determined the amount of Cy5 strands that had been hybridized to the Flu-DNA-GNP. The DNA-GNP was then resuspended and analyzed for Flu content using the DNA cleavage strategy described above. Three experiments were performed in each case to obtain an

average value of each fluorophore, whose standard deviation was used as the error. The total of strands per each experiment was determined by adding each individual set of experiments and then average them. The standard deviation of these values were again reported as the errors. The t values and degrees of freedom were calculated using the t test for populations with different standard deviations,¹¹⁷ p-values were derivated using a web based p-value calculator.¹¹⁸

2.4.6 Fluorescence measurements

The supernatant containing only labeled DNA without GNPs was measured in a Tecan Safire II plate reader using either 96 well or 384 well plates. To analyze the fluorescein concentration, the following instrument settings were used: excitation λ = 495 nm, emission λ = 521 nm, excitation bandwidth = 10 nm, emission bandwidth = 5 nm, number of reads = 5, steps = 1 nm, gain = 60, integration = 40 μ s. To analyze the Cy5 concentration, the following instrument settings were used: excitation λ = 648 nm, emission λ = 671 nm, excitation bandwidth = 10 nm, emission bandwidth = 5 nm, number of reads = 5, steps = 1 nm, gain = 80, integration = 40 μ s.

2.4.7 Sequences

Table 2.1 DNA sequences corresponding to DNA structures described in Figures 2.1–7.

Figure	Sequence
2.2a	I 5'-Fln-T CGT CCA CAT TAT TAA TAT TTT TTT TTT-SH-3'
	II 5'-Cy5-T CGT CCA CAT TAT TAA TAT TTT TTT TTT-SH-3'
2.2b	[5'-Fln-AGA GTT ATT CC- to doubler (arm 1)]
	I 5'-Cy5-AGA GTT ATT CC- to doubler (arm 2) -Doubler-TTT TTA AAA ATT TTT TTT TT-SH-3' (stem)]
2.5a	I 5'-TCT GCC ACT TTT TAA AAA TTT TTT TTT T-SH-3'
	II 5'-TTT TT A AAA AGT GGC ATC-Fln-Phos-3'
	III 5'-TTT TT A AAA AGT GGC ATC-Cy5-Phos-3'
2.5b	I 5'-HS-TTT TTT TTT TAAAA TTT TICGGCCGAC-3' [5'-AGA GTT ATT CC- to doubler (arm 1)]
	II 5'-Fln-TCG TTA TTC AC- to doubler (arm 2) -Doubler-GTC GGC CGA AAA AT-3' (stem)]
	III 5'-Cy5-TCG TTA TTC AC- to doubler (arm 2) -Doubler-GTC GGC CGA AAA AT- 3' (stem)] [5'-CAG CCG GCT TTT- to doubler (arm 1)]
2.5c	I 5'-CGC AGC TTG CTT- to doubler (arm 2) -Doubler-TTT TTA AAA ATT TTT TTT TT-SH-3'(stem)]
	II 5'-AGC AAG CTG CGA-Cy5-Phos-3'
	III 5'-AAA GCC GGC TGA-Fln-Phos-3'
2.7	I 5'-Fln-AGA GTC CAC GTG CTT TTT AAA AAT TTT TTT TTT-SH-3'
	II 5'-ATT TTT AAA AAG CAC GCA CCT GCT-Cy5-Phos-3'
	III 5'-AAA ATT TTT AAA AAG CAC GTG GAC TCT-3'

Chapter 3 Supramolecular spacing control using DNA as scaffold²

²The research involving the supramolecular spacing control using DNA as scaffold described in this chapter was published in J.A. Díaz, D.M. Grewer and J.M. Gibbs-Davis, *Small*, 2012, **8**, 873–883. D.M. Grewer collaborated with the titrations described in Figure 3.2.

3.1 Introduction

Programmability is key to self-assembly, and consequently DNA-based materials and systems have emerged as major examples of nanotechnology. Using complementary interactions between DNA sequences, new materials as well as highly ordered arrays have been assembled in the nanoscale and microscale domain.^{19, 119} In addition to controlling the position of objects, more sophisticated examples of functional DNA systems have emerged such as, molecular switches, motors, walkers, and light harvesting assemblies.^{120, 121} In the previous chapter we showed different ways of controlling the ratio and amount of functional groups of DNA-GNPs. But not only modulating the ratio and amount of functional groups is important, also controlling their spatial distribution on the surface of the nanomaterial is also desirable. For example, matching the ligand arrangement on the nanomaterial with the receptor arrangement on a diseased cell should increase the specificity of cell recognition in targeted drug delivery.^{88, 89, 122-130} Therefore, using the programmability and recognition properties of DNA, we also demonstrated a strategy for controlling the distance between functional groups using DNA clamp complexes. These clamps have promise as drug delivery materials with tailorable affinities for cell targets. Moreover, our results indicate that these clamp structures can also form on the GNP surface, although more work must be done to quantify the distance between labels in functionalized DNA-GNPs.

3.2 Results and discussion

3.2.1 Spacing control using Y-shaped DNA clamps

3.2.1.1 Y-shaped DNA clamps

As previously mentioned, incorporating heterovalency into targeting strategies will require that the position of the two different ligands are in

close enough proximity that both can bind cell surface receptors simultaneously. To fine-tune the distance between the labels, a third *adjuster* strand can also be introduced that clamps the bifunctional structure shut by hybridizing to both labeled arms simultaneously. Such DNA-adjustable clamps bearing targeting ligands can be tuned to match the distance between receptors on cells to increase binding affinity and selectivity.¹²⁷ Figure 3.1 illustrates the design of the *Y-clamp* consisting of two partially complementary strands, the *left* strand containing a 5'- Cy3 terminus and the *right* strand bearing a 3'- Cy5 terminus. The hybridized region of the Y-clamp is denoted as “stem”, the non-complementary regions are the “arms” and the *adjuster* is a strand of linear DNA complementary to both arms and bearing a non-complementary “bridge”. By controlling this bridge sequence and the length of the arms, the distance of the fluorophore (ie. ligands) can be programmed.

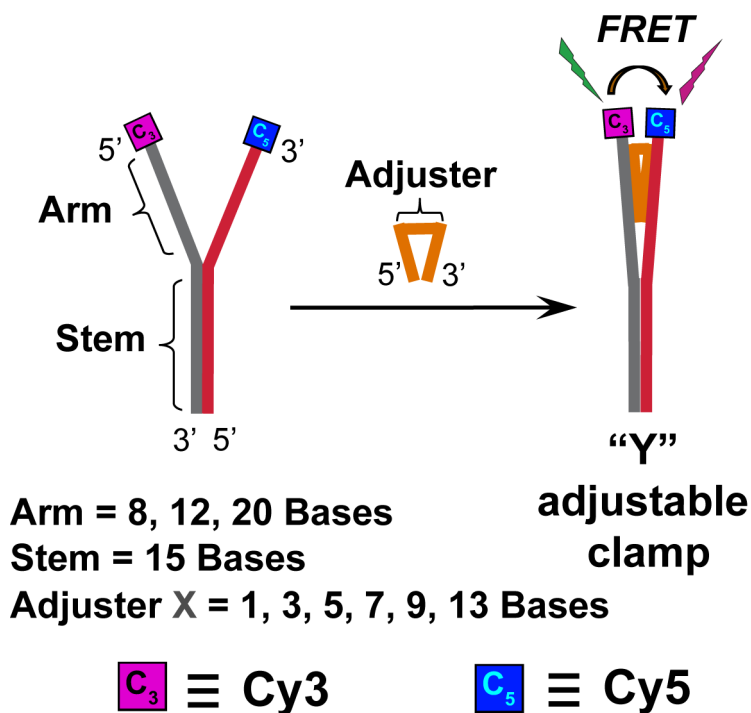


Figure 3.1 Two strands hybridize to form the *left* half (gray) and *right* half (red) of the Y-complex. Adding the *adjuster* strand (orange), complementary to the arms and bearing a central *bridge* sequence, leads to the Y-clamp

3.2.1.2 FRET experiments on Y-shaped DNA clamps

To determine the intra-complex spacing in these DNA-adjustable clamps, we measured Förster Resonance Energy Transfer (FRET) between the Cy3 (donor) and Cy5 (acceptor) by exciting the former at 525 nm (Figure 3.2).

These FRET experiments for the Y-clamp were carried out by first hybridizing a Cy3-modified *left* strand with an adjuster strand (Figure 3.2, 0 equiv) and then titrating in the Cy5-modified *right* strand to form the adjustable Y-clamp (Figure 3.2, varying equivalents). The distance was then determined from the initial emission of the Cy3 when no Cy5 was present and the final Cy3 emission after adding 3 equiv of the Cy5-modified *right* strand to ensure that all of the Cy3 strands were incorporated into clamps (Figure 3.2b). We performed these FRET

titrations for several systems in which the length of the adjuster bridge sequence and the arms were varied.

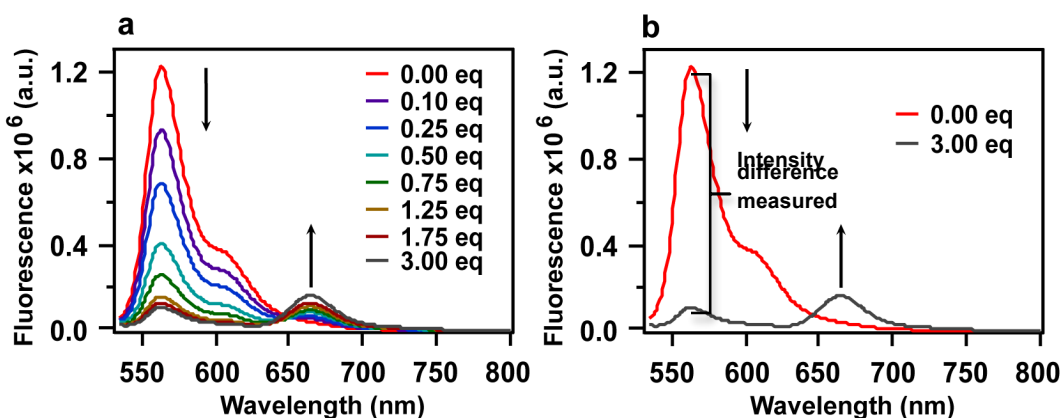


Figure 3.2 Typical FRET titrations of hybridization mixtures containing 1 equiv of Cy3-labeled *left* strand and *adjuster* and varying equivalents of the Cy5-labeled *right* strand ($\lambda_{\text{ex}} = 525$ nm). a) Titration experiment. b) Difference of intensities used to determine the distance between fluorophores

For a short Y-clamp containing 8-base arms, the distance between the fluorophores was measured from 3.6 ± 0.1 nm to 4.3 ± 0.1 nm, depending on the length of the bridging sequence in the adjuster strand used (Table 3.1). For this short Y-clamp, there was a linear trend between the adjuster bridge length (x) and the distance between the fluorophores that corresponded to approximately 0.1nm/bridge base. When no adjuster strand was present the spacing between the two fluorophores was similar to that of a Y-clamp hybridized with an adjuster containing a seven-base bridge, indicating that the adjuster could indeed close the clamp. For a larger clamp with twelve bases in each arm, we looked at a series of adjusters with 1 – 13 bridging bases and observed fluorophore spacing from 4.5 ± 0.1 nm – 5.4 ± 0.1 nm. Specifically, increasing the bridge from 1 – 5 bases led to an increase of approximately 0.4 nm between the fluorophores, consistent with the small Y-clamp system. As the bridge was further increased to 9 and 13 bases, we observed less dependence on bridge length versus distance, which was attributed to increased clamp

flexibility. It was also observed that the clamp without adjuster was more open than the clamp with the longest bridge (Table 3.1).

Table 3.1 Intra-complex spacing with varying adjuster bridging nucleotides (x) for a series of Y-shaped clamps.

System	Adjuster (nm)			
	X = 1	3	5	7
“Y” complex Arm = 8 Bases Stem = 15 Bases	3.6 ± 0.1	3.8 ± 0.1	4.0 ± 0.1	4.3 ± 0.1
	<p style="text-align: center;"> p = 0.05 p = 0.05 p = 0.01 </p>			
		No adjuster	4.2 ± 0.2	
	X = 1	5	9	13
“Y” complex Arm = 12 Bases Stem = 15 Bases	4.5 ± 0.1	5.0 ± 0.1	5.2 ± 0.1	5.4 ± 0.1
	<p style="text-align: center;"> p = 0.0009 P = 0.05 p = 0.05 </p>			
		No adjuster	5.5 ± 0.1	

These results demonstrated that the distance between the two labels could be controlled from the Ångstrom to the nanometer regime by the use of adjuster strands. However, the flexibility of the adjuster bridge and the influence of probe orientation on energy transfer,¹³¹ sensitive to DNA conformation, appeared to cause deviations from the expected linearity.

The simplicity of the DNA adjustable clamp design allowed us to explore alternative hybridization strategies for closing the clamp. Specifically we investigated the influence of the extent of hybridization and position of the adjuster strand on intra-complex spacing. Using a long Y-clamp and a one-base bridge adjuster strand complementary to only the upper arm sequence (Figure 3.3, *Upper*) we observed a distance of 4.09 ± 0.01 nm between the two fluorophores. In comparison, the fluorophore distance for the same Y-clamp hybridized to an adjuster strand fully complementary to the arms led to the same value of 4.09 ± 0.02 nm (Figure 3.3, *Full*). This suggested that the extent of hybridization of the arms did not play a role on the spacing between the strand termini. Next, we explored the effect of the position of the adjuster by hybridizing it with the lower half of the arms

adjacent to the stem (Figure 3.3, *Lower*). For this system, the fluorophore spacing increased to 4.85 ± 0.02 nm despite the same 1-base bridge length. This increase is particularly interesting when comparing the *Lower* adjuster clamp with that of 4.62 ± 0.04 nm for the clamp containing no adjuster (Figure 3.3, *no adjuster*). This suggests that the *Lower* adjuster actually opened the clamp rather than closing it. Overall, these observations reveal that control can be effectively exerted in adjustable Y-clamps by changing the position of the adjuster as well as the length of the bridge sequence (Figure 3.3).

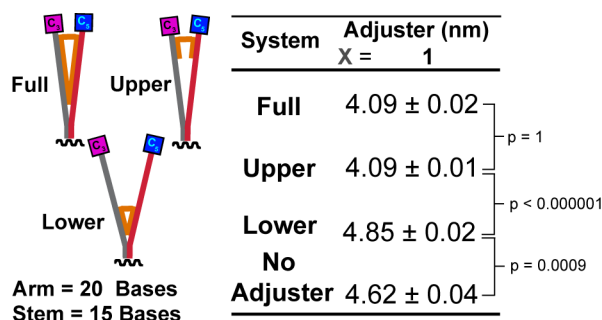


Figure 3.3 A long Y-clamp (20-base arm) hybridized with three different adjuster sequences, all bearing a one-base bridge. The *Upper* adjuster, *Lower* adjuster, and *Full* adjuster are complementary to the upper half, lower half, and all of the arms, respectively, where upper corresponds to the half adjacent to the fluorophores.

3.2.1.3 PAGE experiments Y-shaped clamp formation

To provide more evidence that the clamps were indeed forming we monitored their thermal dissociation temperatures (Table 3.2) and determined that all complexes were stable under the conditions of the FRET experiments (supporting information). We also monitored formation of the clamp complexes with non-denaturing polyacrylamide gel electrophoresis (PAGE) (Figure 3.4). In the PAGE experiments a Fln-labeled *left* strand was used without any label on the *right* strand. We employed only one fluorophore to simplify imaging of the gel using our fluorescent imager. As shown in Figure 3.4, upon combining the labeled *left* strand, *right* strand and adjuster, a new band appeared in the gel that

is attributed to the clamp complex, which exhibited lower electrophoretic mobility than the smaller Y-complex made from only the *left* and *right* strands. Under conditions corresponding to the end of the FRET titrations, 88% of the *left* strand was incorporated into a Y-clamp, with the remaining amount consisting of oligomers of adjuster-linked Y-complexes (Figure 3.9). Despite the presence of the small amount of oligomers, the distances measured from the FRET experiments are highly reproducible as indicated by the small error values (Table 3.1).

Table 3.2 Melting temperatures of the hybridized adjuster:Y-Complex (DNA Adjustable Y-clamps) x = *The number of bridging bases in the adjuster strand.*

System	Melting Temperatures °C					
	X =	Free*	1	3	5	7
“Y” complex Arm = 8 Bases Stem = 15 Bases		39.4	44.0	44.3	41.8	42.3
	X =	Free*	1	3	5	7
“Y” complex Arm = 12 Bases Stem = 15 Bases		44.2	50.9	48.2	47.9	49.8
	X =	Free*	Full	Upper	Lower	
“Y” complex Arm = 20 Bases Stem = 15 Bases		26.0	45.1	38.3	30.6	

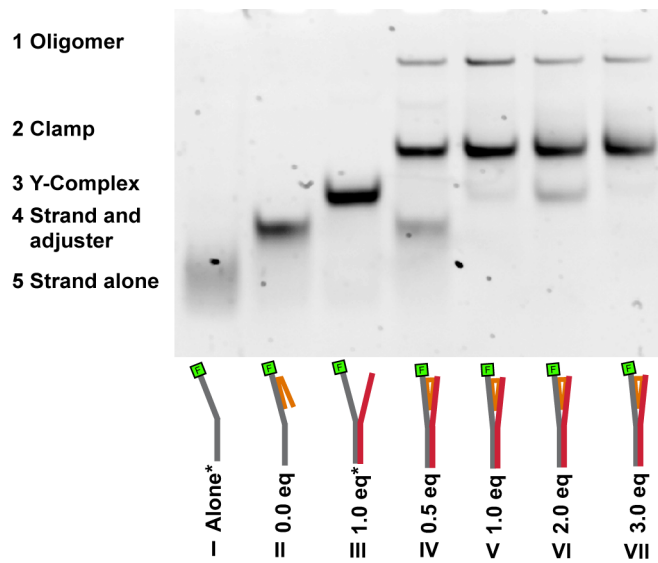


Figure 3.4 Non-denaturing PAGE fluorescent image tracking the clamp formation. All lanes contained left strand (1 equiv) and adjuster (1 equiv), unless noted, and the following amounts of the right strand: I) 0 equiv;* II) 0 equiv; III) 1 equiv;* IV) 0.5 equiv; V) 1.0 equiv; VI) 2.0 equiv; VII) 3.0 equiv. (*No adjuster present.) The Fln label was used instead of the Cy3 and Cy5 for optimal imaging with our fluorescent imager, which should not affect the stability of the complexes. *Conditions:* 1 equiv = 1.3 μ M in buffer (10 mM PBS, pH 7, 0.5 M NaCl).

3.2.2 Spacing control using DNA-doublers clamps

3.2.2.1 DNA-doublers clamps

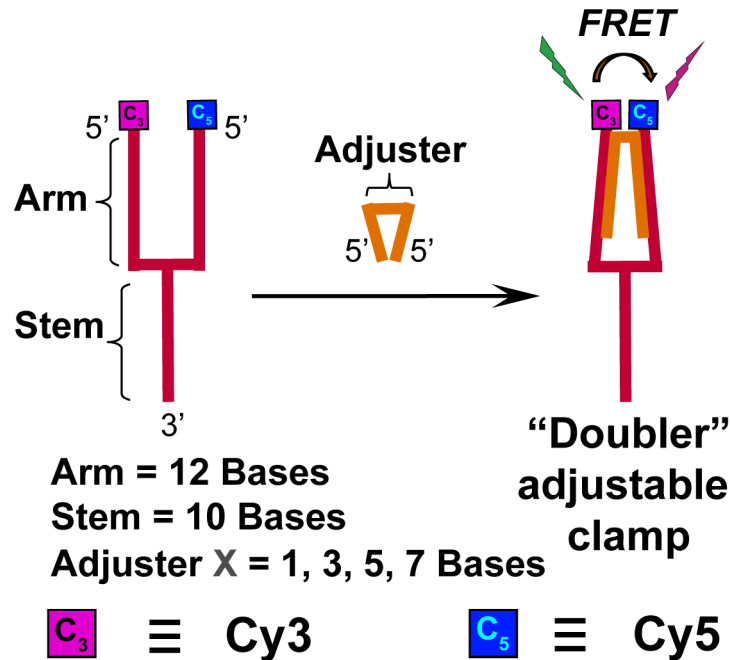


Figure 3.5 Adjustable DNA-doubler clamp design.

The *DNA-doubler clamp* is based on essentially the same design as the Y-clamp, but the DNA arms were connected covalently using a branched phosphoramidite rather than connected through hybridization (Figure 3.5). Therefore, the adjuster strands for these DNA-doubler clamps required that the 3'-5' directionality of the strand changed half-way through the sequence in order to hybridize with both arms.

3.2.2.2 FRET experiments on DNA-doublers clamps

As in the previous example, FRET was used to determine the intra-complex spacing of the two fluorophores in the DNA-doubler clamp (Figure 3.6a). Here the adjuster strand was titrated in, unlike the Y-clamp experiments where the Cy5-modified strand was added, as the DNA-doubler already contained both fluorophores. Figures 3.6b illustrates the observed change in energy transfer as titration proceeded. As adjuster

was added the donor emission decreased, but an increase in FRET emission from the acceptor was not observed. We attributed these results to the small change in donor emission for this system compared with that of the Y-complex. To quantify the intra-complex distance, the donor emission without any FRET was determined from a reference Cy3-DNA solution, and that value and the donor emission in the presence of 0.5 equivalents of adjuster strand were used. From analysis of these FRET titrations, we observed a similar trend relating bridge length to intra-strand distance as observed for the Y-clamp, when the bridging bases were varied from 1-7 (Table 3.3). The resulting intra-complex distances were less than that of the Y-clamps exhibiting values from 2.85 -3.28 nm.

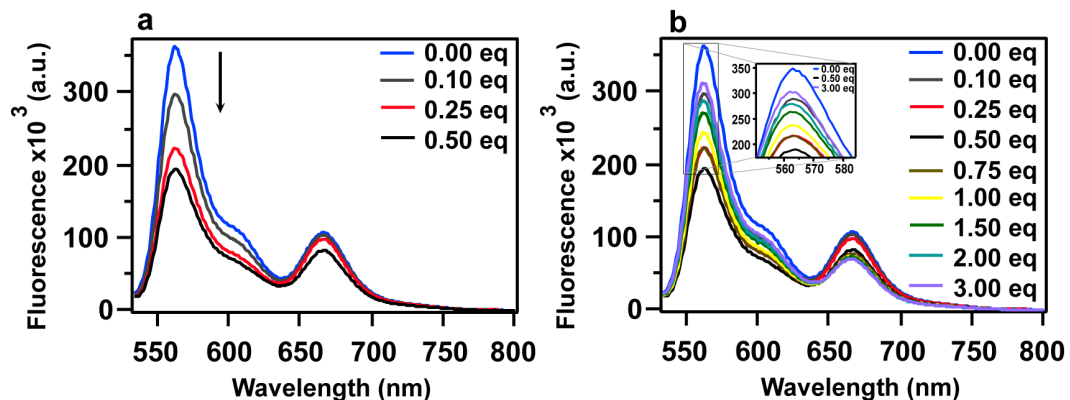


Figure 3.6 Example of a titration where varying equivalents of an adjuster strand were added to a solution of bifunctional Cy3-Cy5-DNA-doubler a) decrease in donor intensity from 0.00 equivalents up to 0.50 equivalents of adjuster. b) Titration experiment of the Cy3-Cy5 bifunctional DNA-doubler. When more than 0.5 equivalents of the adjuster strand were added, the Cy3 emission increased, suggesting the formation of oligomers and open clamp species.

Table 3.3 Intra-complex spacing with varying adjuster bridging nucleotides (x) for a Series of DNA-doublers clamps

System	Adjuster (nm)			
	X = 1	3	5	7
“Doubler”	2.85 ± 0.01	3.02 ± 0.01	3.16 ± 0.01	3.28 ± 0.01
Arm = 8 Bases		p = 0.00007		p = 0.0001
Stem = 15 Bases	No adjuster	3.22 ± 0.01		
			p = 0.003	

When more than 0.5 equivalents of adjuster strand was added to the bifunctional DNA-doubler, the Cy3 emission was shown to increase rather than decrease (Figure 3.6b). The fluorescent behavior suggested that at these higher concentrations, adjuster strands hybridized to only one arm of the doubler forming an open clamp, which led to a decrease in FRET emission. Indeed, the presence of additional bands in the PAGE gel of the DNA-doubler clamp system were consistent with the presence of both an open and closed clamp complex (Figure 3.7). As more of the adjuster strand was added, oligomers of DNA-doubler-adjuster complexes were also observed. We attributed the apparent tendency of the DNA-doubler to form both the open and closed clamp to the change in directionality in the adjuster sequence that could cause strain in the close clamp structure. In the future, avoiding open complexes or oligomerization may be possible by minimizing strain in the DNA-doubler-adjuster complex through modification of the adjuster structure.

3.2.2.3 PAGE experiments DNA-doubler clamp formation

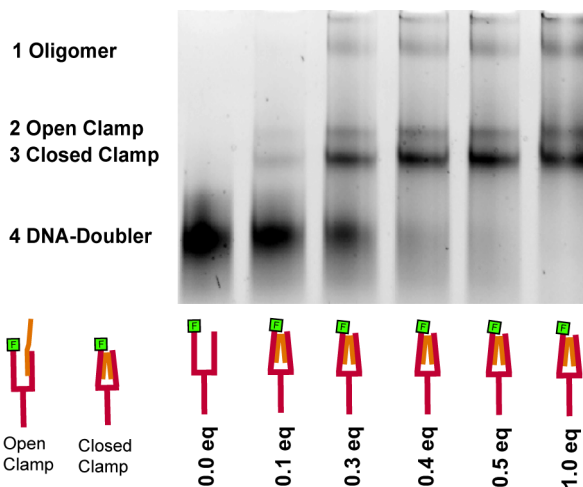


Figure 3.7 Fluorescent image of a non-denaturing PAGE experiment tracking the formation of the DNA-doubler-clamp using Fln-labeled DNA doubler. (*Eq*) refers to the added equivalents of the adjuster strand containing a one-base bridge. As adjuster is added, a new band appears above the original band of the DNA-doubler, which is attributed to the clamp (*Closed Clamp*, shown in part a). Another faint band appears above, which we attributed to an *Open Clamp*, where the adjuster is only hybridized to one arm. Oligomers are also observed. *Conditions*: 1 equiv = 1.3 μ M in buffer (10 mM PBS, pH 7, 0.5 M NaCl).

DNA-doublers PAGE experiments were performed in a similar way to the Y-shaped ones. Just as in the FRET experiments, we titrated a DNA-doubler Fln-labeled solution with different equivalents of the corresponding adjuster. We observed in this case, that the free doubler band faded away when adding about 0.5 equivalents. These results further support our FRET experiments findings, suggesting that the clamp is unstable and leads to open clamps causing oligomerization.

3.2.3 Supramolecular spacing control on GNPs

To demonstrate that the clamp method for tuning label spacing could be applied to DNA-modified nanoparticles, we monitored the change in fluorescence for Y-clamps and DNA-doubler clamps hybridized to DNA-GNPs in the presence of an adjuster strand. In this case the Y-complex and the DNA-doubler were modified with Cy5 and fluorescein, also known

to exhibit FRET. Interestingly, when adjuster was added to the Y-DNA-GNP complex, we observed a steady increase in both fluorescein and Cy5 emission (Figure 3.8a). As the concentration of the adjuster increased to 1.25 equivalents, a plateau was reached. The counterintuitive increase in fluorescein emission upon adding the adjuster strand can be explained by the ability of 13-nm gold nanoparticles to quench fluorescein. We infer from these results that the adjuster hybridized to the Y-complex, rigidifying the DNA and pulling the fluorophores from the gold nanoparticle surface. Therefore, quenching of the fluorescein decreased, and fluorescein emission increased as did FRET emission from the Cy5 (Figure 3.8a). These results qualitatively suggest that the strand termini spacing can also be controlled on the surface of Y-DNA-GNP complexes. Quantitative determination of the spacing, however, is not straightforward owing to the quenching properties of the gold nanoparticles. To overcome this challenge a FRET pair must be identified that is not quenched by gold nanoparticles and is easily incorporated into DNA. Consequently, more work must be done to establish the tunability of label spacing using Y-clamp-GNP conjugates, but this first demonstration is promising.

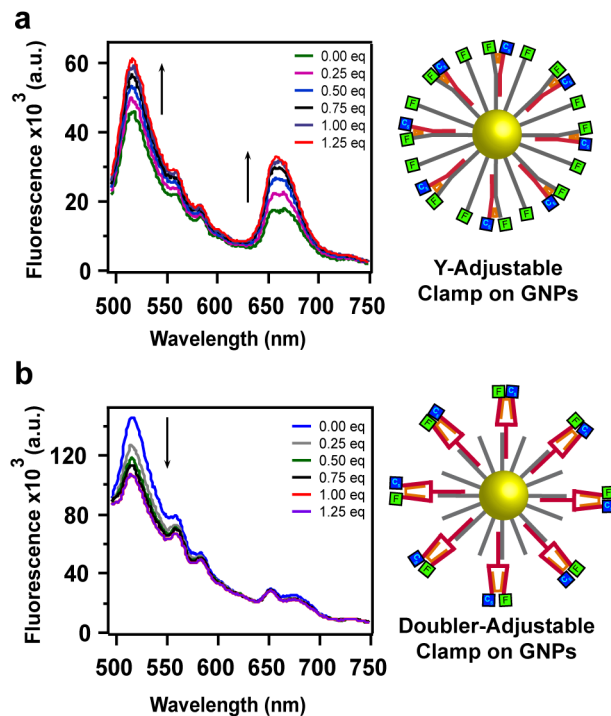


Figure 3.8 Y-clamp and DNA-doubler clamp complexes hybridized to DNA-GNPs. Emission spectra as a function of the amount of adjuster strand for a) Fln and Cy5 labeled Y-DNA-GNP complexes and b) Fln and Cy5 labeled DNA-doubler-GNP complexes. The excitation wavelength was 460 nm, which corresponded to excitation of the Fln donor. Equivalentents refer to the amount of adjuster strand added.

We observed that adding adjuster strands to a suspension of bifunctional DNA-doubler-GNP complexes changed the fluorescent behavior of the modified DNA-GNPs. Upon titration of the DNA-doubler-GNP complex with an adjuster strand, we observed a slight decrease in emission of the fluorescein, yet little change was observed in the Cy5 emission (Figure 3.8b). This lack of FRET emission from the Cy5 could be because the two fluorophores only undergo a small change in distance upon adding the adjuster strand. The resulting amount of energy transfer is significant enough to observe quenching but not significant enough to observe an increase in FRET. The overall lack of FRET in this system, however, suggests that the FRET pairs are not positioned optimally for energy transfer when bifunctional DNA-doublers are attached to the GNP surface. Additionally, within one-day aggregation of the DNA nanoparticles

was also observed, which suggested that opening of the clamp and oligomerization was also a problem for the Doubler-clamp-GNP complexes (Figure 3.10). Once again, modifying the directionality of the adjuster strand might prove useful to avoid oligomerization. Overall, the Y-clamp-GNPs appear to be a better choice for tuning label spacing on nanoparticles than the Doubler-clamp-GNP conjugates.

3.3 Conclusions

Using DNA hybridization we were able to demonstrate control over the spacing of functional groups in DNA adjustable clamp complexes in the absence of nanoparticles. These clamps should prove useful in bivalent targeting of cells, but more work is required to quantify their effects on label spacing when these clamps are incorporated into DNA-modified GNPs. As strategies are developed for controlling the ratio, density and spacing of multifunctional groups on DNA materials, we anticipate that new applications will emerge, particularly in the area of heterovalent targeting in nanomedicine but also in the construction of molecular electronics and light-harvesting materials using highly functional DNA architectures.

3.4 Materials and methods

3.4.1 FRET experiments

The FRET experiments to determine the intra-complex distance (FRET pair distance) were performed on a PTI MP1 SER# 1621 fluorometer. Instrument settings using Cy3 as the donor fluorophore: excitation λ at 525 nm, emission and excitation bandwidth = 4 nm, number of reads = 3, integration = 0.1 s, steps = 1 nm, scan 535-800 nm. Instrument settings using FlIn as the donor fluorophore: excitation λ at 460 nm, emission and excitation bandwidth = 6 nm (for Y-complex) and 8 nm (for DNA-doublers), number of reads = 3, integration = 0.1 s, steps = 1 nm, scan 495-750 nm.

Each FRET titration was performed twice. For each titration experiment, the intra-complex distance was calculated as described below. The reported value is the average value and the error is the standard deviation.

FRET experiments for the Clamps *not bound to the GNPs*: a hybridization mixture of the adjuster strand and the corresponding Cy3-modified strand (1.3 μM each) containing both an *arm* and *stem* sequence was made in buffer (485 μL , 0.5 NaCl 0.1 M PBS pH = 7.00) and allowed to sit for 15 minutes. The fluorescent emission spectrum was measured from 535-800 nm, with excitation of the Cy3 fluorophore at 525 nm. Next, aliquots (~ 0.1 equivalent/ μL) of the Cy5-modified strand complementary to the stem sequence of the Cy3-strand were added in various amounts from 0.1 – 3 equivalents. After each addition of the Cy5-modified strand the solution was allowed to sit for a couple of minutes and an emission scan was acquired. For the *DNA-Doubler-Clamps*, a solution of the Cy3-Cy5 bifunctional DNA doubler (1.3 μM) was made in buffer (485 μL , 0.5 NaCl 0.1 M PBS pH = 7.00), and an emission spectrum was measured. To this solution, aliquots of the adjuster strand (~ 0.1 equivalent/ μL) were added in various amounts from 0.1 – 3 equivalents. After each addition of the adjuster strand an emission scan was acquired.

Calculating FRET Distances: distance calculations were obtained using the following relations:

$$E = \frac{1}{1 + \left(\frac{r}{R_0}\right)^6} \quad (1)$$

and

$$E = 1 - \frac{I'_d}{I_d} \quad (2)$$

where E is the energy variation with the change of distance between donor and acceptor fluorophore, R_0 is the distance at which energy transfer is 50% efficient ($R_0 = 54 \text{ \AA}$ Förster radius for Cy3/Cy5 pair)¹³² and r is the separation of fluorophores in \AA . I_d is the donor fluorescence intensity after the addition of 3 equivalents of acceptor (or 0.5 equivalents of adjuster for the DNA-doubler experiment) and I_d is the donor intensity without acceptor.¹³² Each experiment was performed three times to obtain an average value, the standard deviation of this mean was used as the error. The t values and degrees of freedom for the experiments described were calculated using the t test for populations with different standard deviations,¹¹⁷ p-values were derived using a web based p-value calculator.¹¹⁸

FRET experiments for the DNA adjustable clamps on the GNPs: For the *Y-Clamp modified GNPs*, a 0.25 μM suspension of Y-DNA-GNPs with respect to Cy5 was prepared in buffer (Table 2.1, sequences 2.7-I,II and Table 3.4, 3.1_s-III₁). We assumed 80 Cy5 strands per GNP based on the fluorescent data (see Figure 2.7). After acquiring an emission scan with fluorescein excitation at 460 nm, to this suspension was added aliquots of a solution containing the adjuster strand (~0.1 equivalent in 1 μL) until 3 equivalents had been reached. After the addition of each aliquot, the solution was allowed to hybridize for a few minutes and then an emission scan was measured. For the *DNA-doubler-clamp modified GNPs*, a 0.10- μM suspension of DNA-Doubler-GNPs with respect to Cy5 was prepared in buffer (Table 3.4, sequences 3.8b-I and 3.5a-II₁). We assumed 40 Cy5 strands per GNP based on the fluorescent results (see Figure 2.5b and 2.6b). These suspensions were also titrated by adding aliquots of the adjuster solution containing 0.1 equivalent in 1 μL until 3 equivalents of adjuster were reached.

3.4.2 PAGE experiments

We prepared DNA solutions of the clamp components using one fluorescently labelled strand of the Y-complex or a fluorescently labelled DNA-doubler (1.3 μ M per equivalent) in TAEMg buffer (40 mM Tris, 2 mM EDTA \cdot 2Na \cdot 2H₂O, 12.5 mM MgCl₂ \cdot H₂O, 20 mM acetic acid, pH = 7.5). For the Y-complex experiments, 0 or 1 equivalent of adjuster strand was used. The sample was then heated up to 50 °C for 1 minute and cooled down to room temperature and allowed to sit overnight.

Before running the gel, the samples were cooled down to 4 °C for 30 minutes. PAGE was performed at 4 °C using TAEMg as a running buffer and 120 V. The gels were imaged and the band intensities quantified using ImageQuant RT ECL imager from GE Healthcare Life Science using UV transillumination.

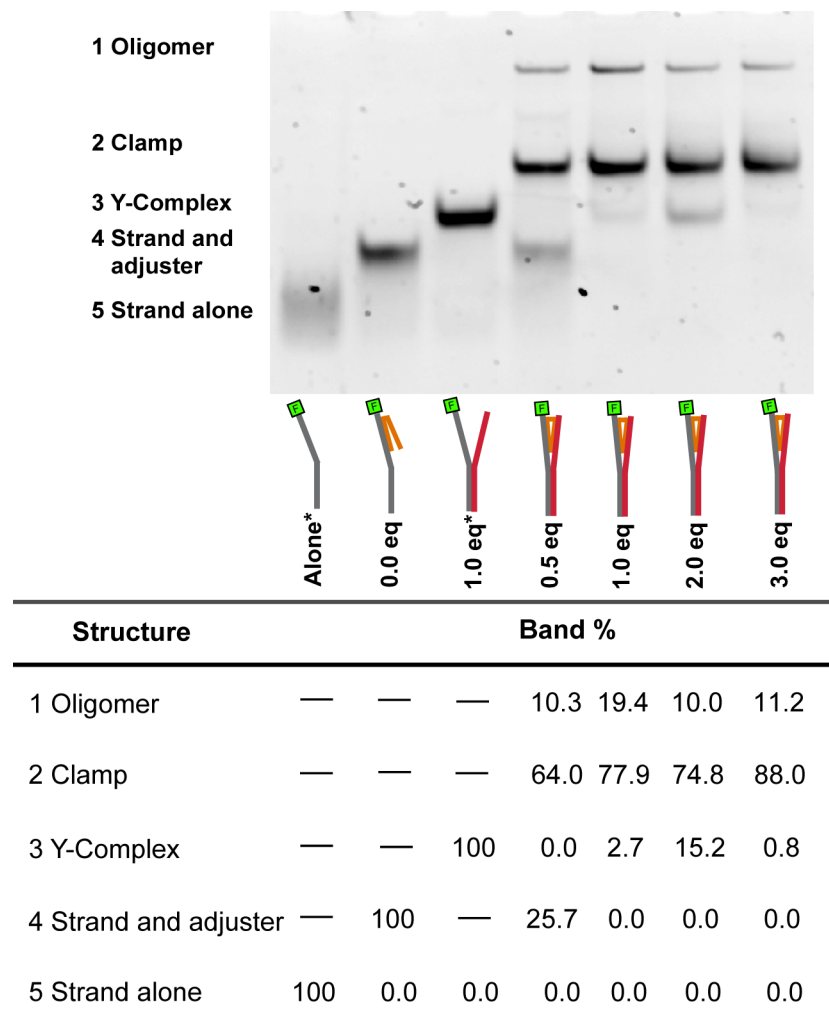


Figure 3.9 Fluorescent image of a non-denaturing polyacrylamide gel electrophoresis experiment tracking the formation of the Y-clamp. The Y-complex contains a Fln-labeled strand and an unlabeled strand, and the adjuster strand contains a 3-base bridge. (Eq) refers to the added equivalents of the unlabeled Y-complex strand and (*) indicates that no adjuster strand is present. A band corresponding to the DNA-adjustable clamp (Clamp) is the dominant species when the adjuster and both Y-complex strands are present. Oligomers are also observed (top band) but they make up only 10-20% of the complexes. *Table:* the percent intensity of each band, which corresponds to the relative amounts of each structure. *Experimental conditions unless noted:* 1 equivalent Fln-labeled Y-complex strand (1.3 μ M), 1 equivalent adjuster strand (1.3 μ M), varying equivalents of unlabeled Y-complex strand (0 – 3.9 μ M); 15% polyacrylamide gel, TAEMg running buffer, 4°C, 120 V.

3.4.3 Agregation experiments

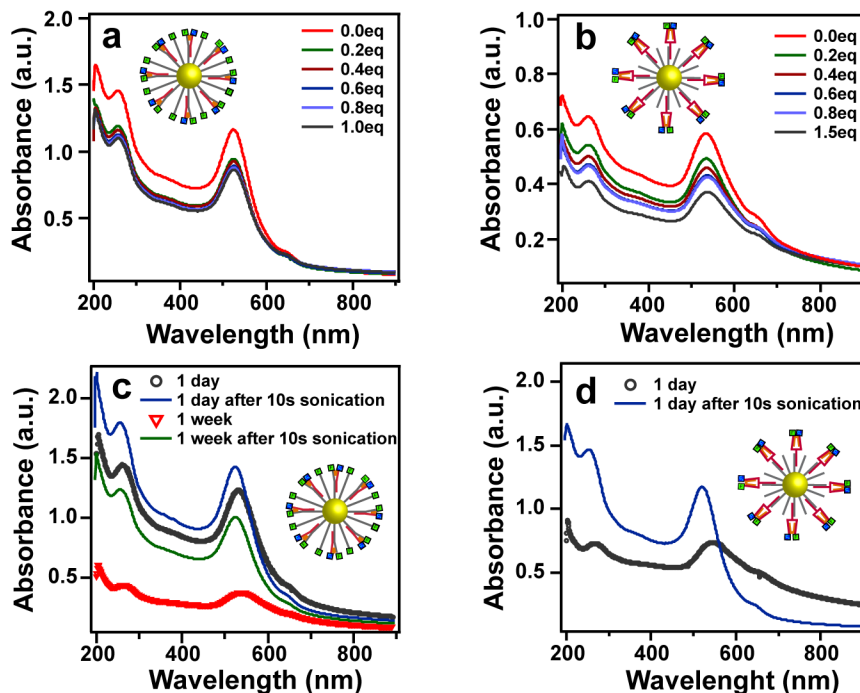


Figure 3.10 UV-vis absorbance spectra for Clamp-GNP complexes. a) Absorbance as a function of equivalents of the adjuster strand added to the Y-DNA-GNPs. b) Absorbance as a function of equivalents of the adjuster strand added to the DNA-doubler-GNPs. c) UV-vis absorbance of the Y-Clamps on GNPs after standing for one day (grey circles) and after sonicating the suspension (blue line) showing the redispersion of the particles; (red circles) are the same GNPs after standing for a week and then after sonication (green line). d) UV-vis absorbance of the doubler-clamp on GNPs after standing for one (grey circles) circles and after redispersion by sonicating 10 seconds (blue line). The experiments of a and b are different batches than those corresponding to c and d.

3.4.4 Sequences

Table 3.4 DNA sequences corresponding to DNA structures described in Figures 3.1, 3.3, 3.4, 3.5, 3.7 and 3.8.

Figure	Sequence
3.1 ^a _s	I 5'-Cy3-AGA GTC CAT TTT TTT TTT AAA A-3'
	II 5'-TTT TTA AAA AAA AAA CAC CTG CT-Cy5-Phos-3'
	III₁ 5'-TGG ACT CTT AGC AGG TG-3'
	III₃ 5'-TGG ACT CTA TGA GCA GGT G-3'
	III₅ 5'-TGG ACT CTA TGT AAG CAG GTG-3'
	III₇ 5'-TGG ACT CTG ATG TAG AGC AGG TG-3'
	3.1 ^a _m
II 5'-TTT TTA AAA AAA AAA CAC CTT TTT GCT-Cy5-Phos-3'	
III₁ 5'-TGG AAA AAC TCT GAG CAA AAA GGT G-3'	
III₅ 5'-TGG AAA AAC TCT ATG TAA GCA AAA AGG TG-3'	
III₉ 5'-TGG AAA AAC TCT TGA TGT AGT AGC AAA AAG GTG-3'	
III₁₃ 5'-TGG AAA AAC TCT CCT GAT GTA GTC CAG CAA AAA GGT G-3'	
3.3 ^a ₇	
	II 5'-TTT TTA AAA AAA AAA CAC CTG CTT TGC CAG TTC TC-Cy5-Phos-3'
	III₁ 5'-TGG ACT CTT GTA AAG CAG GTG-3'
	III_u 5'-TGC CAG ACA ATG AGA ACT GGC-3'
	III_r 5'-TGG ACT CTT GTG CCA GAC AAT GAG AAC TGG CAA -AGC AGG TG-3'
3.4	I 5'-Flu-AGA GTC CAT TTT TTT TTT AAA A-3'
	II 5'-TTT TTA AAA AAA AAA CAC CTG CTT-3'
3.5	I [5'-Cy3-CCT TAT TGA GAC- to doubler (arm 1) 5'-Cy5-CCT TAT TGA GAC- to doubler (arm 2) Doubler-TTT TTT TTT T-3' (stem)]
	II 5'-GAA TAA CTC TGT-3'-G [*] T [*] C [*] T [*] C [*] A [*] A [*] T [*] A [*] A [*] G [*] -Phos-5'
3.5 ^b ₁	II 5'-GAA TAA CTC TGT TT-3'-G [*] T [*] C [*] T [*] C [*] A [*] A [*] T [*] A [*] A [*] G [*] -Phos-5'
3.5 ^b ₃	II 5'-GAA TAA CTC TGT TTT T-3'-G [*] T [*] C [*] T [*] C [*] A [*] A [*] T [*] A [*] A [*] G [*] -Phos-5'
3.5 ^b ₅	II 5'-GAA TAA CTC TGT TTT TTT T-3'-G [*] T [*] C [*] T [*] C [*] A [*] A [*] T [*] A [*] A [*] G [*] -Phos-5'
3.7	I [5'-AGA GTT ATT CC- to doubler (arm 1) 5'-Flu-TCG TTA TTC AC- to doubler (arm 2) -Doubler-GTC GGC CGA AAA AT-3' (stem)]
	I [5'-Flu-CAG AGT TAT TCC- to doubler (arm 1) 5'-Cy5-CAG AGT TAT TCC- to doubler (arm 2) Doubler-GTC GGC CGA AAA AT-3' (stem)]

^a Y-complexes with arm lengths of 8, 12, 20 bases, corresponding to *s*, *m*, and *l*, respectively. Adjuster strands for Y-complex with bridge lengths of 1, 3, 5, 7, 9, 13 bases, corresponding to III₁₋₁₃, respectively. For figure 5, III_u, III_l, III_r corresponds to the lower, upper and full adjuster, respectively. ^b Adjuster strand for DNA-doubler synthesized with bridge lengths of 1, 3, 5, 7 bases, corresponding to b_{1-b7}, respectively. * "Backward bases" (3'-DMT-protected, 5'-phosphoramidite nucleotides) were used on the DNA synthesizer to change the direction midway through the sequence. Phos = Phosphate.

Chapter 4 Sharpening the thermal release of DNA from GNPs: towards a sequential release strategy ³

³The research involving sharpening the thermal release of DNA from GNPs: towards a sequential release strategy described in this chapter was published on line in J.A. Díaz and J.M. Gibbs-Davis, *Small*, 2013, in press.

4.1 Introduction

Modern medicine has developed strategies for treating severe illnesses by administering multiple drugs in time-dose-combination specific regimens. These regimens have several benefits over conventional treatments, such as increase in life expectancy and reduction of side effects.^{133, 134} They can be divided into two therapeutic approaches: combination therapy and sequential therapy. In combination therapy, several agents that act synergistically are administered simultaneously—but such an approach often requires low dose amounts to minimize the toxic effects of the combined drugs.¹³³ Sequential therapy involves the successive administration of one or multiple therapeutic agents to sensitize targeted cells to subsequently administered drugs¹³⁵ or to minimize the side effects of potent medications while maximizing their therapeutic effect.^{133, 136} Critical diseases including cancer, HIV and malaria have found improved treatments using approaches such as these.^{91, 133, 134, 137} Due to their multifunctional nature, nanomedicine systems qualify for these therapies, because all acting agents will be at the targeted site in a given time. Yet, strategies for separately controlling the release of different reagents from the same nanostructure are required to make sequential therapies feasible at the nanometer scale.

To incorporate multiple functions and means to selectively release therapeutic agents, researchers often combine well-defined inorganic nanostructures with biomolecules to achieve targeting or stimuli-responsive behavior. For example, DNA-modified gold nanomaterials are widely studied due to the ease of their synthesis and their unique optical, therapeutic, and recognition properties.^{42, 138, 139} Nucleic acids in these systems may play multiple roles acting as a therapeutic agent,^{140, 141} a modifiable component for introducing multiple functions, and an active constituent of the release mechanism.¹⁴² To illustrate the former, interfering oligonucleotide sequences have been introduced that prevent

the expression of specific genes, leading to the destruction of the diseased cell.^{138, 139} Regarding the second, researchers have capitalized on well-established synthetic strategies to modify oligonucleotides with different modifications, one of which binds the strand to the inorganic scaffold, while the other incorporates a functional group like a drug. For example using cis-platin modified oligonucleotides as “warheads” to attack cancer cells, DNA-modified gold nanoparticles have exhibited much greater potency than cis-platin alone.²⁴ Finally, researches have utilized the molecular recognition properties of DNA to introduce therapeutic or imaging agents onto nanostructures by DNA hybridization rather than covalent attachment.¹⁴³ Due to the reversible nature of the resulting DNA duplex, controlled release becomes possible through modulation of the local temperature around the nanoparticle.

Indeed, several investigations have focused their attention on the externally controlled release of oligonucleotides from different types of structures including gold nanorods,^{91, 144, 145} gold nanoparticles (GNPs),¹⁴⁶ silica-gold nanoshells,^{138, 145} and gold nanoprisms¹⁴⁷ based on photothermal modulation. All of these examples take advantage of the heat generated by gold nanostructures when they are laser-irradiated at specific wavelengths that excite surface plasmons, which in turn promotes dehybridization of the nucleic acids or breakage of the Au-S bond. For instance, Lee and co-workers interfered gene expression in a single cell using a nanoplasmonic carrier-based optical switch, allowing the release of the oligonucleotide payload at specific times and locations.¹⁴⁴ This method provides not only remote activation of the nanostructures but also optical tunability due to the different plasmon absorption frequencies that arise from distinct shapes, sizes, and compositions.¹³⁹

To incorporate the benefits of combination, and particularly sequential therapies, into one drug delivery vehicle, mechanisms that independently control the release of separate therapeutic agents are essential.⁹¹ Hamad-

Schifferli and colleagues demonstrated one such approach to sequential release based on plasmon excitation. By taking advantage of the different excitation wavelengths of “nanobones” and “nanocapsules,” they selectively released two different types of oligonucleotides upon thermally melting the corresponding gold nanostructure.⁹¹ More recently, Lee and co-workers have developed a photonic gene circuit using two nanoantennae with different excitation frequencies.¹⁴⁸ However, there are two disadvantages to this approach to sequential therapy. First, both nano-agents would have to be localized on the same cell, which would be difficult to achieve even with targeting strategies. Second, most nanostructures with plasmon resonances in the water window exhibit overlapping absorbance profiles, which complicates the selection of specific excitation wavelengths.^{148, 149} Consequently, achieving a high degree of selectivity by excitation of different nanostructures remains a challenge.

An alternative route that avoids both of these issues involves releasing two hybridized agents from the same structure based on different thermal stabilities of each duplex-modified agent. However, achieving independent and sequential release using thermal dissociation requires that each agent exhibits very distinct temperature-dependent behavior. Unfortunately, the usual broad range of temperatures needed to dehybridize nucleic acids limits a strand-by-strand dissociation strategy because the release of one strand will be contaminated by the other even if the stability of the two corresponding duplexes differed substantially. To overcome this problem and increase selectivity, DNA agents that exhibit very narrow, or sharp, melting transitions are desired. Such sharp melting should allow all of one agent to be released over a narrow temperature range without liberating the next strand. Although sharp melting transitions are a hallmark of DNA-modified gold nanoparticles (DNA-GNP) hybridized into aggregate

structures,⁷¹ such transitions have never before been observed in colloidal DNA-GNP systems despite their applicability in phototherapy.

The sharp DNA melting phenomenon first observed in DNA-GNP aggregates, and now reported in several aggregated nanomaterials,^{71, 150-155} is generally attributed to the multivalent rigid structure of the nanomaterial and the high density of DNA resulting when they assemble into DNA-linked aggregates. As a consequence of the dense local environment, cooperative interactions occur between DNA duplexes parallel and close to one another (< 5 nm).¹⁵⁰ The specific origin of this cooperativity involves the condensed cation cloud associated with each negatively charged duplex. When one of the interacting duplexes dissociates some of the condensed cations are released to solution, decreasing the local cation concentration, and leading to a melting cascade.⁷¹ Recently Nguyen, Schatz, and co-workers^{72, 156, 157} and the Sleiman group¹⁵⁸ have studied several DNA-small molecule systems that have the ability to form caged dimers resulting in two or three neighboring DNA duplexes. They discovered that all the caged dimers displayed sharpened melting transitions despite the lack of aggregate.^{72, 156, 157} We hypothesized that similar behavior would result using DNA-modified GNPs to complete the cage because of the high density of oligonucleotides on the gold nanoparticle surface. Such cage assemblies formed on the surface of gold nanoparticles should exhibit sharper melting, thereby permitting the sequential release of several strands without cross contamination due to overlapping melting transitions. Herein, we demonstrate how branched DNA, referred to as DNA-doublers, exhibit sharper melting transitions than linear DNA when hybridized to complementary DNA-GNPs. We also compare two strategies for varying the sequence of the DNA-doublers that allow us to control the melting temperature (T_m) while maintaining the sharpness. Finally, we show how a system composed of two DNA-doubler strands with different melting

temperatures leads to sequential, selective release behavior. Our strategy has promise in photothermal therapies based on the selective dehybridization of several strands by remotely increasing the temperature of the gold nanostructures via plasmonic excitation.^{145, 146, 159, 160} Furthermore, this approach could find application in systems like DNA-liposome or DNA-polymer hybrids using exposure to radio frequencies (RF),^{161, 162} magnetic fields,^{163, 164} or high intensity focused ultra sound (HIFU)¹⁶⁵⁻¹⁶⁸ to induce localized hyperthermia. Finally, introducing cooperativity into DNA complexes formed on colloidal nanoparticles provides insights into general methods for tuning molecular recognition in nanomaterials, and consequently our approach could be useful in other applications involving smart DNA-based materials like molecular machines and functional assemblies.¹⁴²

4.2 Results and discussion

4.2.1 System design

To determine whether sharp melting of DNA from the surface of gold nanoparticles could be induced by cooperative interactions in branched DNA structures, we compared the melting behavior of linear, single-stranded DNA (ss) and DNA–doublers (DT_x) from the surface of gold nanoparticles modified with complementary linear DNA or DNA–doubler constructs (ss-GNP and DT_x -GNP, respectively). Figure 4.1 depicts all of the hybridization combinations evaluated in our investigation. To monitor the dissociation behavior of these hybridization mixtures, 13-nm GNPs were first functionalized with either thiolated DNA–doublers or single-stranded DNA of the analogous sequence from commercially available phosphoramidites (Figure 4.9). Complementary DNA–doublers or single-stranded DNA containing a fluorescein label were also prepared (Figure 4.9). Owing to the ability of 13-nm GNPs to quench the emission of fluorescein, fluorescence was used to monitor the thermal dissociation in

which an increase in signal indicated that the fluorescein-labeled complement had dissociated from the GNP-bound surface strand. Each hybridization mixture consisted of ss-GNPs or DT_x-GNPs and complementary DNA (ss or DT_x), resulting in a final concentration of 6 nM for both the nanoparticles and the complementary agent (0.3 M NaCl, 10 mM PBS, 0.01% SDS buffer). After hybridization overnight, the fluorescence of the colloidal hybridization mixture was monitored at 520 nm using an excitation wavelength of 480 nm, as it was heated with a Peltier temperature controller using a temperature ramp from 20 °C to 74 °C at increments of 2 °C, allowing equilibration for 5 minutes between each measurement (Figure 4.2). To analyze the influence of strain from the DNA-doubler on the molecular recognition behavior, we added two or four thymidines between the complementary sequence and the branching site in each arm (DT_x; x = 2 or 4, respectively).

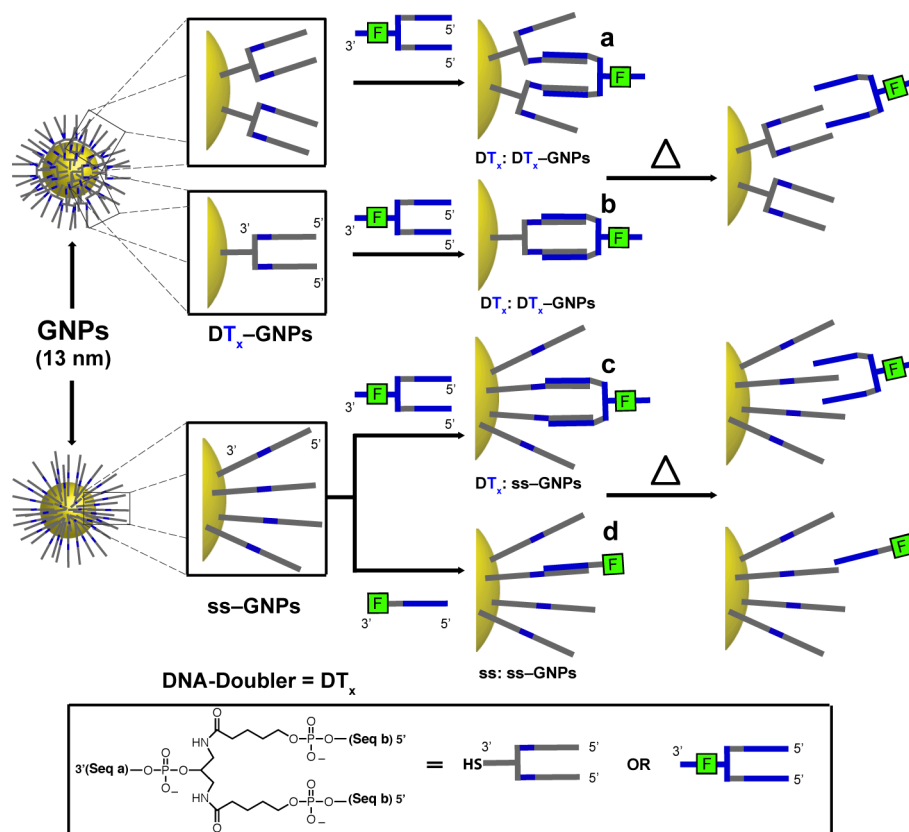


Figure 4.1 Schematic representations of hybridization combinations consisting of DNA-doublers (DT_x) and single-stranded DNA (ss) with DNA-doubler or single-strand Modified GNPs.

4.2.2 Melting behavior

Figure 4.2 illustrates the melting behavior of the hybridization mixtures explored. To begin, we compared the melting behavior of the ss:ss-GNP complex with that of the analogous free duplex (ss:ss, Figure 4.2a). The melting temperature at which half the duplexes had dissociated (T_m) was higher by 3.4 °C for the ss:ss-GNP hybrid compared with the free ss:ss duplex (Figures 4.2a and b). This enhancement in stability for DNA hybridized to GNP surfaces, as indicated by the increase in T_m , has been previously observed and attributed to the high-density of DNA on the nanoparticle surface.¹⁶⁹ Next, to quantify the sharpness of these transitions we measured the full width half maximum (FWHM) of the first derivative of the melting profile. The FWHM for the dissociation of the free

duplex was 11.5 ± 0.3 °C (ss:ss, Figure 4.2b). In contrast, the ss:ss-GNP hybrid exhibited a FWHM of 10.3 ± 0.2 °C, which indicated that the high-density of DNA on the nanoparticle surface led to a slightly more cooperative transition.

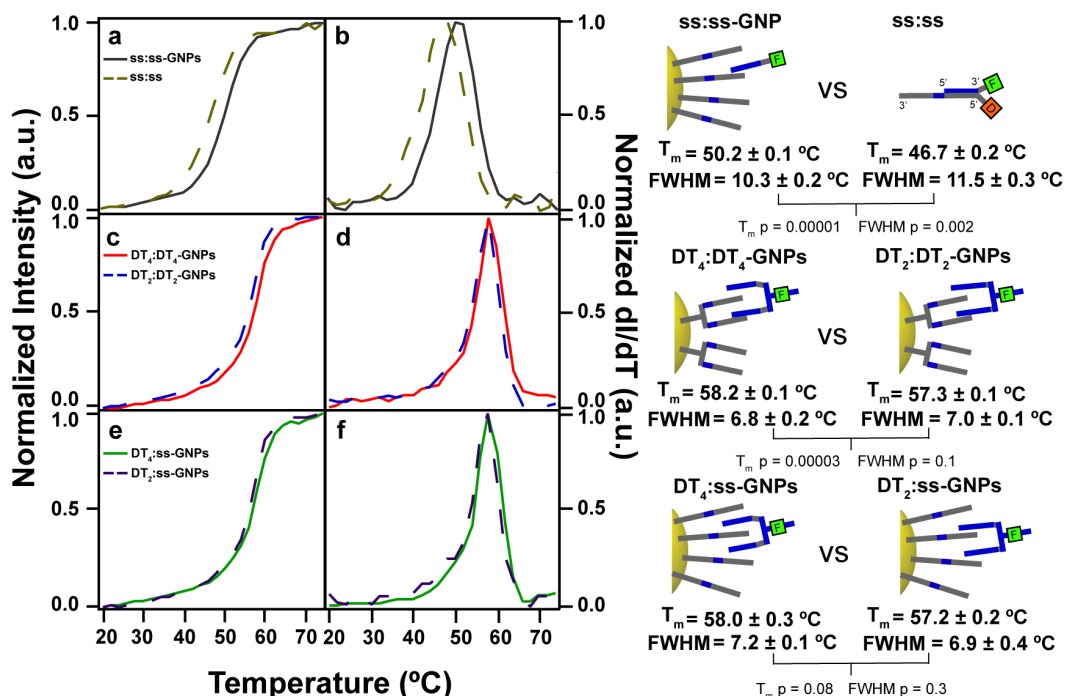


Figure 4.2 Melting profiles determined from the change in fluorescent intensity at 520 nm with temperature and the corresponding melting temperatures (T_m) and full-width half maximum values of the first derivatives (FWHM). a) The melting profiles of single-stranded DNA hybridized with: single-strand modified GNPs (ss:ss-GNP, black line) or a dabcyll-modified complementary strand (ss:ss, dashed line). b) The normalized first derivatives of the melting profiles in part A illustrating the sharpness of the transition. c) The melting profiles and d) respective normalized first derivatives of: DNA–doublers hybridized with complementary DNA–doubler modified GNPs containing a T_4 bridging spacer ($DT_4:DT_4$ -GNP, solid line) or a T_2 bridging spacer ($DT_2:DT_2$ -GNP, dashed line). e) The melting transitions and f) respective normalized first derivatives: of single-strand modified GNPs hybridized with DNA–doublers with T_4 ($DT_4:ss$ -GNP, solid line) or T_2 ($DT_2:ss$ -GNP, dashed line) bridging spacers.

To determine the influence of the cage structure on nanoparticle-bound DNA complexes, we next examined the hybridization behavior of DNA–doublers (DT_2 and DT_4) hybridized with DT_x -GNP or ss-GNP (Figure 4.2c

and 4.2e, respectively). When either DT₂ or DT₄ was hybridized to the corresponding DT_x-GNP, the sharpness increased significantly related to the ss:ss-GNP experiment as illustrated by the smaller FWHM of 6.8 ± 0.2 °C for the DT₄ case (Figure 4.2d). The DNA-doubler with a shorter thymidine bridge, DT₂, showed very similar behavior in both melting temperature and FWHM. Interestingly, when DNA-doublers were hybridized to single-strand modified GNPs (DT_x:ss-GNP), we found that they were also quite sharp exhibiting behavior similar to that of the DT_x:DT_x-GNP systems (Figure 4.2f). Specifically, our experiments indicated that the FWHMs for the DT_x:ss-GNPs were 7.2 ± 0.1) °C and 6.9 ± 0.4 °C for the T₄ and T₂ spaced cases, respectively, which are very close to the FWHM values observed for the DT_x:DT_x-GNPs system. These results supported our initial hypothesis that sharper melting could be achieved from the GNP surface using branched DNA-doublers capable of cooperative interactions. Moreover, the success of the DT_x:ss-GNP system indicated that the nanoparticle surface possessed a great enough DNA density to facilitate cooperative interactions without needing the corresponding DNA-doubler to form the caged complex.

Overall, utilizing DNA-doublers instead of linear single-stranded DNA led to a decrease in FWHM of approximately 3 °C and 5 °C compared with the ss:ss-GNP and ss:ss complexes, respectively. In addition to increasing the sharpness of the transition, the T_m values also were significantly higher for the DT_x complexes formed on the GNP surface. For example, DT₄:DT₄-GNP and DT₄:ss-GNP exhibited an increase in T_m of 8 °C compared with the ss:ss-GNP complex (Figure 4.2). This increase in melting temperature has been observed for the caged small molecule DNA hybrid (SMDH) dimers of Schatz and Nguyen,⁷² and more recently Sleiman,¹⁵⁸ but the maximum increase observed for caged dimers linked by two DNA duplexes in similar buffer conditions was 4 °C.⁷² It appears the increase in stability manifested by the increase in T_m is more

significant for the GNP system when compared with the SMDH system, but such enhancement could stem from differences in the sequences explored or the structure of the branching site.

In Figure 4.1a and b, we proposed two ways as to how the DNA–doublers could interact with the DNA–doublers on the surface of the gold nanoparticles. The first case represents indiscriminate binding, where the DNA–doubler hybridizes with the arms of two different doublers bound to the GNP (Figure 4.1a). In the second case the DNA–doubler forms a complex with a single DNA–doubler on the GNP (Figure 4.1b). The small differences in the T_m and sharpness between the $DT_x:DT_x$ -GNP and $DT_x:ss$ -GNP systems led us to conclude that hybridization did not necessarily occur in a discriminatory fashion between one DT_x in solution and one on the nanoparticle surface. Consequently, we reasoned that the $DT_x:DT_x$ -GNP and $DT_x:ss$ -GNP systems resulted in similar geometries and extents of cooperativity most likely through hybridization with neighboring DNA–doublers on the GNP surface (Figure 4.1a). Regardless of the origin of the similarity between the $DT_x:DT_x$ -GNP and $DT_x:ss$ -GNP systems, the sharp melting exhibited by the $DT_x:ss$ -GNP hybridization mixtures indicated that gold nanoparticles suffice as a template to hold the neighboring strands in the correct position to enable optimal interaction with the DNA–doubler (*vide supra*). In contrast, DNA–doublers hybridized to two complementary single-strands exhibited very broad melting transitions, even broader than free DNA duplexes, with a FWHM value of 26 ± 3 °C (Figure 4.3). We infer from this result that the DNA doublers are flexible enough to prevent cooperative interactions between the neighboring duplexes when hybridized with two free strands. These transitions are even broader than that of single-stranded DNA hybridized with GNPs,¹⁶⁹ which indicates that the free DNA: DT_4 complex is flexible enough to form an extended structure where no neighboring interactions are possible between the duplexes. In contrast, the ability of DNA–

doublers to form cooperative structures with single strands tethered to the gold nanoparticles is quite remarkable and provides further evidence that rigid structures that promote a parallel arrangement of neighboring duplexes facilitate cooperativity.^{71, 150-155} Finally, achieving cooperative interactions using DNA-doublers hybridized with standard DNA-functionalized gold nanoparticles is advantageous as the functionalization of gold nanoparticles with DNA-doublers may be avoided, thereby decreasing the cost of DNA-GNP synthesis.

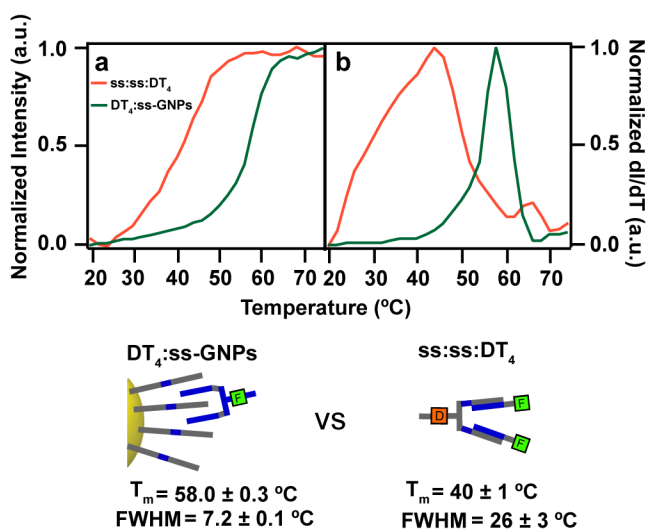


Figure 4.3 a) Melting profiles determined from the change in fluorescent intensity at 520 nm with temperature and b) the corresponding normalized first derivatives of: two single strands hybridized with dabcyl-modified doubler (ss:ss:DT₄, light gray line) and a DNA-doubler hybridized with ss-GNP (DT₄:ss-GNP, black line).

Depending on the DNA-doubler flexibility one could imagine that DNA-doublers could extend their arms and aggregate neighboring GNP-DNA rather than hybridize both arms with one GNP. At the concentrations we worked with, however, we never observed a color change from red to purple, which is indicative of aggregation, upon combining DNA-doublers with either ss-GNP or DT_x-GNP. Furthermore, when the temperature was increased while monitoring the GNP surface plasmon absorption band at 525 nm, no obvious change in the absorption maximum wavelength or intensity was observed that could be attributed to the formation of clusters

(see Figures 4.13 and 4.14). This suggested that the majority of the hybridization-dehybridization events were coming from the proposed caged constructs shown in Figure 4.1.

4.2.3 Controlling melting temperature while maintaining sharpness

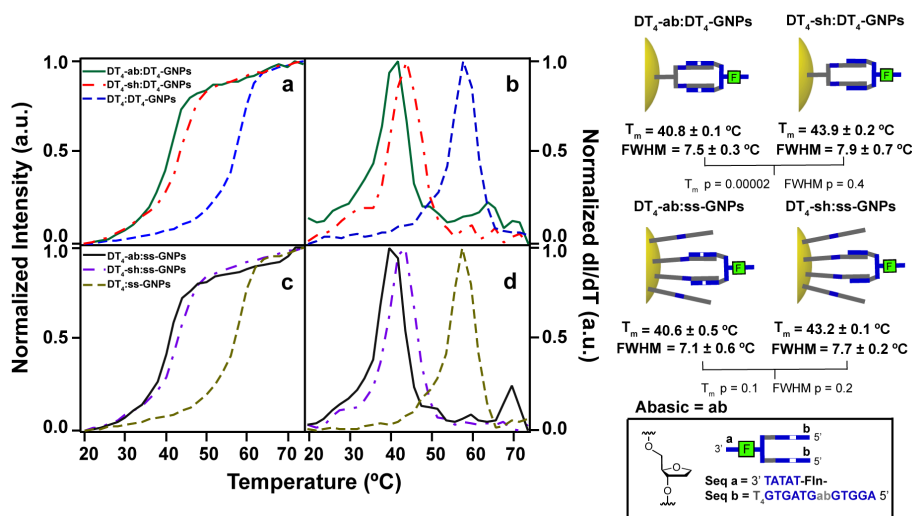


Figure 4.4 Melting profiles determined from the change in fluorescent intensity at 520 nm of destabilized DNA–doublers hybridized with nanoparticles and their corresponding thermodynamic parameters. a) Melting profiles and b) the corresponding normalized first derivatives of DNA–doubler modified GNPs hybridized with the perfect DNA–doubler (DT₄:DT₄-GNPs, dashed line), the destabilized DNA–doubler containing an abasic group (DT₄-ab:DT₄-GNPs, solid line) or a shortened sequence (DT₄-sh:DT₄-GNPs, dot-dashed line). c) Melting profiles and d) the corresponding normalized first derivatives of single-strand modified GNPs hybridized with: the perfect DNA–doubler (DT₄:ss-GNPs, dashed), the abasic-modified doubler (DT₄-ab:ss-GNPs, solid line) or the truncated doubler (DT₄-sh:ss-GNPs, dot-dashed line).

After establishing that DNA–doublers exhibited sharp dissociations from nanoparticle surfaces, our objective was to use these constructs to find routes for the sequential release of different strands by forming multiple cooperative surface structures that had distinct thermal stabilities. Consequently, one agent attached to one DNA construct could be released exclusively with no release of another therapeutic agent, which is the necessary first step to develop sequential therapies using

multifunctional DNA-modified GNPs. To achieve this end, we explored ways in which the T_m of the DNA–doubler complexes could be decreased without loss of sharpness so that the stability of different strands on the GNPs could be tuned without sacrificing the thermal discrimination afforded by the sharp melting.

It is known that the sharpness of double-stranded DNA melting decreases as the length of the duplex decreases.¹⁷⁰ Based on this intrinsic property of DNA and the decrease in shared ion cloud between neighboring strands as the strand length decreases,⁷¹ we hypothesized that shortening the DNA–doubler would not lead to optimal cooperativity in the DT_x :ss-GNP system. In contrast, the introduction of a model abasic site known to decrease the T_m ¹⁷¹ was not expected to affect the sharpness of the transition as the presence of an abasic removes base pair interactions but should leave the ion cloud length intact. To test our hypothesis, we synthesized two new fluorescently labeled DNA-doublers. The design of one doubler consisted of the same sequence used for the DT_4 case explored in Figures 4.2c and 4.2e, but an abasic group was substituted for a deoxyguanosine unit (Figure 4.9, DT_4 -ab). The second doubler design consisted of a truncated sequence of DT_4 by removing three bases at the 5' end, thus decreasing the melting temperature of the resulting complex and possibly the sharpness (Figure 4.9, DT_4 -sh).

We ran similar melting experiments between these DNA–doublers and DT_4 -GNP or ss-GNP as discussed previously. As shown in Figure 4.4a-b, the presence of the abasic group led to a T_m of 40.8 ± 0.1 °C for the DT_4 -ab: DT_4 -GNP system, which was ~ 17 °C less than that of the corresponding DT_4 : DT_4 -GNP hybrid. The truncated system also exhibited a decreased T_m (43.9 °C, DT_4 -sh: DT_4 -GNP) although it was higher than the abasic system by 2 °C. The sharpness of the melting profiles corresponding to the abasic and truncated DNA–doublers were similar exhibiting FWHM values of 7.5 ± 0.3 °C and 7.9 ± 0.7 °C ($p = 0.4$),

respectively, which were slightly greater than that of the DT₄:DT₄-GNP profile (6.8 ± 0.2 °C, $p = 0.02$ and $p = 0.08$ respectively, Figure 4.2c-d). The effect of the abasic group in the DT₄-ab:ss-GNP system was especially promising, since the removal of only one base pair interaction caused a decrease in T_m of almost 18 °C without decreasing the sharpness of the thermal transition. Moreover, the abasic-modified doubler showed a trend towards a sharper transition than the truncated DNA-doubler (DT₄-sh) when hybridized to ss-GNPs, even though the statistical significance of this difference is small ($p = 0.2$), it still suggests a relationship between the length of the DNA sequence and its ion cloud and the extent of cooperativity as illustrated by the sharpness of the dissociation curve. This trend was also supported by the off-particles experiments, as shown in Figure 4.5, which had more statistical significance ($p = 0.000006$) than the on-particle experiments, demonstrating that the abasic groups can find potential application as a destabilizing group to fine-tune the T_m while maintaining the sharpness of the transitions.

4.2.4 Off-particles experiments: Sharp melting of DNA-doublers and modified DNA-doublers

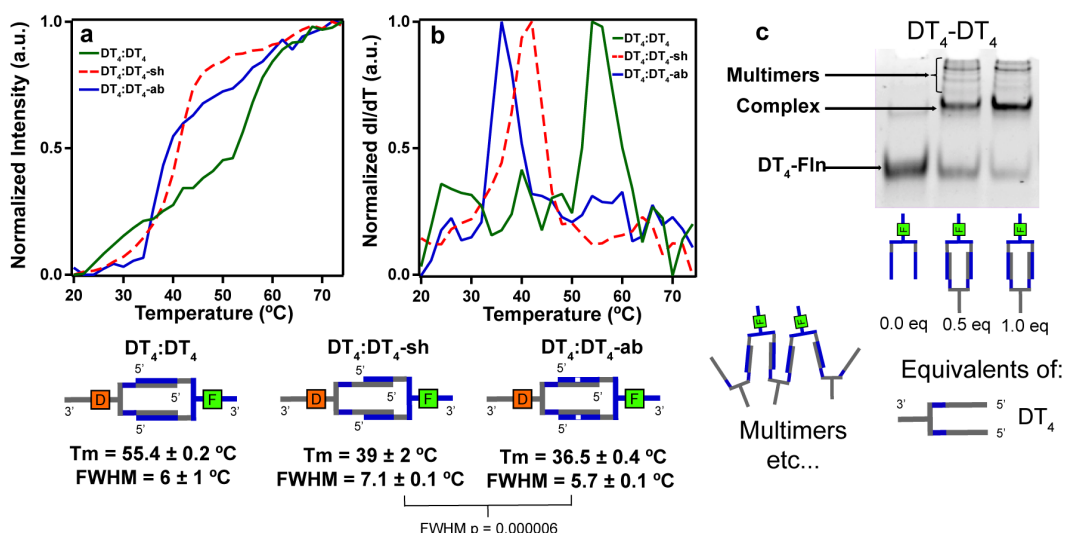


Figure 4.5 The formation and melting behavior of solution-phase caged dimers made from complementary DT₄ constructs. a) Melting profiles determined from the change in fluorescent intensity at 520 nm with temperature and b) the corresponding first derivative of the following hybridization mixtures: (DT₄:DT₄, gray solid line); (DT₄:DT₄-sh, dashed line); and (DT₄:DT₄-ab, black solid line). The melting temperatures (T_m) and full-width half maximum values (FWHM) from the first derivatives are shown for the corresponding melting transitions. c) Fluorescent images of non-denaturing PAGE gels illustrating the formation of a DT₄:DT₄ complex upon adding increasing equivalents of complementary DT₄ to a fluorescently labeled DNA-doubler (DT₄-Fln).

To determine whether the sharpness exhibited by caged dimers in solution was similar to caged dimers formed on the gold nanoparticle surface, we prepared hybridization mixtures of the fluorescently labeled DNA-doublers used in the previous experiments and a dabcyf-modified DT₄ doubler that was not bound to a GNP but could similarly quench fluorescein (Figure 4.5a-b). This allowed us to use fluorescence to monitor thermal dissociation under the same conditions as the GNP experiments. Polyacrylamide gel electrophoresis was utilized to determine whether discrete caged dimers formed, which required working with more concentrated hybridization mixtures (1.3 μM with respect to DNA-doubler concentration). Even at this concentrations which were much greater than

that used in the melting experiments (6 nM), the dominant species present were caged dimers (Figure 4.5c). Multimeric assemblies were also observed, but the relative amount of these assemblies should decrease with respect to dimer at the lower concentrations used for the melting experiments, thereby contributing only slightly to the thermal denaturation profile. As shown in Figure 4.5a and b, these mixtures exhibited sharp melting dissociations for all of the hybridization mixtures explored with FWHM values between $\sim 6\text{-}7$ °C. The FWHM values obtained were all in the range of those previously reported for the small-molecule DNA hybrid two-strand systems of Schatz and Nguyen, indicating that we had similarly cooperative behavior in our caged dimers. Comparing these results with those for the GNP systems revealed that the FWHM values of the solution species were approximately 1 °C less than that observed for the DT₄-GNP mixtures indicating that hybridization on the nanoparticles led to a subtle decrease in cooperativity which also supports that the DNA-doublers are hybridizing indiscriminately with doublers on the surface (Figure 4.1a). As observed for linear duplexes, we also found that the T_m values for GNP systems were higher than the corresponding caged dimers in solution: for example, the T_m of DT₄:DT₄-ab was 36.5 ± 0.4 °C, while for the DT₄-ab:DT₄-GNP and DT₄-ab:ss-GNP mixtures the T_m values were 40.8 ± 0.1 °C and 40.6 ± 0.1 °C, respectively. This corresponds to a $\sim 4\text{-}5$ °C increase in stability for the GNP compared with the solution systems, which was also observed for linear single-stranded DNA (Figure 4.2a-b). Once again we attribute these differences in stability to the unique confined environment on the GNP surface, which is thought to promote a higher ionic concentration than the surrounding solution due to the high density of negatively charged DNA packed on the GNP surface.¹⁶⁹ As the T_m increases with increasing salt concentration, this could explain the enhanced stability of the DNA-doublers on the surface.

4.2.5 Sequential release

Thus far, we have demonstrated how to obtain sharpened thermal release of DNA strands from gold nanoparticles, as well as strategies to decrease the melting temperature while maintaining the sharpness of the transitions. To determine whether this strategy would lead to discrimination in thermally initiated sequential release of different strands, we hybridized two DNA sequences with different stabilities to a complementary DNA-modified GNP. In one strategy, linear single-stranded DNA was used consisting of a 1:1:1 mixture of destabilized DNA (ss-ab), regular single-stranded DNA (ss) and the complementary ss-GNP (Figure 4.6). We also explored an analogous DNA-doubler based strategy using DT₄ and DT₄-ab hybridized in a 1:1:1 ratio with either ss-GNPs (Figure 4.6) or DT₄-GNPs. Two melting events were expected for each system: one melting transition should occur at lower temperature corresponding to the dissociation of the destabilized duplex, while the other should occur at higher temperature corresponding to that of the perfectly complementary duplex. For the linear DNA system, the release profile should overlap because of the broadness of each melting transition. When DNA-doublers were used, we predicted a reduction of this overlap.

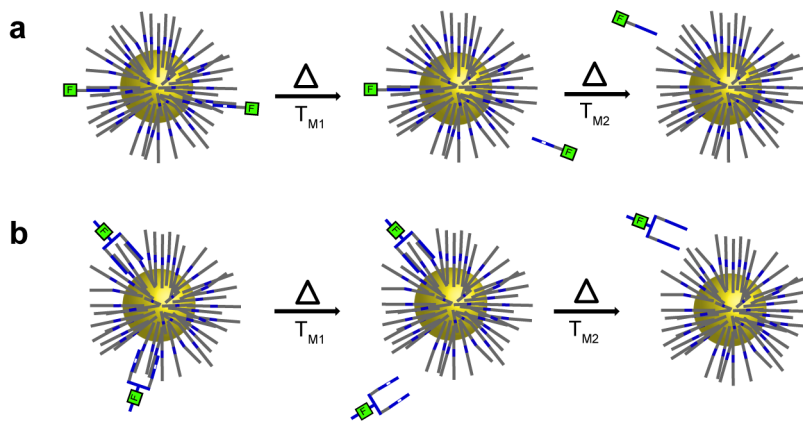


Figure 4.6 Schematic representation of the sequential thermal release of DNA using a mixture of destabilized and perfectly complementary a) single-stranded DNA and b) DNA-doublers.

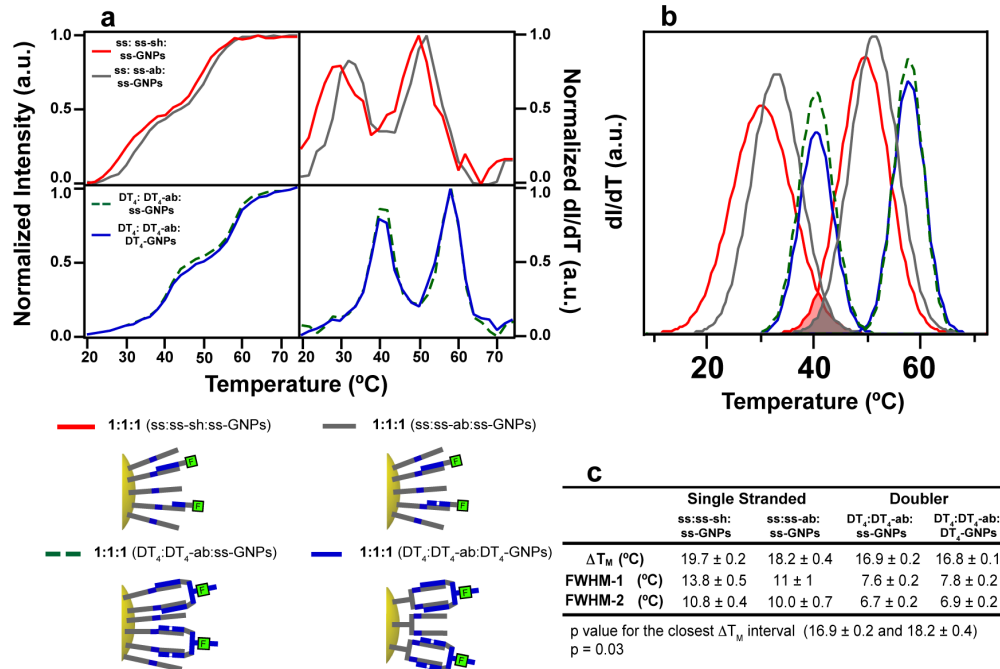


Figure 4.7 Sequential release of DNA in tri-component mixtures consisting of single-strand or DNA-doubler modified GNPs hybridized with a 1:1 mixture of the perfect complement (ss or DT₄) and the destabilized complement (ss-sh, ss-ab, or DT₄-ab). a) Melting profiles determined from the change in fluorescent intensity at 520 nm and the normalized first derivatives of: a mixture of single-stranded complement (ss), truncated complement (ss-sh), and the corresponding ss-GNP (ss:ss-sh:ss-GNP, black line); single-stranded complement (ss), the abasic containing complement (ss-ab), and ss-GNP (ss:ss-ab:ss-GNP, gray line); the complementary doubler (DT₄), the abasic-modified doubler (DT₄-ab), and the corresponding ss-GNPs (DT₄:DT₄-ab:ss-GNP, black dashed line); the complementary doubler (DT₄), the abasic-modified doubler (DT₄-ab), and the corresponding DT₄-GNPs (light gray solid line). b) The two Gaussian peak fit to the first derivative traces shown in part (a). c) Table comparing the differences in melting temperatures (ΔT_m) between the first and second transitions, and the full width half maximum values corresponding to the transitions at low and high temperatures (FWHM-1 and FWHM-2, respectively).

We prepared suspensions of a 1:1:1 ratio of destabilized DNA (ab or sh), unmodified DNA, and complementary DNA-GNPs for each of the experiments and examined their melting behavior (Figure 4.7). For the tri-component single stranded DNA systems, both of the melting transitions were broad when hybridized to ss-GNPs whether or not the abasic or truncated sequence were used (Figure 4.7a, upper panels, gray and black

trace, respectively). For the abasic modification, we observed that its melting transition was only slightly broader than the second transition that corresponded to the perfect strand ($\Delta\text{FWHM} = 1\text{ }^{\circ}\text{C}$, Figure 4.7c). On the other hand the truncated complement (ss–sh) displayed a much broader transition when compared with the transition at higher temperatures ($\Delta\text{FWHM} = 3\text{ }^{\circ}\text{C}$, Figure 4.7c). This difference in sharpness once again supports that the abasic group was ideal for significantly reducing the T_m while not increasing the broadness of the melting transition, even in linear DNA systems. Fitting the first derivative of the melting profile with two Gaussian peaks allowed us to measure the overlap between the single-stranded species (Figure 4.7b, gray region). For both ss experiments containing either the truncated sequence or abasic modification, the thermal discrimination was poor as illustrated by the large shaded region illustrating the overlap of the two peaks from the fit of the melting derivative. This overlap occurred despite the large difference in T_m of 19.7 ± 0.2 and $18.2 \pm 0.4\text{ }^{\circ}\text{C}$ for the perfect single strand with the abasic or truncated strand, respectively. Moreover, as a result of these broad transitions, the thermal release of DNA occurred over a range of approximately 45-55 $^{\circ}\text{C}$ for the single-stranded tri-component system.

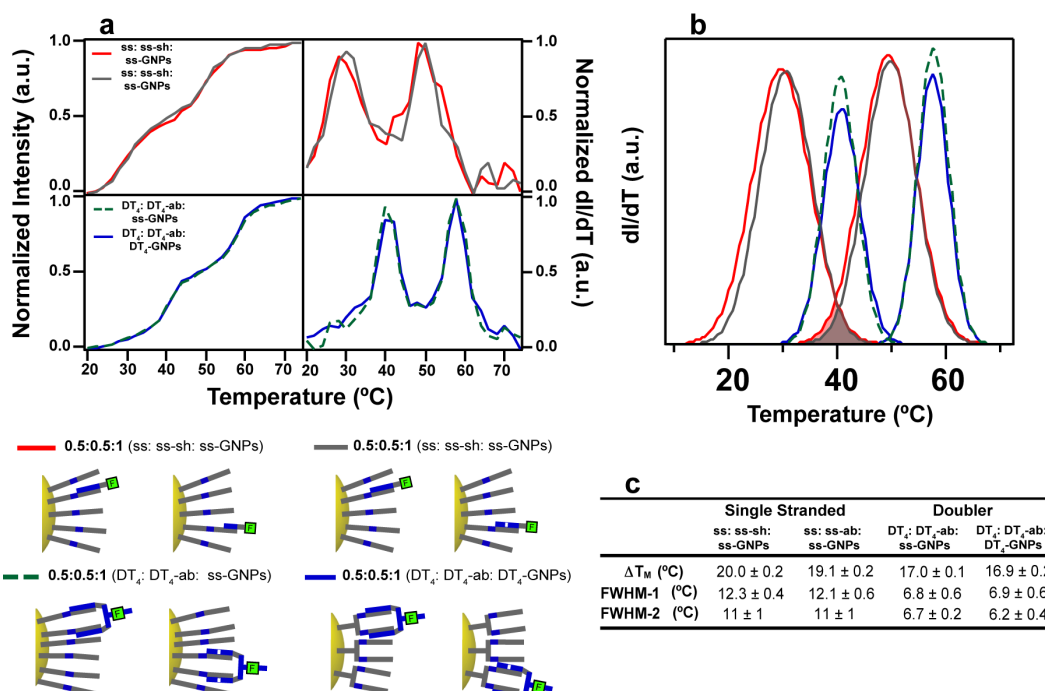


Figure 4.8 A) Melting profiles (monitored at 520 nm) and the corresponding normalized first derivatives of the systems studied. a) 0.5:0.5:1 molar suspension of: *red line*: ss, ss-sh, and ss-GNPs; *grey line*: ss, ss-ab and ss-GNPs; *green dashed line*: DT₄, DT₄-ab, and ss-GNPs; *blue line*: DT₄, DT₄-ab, and DT₄-GNPs. b) The two-Gaussian-peak fitting to the melting profiles in part (a). c) Table comparing the differences in melting temperatures (ΔT_m) for the transitions at low and higher temperature and the full width half maximums values for the low and high temperature transitions (FWHM-1 and FWHM-2, respectively). *Experimental conditions: 1 equivalent = 6 nM in 0.3 M NaCl, 10 mM PBS, pH 7.0*

When the ratio of destabilized and perfect DNA were reduced with respect to GNPs, we still observed that the branched DNA had similar differences in T_m and FWHM values compared with the 1:1:1 mixture (see Figure 4.8)

4.3 Conclusions

In summary, we have demonstrated how sharper melting transitions for releasing DNA from GNPs are possible using branched DNA-doubler constructs, which are commercially available and easy to synthesize. The DNA complexes that result upon hybridizing DNA-doublers to DNA bound

to GNPs benefit from the cooperative properties exhibited when at least two DNA duplexes are in close proximity and parallel to each other. Importantly, these cooperative, sharp transitions could be achieved whether DNA–doublers were hybridized to DNA–doubler or single-strand modified GNPs. Consequently, new thermal release profiles are possible using standard single-strand DNA modified gold nanoparticles in conjunction with DNA–doublers made using standard solid-phase methods. To achieve the separate thermal release of different DNA strands from the GNP surface, we compared two strategies to decrease the melting temperature of the DNA–doublers without altering the sharpness of the transition. We found that the introduction of one abasic group into the center of the hybridizing strand substantially decreased the T_m without affecting the sharpness making it the ideal candidate for use in sequential release strategies. Using a three-component hybridization mixture consisting of a DNA-doubler, an abasic-modified DNA–doubler and a complementary single-strand modified GNP, we demonstrated sequential thermal release of the two DNA doublers with excellent thermal discrimination. This type of cooperative release could find applications in sequential drug delivery systems or in any device that require means to trigger the release of one DNA strand over another from a nanoparticle surface.

4.4 Materials and methods

4.4.1 Sequences

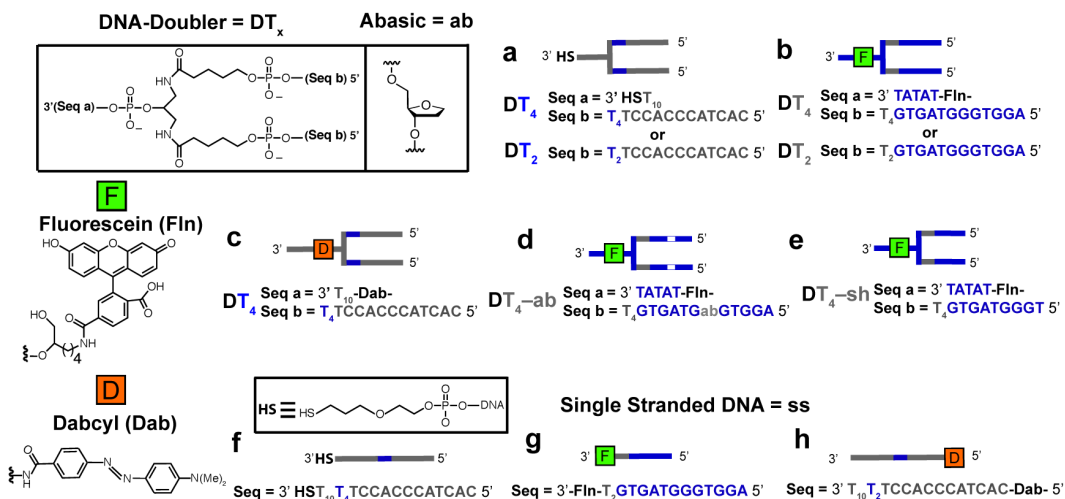


Figure 4.9 Commercially available DNA modifications and sequences used. a) 3'-Thiolated DNA-doubler (DT_x) for covalent attachment to the GNPs. b) Fluorescently-labeled DNA-doublers (DT_x) for hybridization with DNA on GNPs. c) A dabcyl labeled DNA-doubler (DT_4) used in the experiments without GNPs. d) The fluorescently-labeled DNA-doubler containing an abasic group instead of a central deoxyguanosine (DT_4-ab). e) The fluorescently labeled DNA-doubler with a truncated (shorter) sequence (DT_4-sh). f) 3'-Thiolated single-stranded DNA (ss) for covalent attachment to the GNPs. g) Fluorescently labeled single-stranded DNA (ss). h) Dabcyl labeled single-stranded DNA for the solution-phase experiments without GNPs (dab-ss).

4.4.2 Preparation of DNA strands and gold nanoparticle

See section (2.4.2) In addition to the standard nucleotide phosphoramidites, the following compounds were used: 6-Fluorescein phosphoramidite (cat. 10-1964-95), symmetric doubler phosphoramidite (cat. 10-1920-90), (abasic) dSpacer phosphoramidite (cat. 10-1914-95).

4.4.3 DNA loading and hybridization

Thiolated DNA was covalently attached to the GNPs following the procedure outlined by Hurst *et al.* with slight modifications. First, the

purified, lyophilized, disulfide-modified oligonucleotide was cleaved with a solution of dithiothreitol (DTT) (0.1 M DTT in 0.18 M PBS buffer, pH 7.99), which was allowed to react for 2 hours. Immediately after cleavage, the thiolated oligonucleotides were purified in a 0.2 Gel-Pak column (cat. 61-5002-05 Glen Research). The DNA was eluted on these columns with PBS buffer (0.05 M PBS, SDS 0.01%, pH 7.40). The purified DNA (20 nmol total) was added to a vial of concentrated buffer (0.05 M PBS, 0.05% SDS pH = 7.4) to reach a final volume of 1 mL. Next, citrate-stabilized GNPs (10 pmol) and Millipore water were added to reach a final volume of 5 mL. These GNP -thiolated DNA solutions were sonicated and allowed to sit for 20 minutes, at which point they were “salted” with buffer (0.01 M PBS, 0.01% SDS) containing concentrated NaCl (2 M). First, one aliquot of NaCl buffer was added to the thiolated DNA-GNP mixture to reach a NaCl concentration of 0.05 M. Next, another aliquot of NaCl in buffer was added to reach a NaCl concentration of 0.1 M. Thereafter, aliquots were added to increase the NaCl concentration stepwise by 0.1 M up to 0.7 M. After the addition of each aliquot of NaCl solution, the suspensions were sonicated for ~ 1 min and allowed to sit for 15 to 20 minutes. The salted samples were then incubated overnight in the dark at room temperature. To purify them and remove free thiolated DNA, functionalized DNA-GNPs were centrifuged (15 °C, 14000 rpm, 30 minutes) at which point the liquid was decanted from the DNA-GNP pellet. The pellet was then resuspended in NaCl containing buffer (500 μ L, 0.3 M NaCl, 0.10 M PBS, 0.01% SDS pH = 7.01), vortexed for 1 min and then centrifuged once again. This washing step was repeated four times ending with the DNA-GNPs suspended in buffer.

Hybridization of oligonucleotides: DNA-modified gold nanoparticles and the corresponding complementary single strand or DNA-doublers were combined in buffer (1.5 mL, 0.3 M NaCl 0.10 M PBS, 0.01% SDS, pH 7.01) to reach final concentrations of 6 nM (with respect to [single

strands], [DNA-doublers] and [GNPs]). The hybridization mixtures were then vortexed, sonicated for ~ 10 seconds and left overnight in the dark. No centrifugation was performed at this stage. Hybridization mixtures of complementary single strands and DNA-doublers lacking any nanoparticles were prepared in the same manner.

4.4.4 Excitation and emission spectra as a function of temperature

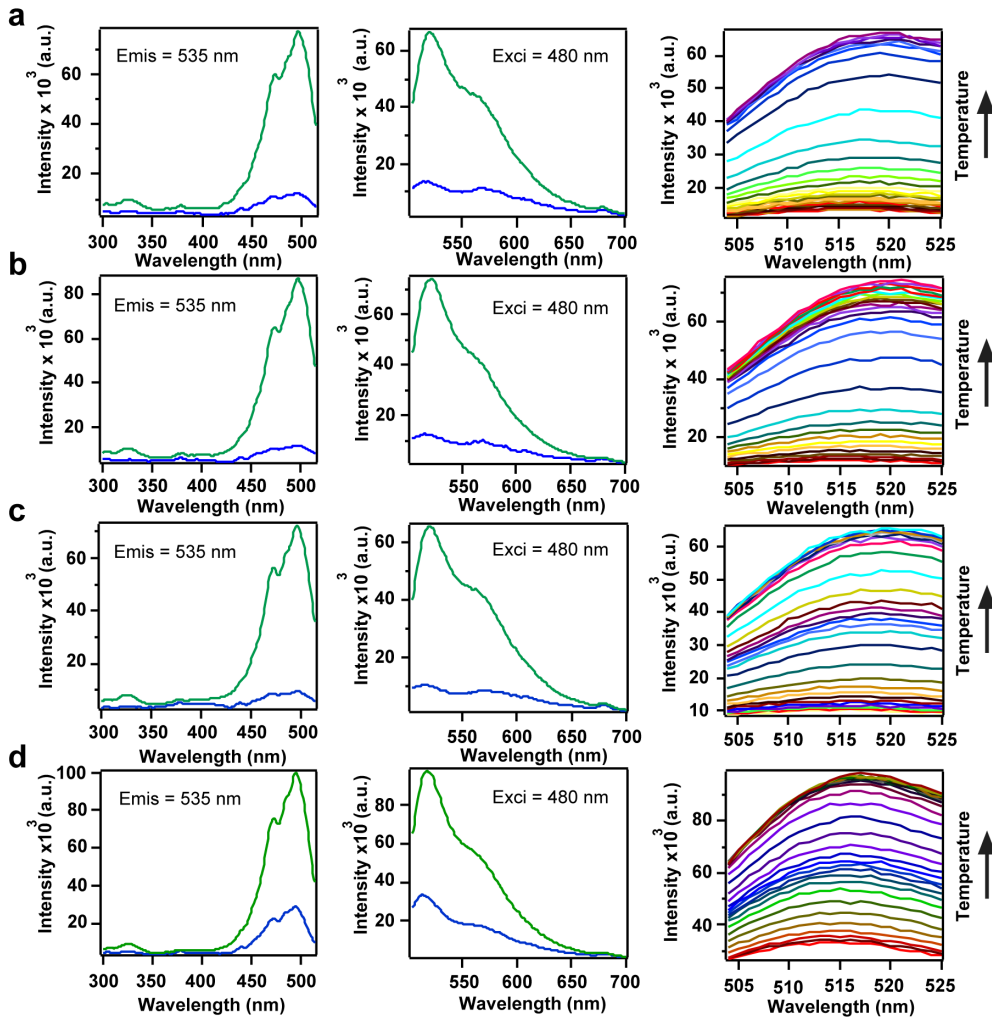


Figure 4.10 Excitation spectra (first column), emission spectra (second column) and emission versus temperature traces (third column) of the experiments a) DT₄ hybridized to DT₄-GNPs (Figure 4.2D). b) DT₄-ab hybridized to ss-GNPs (Figure 4.4D). c) Combination of DT₄ and DT₄-ab hybridized with ss-GNPs (Figure 4.7A Bottom). d) Combination of ss and ss-sh hybridized with ss-GNPs (Figure 4.7A Top). The blue and green lines represent the fluorescence intensity before and after melting, respectively.

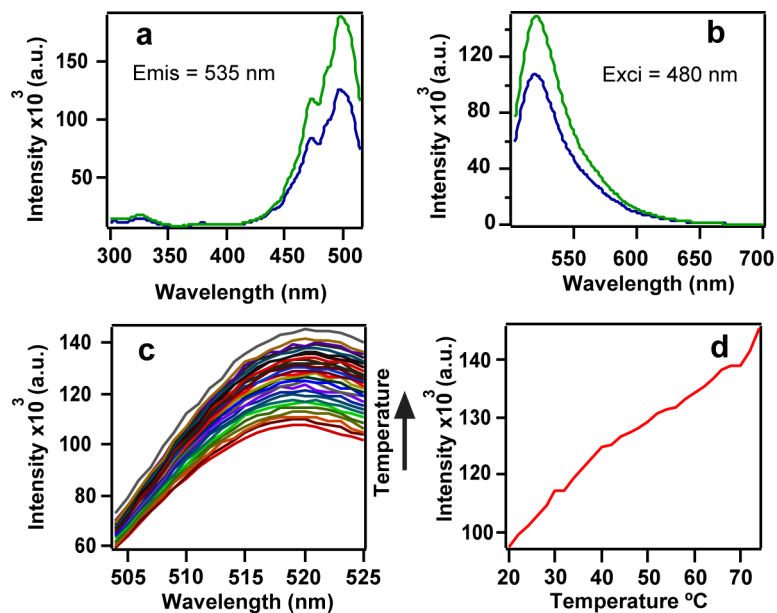


Figure 4.11 Changes in fluorescence of an Fln-DT₄ strand solution in PBS buffer as the temperature increases. A) Excitation spectrum: before heating (blue) and at 74 °C (green). B) Emission spectrum before heating (blue) and at 74 °C (green). C) Emission changes at several wavelengths while a temperature ramp is applied. D) Fluorescence intensity at 520 nm vs. temperature ($\lambda_{\text{ex}} = 480 \text{ nm}$). The intrinsic fluorescence of the fluorophore varies linearly with temperature, which may account for the linear portions of the melting profiles at low and high temperature.

4.4.5 Fluorescence intensity dependence on temperature and DNA length of Au-S bounded strands to GNPs

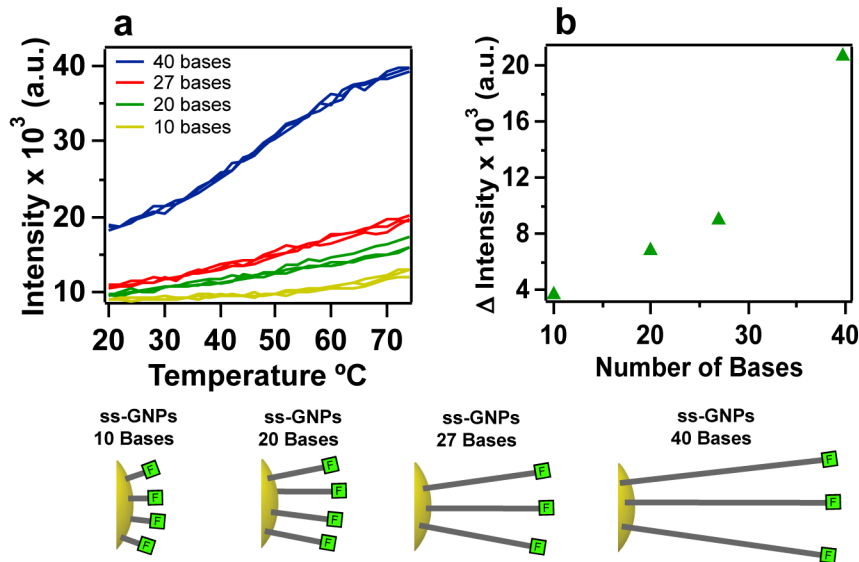


Figure 4.12 a) Changes in fluorescence intensity as the temperature increases for Fln-modified single strands of different lengths covalently linked to GNPs via S-Au bond. b) Maximum intensity difference with temperature as a function of strand length.

These results indicate that the large change in fluorescence observed in our melting experiments is due to DNA dehybridization rather than S-Au bond breakage. If the S-Au bond was breaking then the fluorescent change should not depend on the strand length as it clearly does. We suggest that the increase in fluorescence observed in the experiments shown in Figure 4.12 is due to extension of the single-strand bound to the GNP with increasing temperature, which results in an increase in Δ fluorescence with strand length.

4.4.6 Aggregation experiments

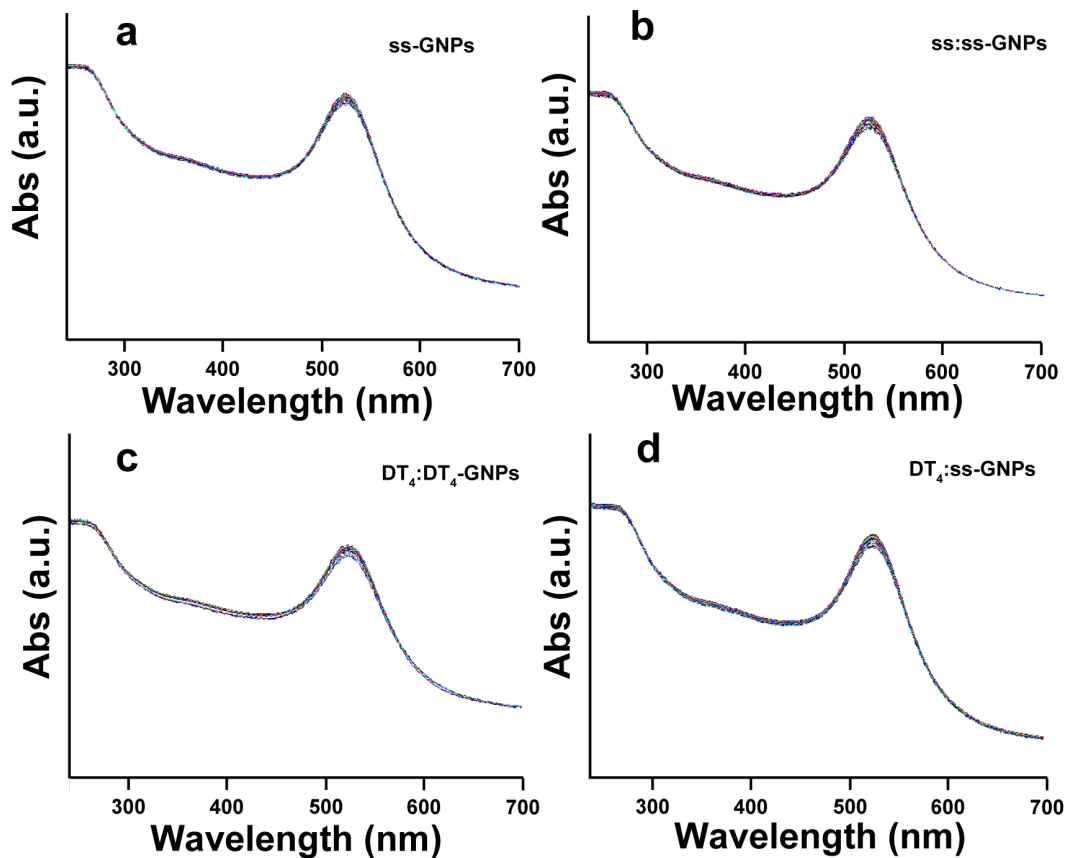


Figure 4.13 Aggregation control experiments showing the absorbance of GNPs as the temperature is increased for the concentrations explored in the fluorescence experiments. a) A suspension of only ss-GNPs with no complementary strands present. b) A mixture of complementary ss and ss-GNPs. c) A mixture of complementary DT₄ and DT₄-GNPs. d) A mixture of complementary DT₄ and ss-GNPs. No substantial difference is observed when comparing the non-hybridized (a) data with that of the hybridization mixtures (B-D), indicating no significant GNP cluster formation.

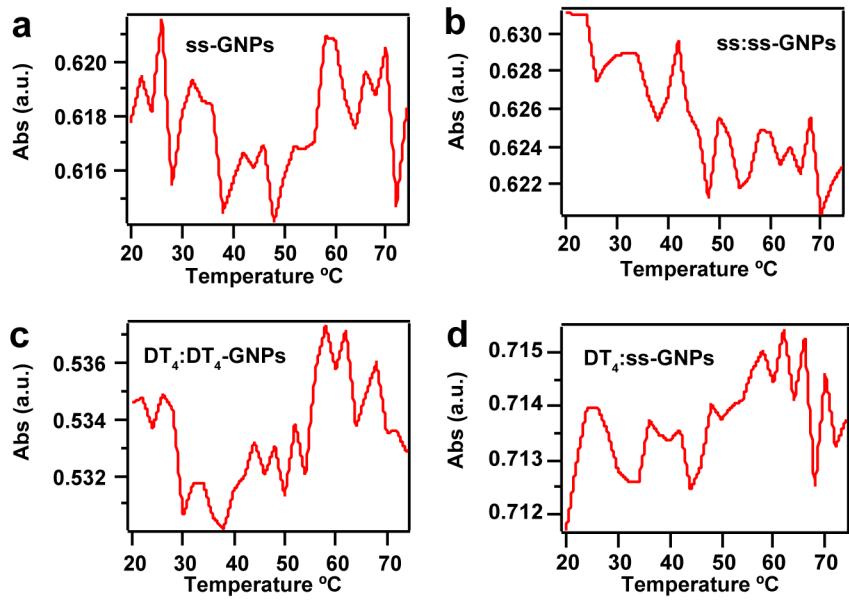


Figure 4.14 The same aggregation control experiments shown in Figure 4.13 following the absorbance at the surface plasmon resonant frequency of DNA-modified 13-nm GNPs ($\lambda_{\text{max}} = 525 \text{ nm}$) versus temperature. a) A suspension of only ss-GNPs with no complementary strands present. b) A mixture of complementary ss and ss-GNPs. c) A mixture of complementary DT_4 and DT_4 -GNPs. d) A mixture of complementary DT_4 and ss-GNPs. The lack of systematic change in absorbance with temperature indicates that there is no appreciable aggregation.

4.4.7 PAGE experiments

Caged dimer formation was monitored using polyacrylamide gel electrophoresis using non-denaturing gels, which required higher concentrations of DNA-doublers than used in the fluorescent melting experiments. In these experiments, we prepared DNA solutions in buffer (0.3 M NaCl, 0.01 M PBS, 0.01% SDS pH 7.01) containing the fluorescent DT_4 (1.3 μM) and the corresponding complementary DT_4 at concentrations of 1.3 μM (1 equivalent) or 0.65 μM (0.5 equivalent). The hybridization mixture was left at room temperature and allowed to sit overnight. Before running the gel (0.75 mm thick, 10 well), the samples were cooled down to 4 °C for 20 minutes and then a 3- μL aliquot was combined with 1 μL of a running dye mixture and vortexed. Of this mixture, 3.5 μL were loaded into each well. PAGE was performed at 4 °C using TAEMg (40 mM Tris, 2 mM

EDTA·2Na·2H₂O, 12.5 mM MgCl₂·H₂O, 20 mM acetic acid, pH = 7.5) as the running buffer and 100 V. All gels were immediately imaged in a fluorescent imager with trans-UV illumination.

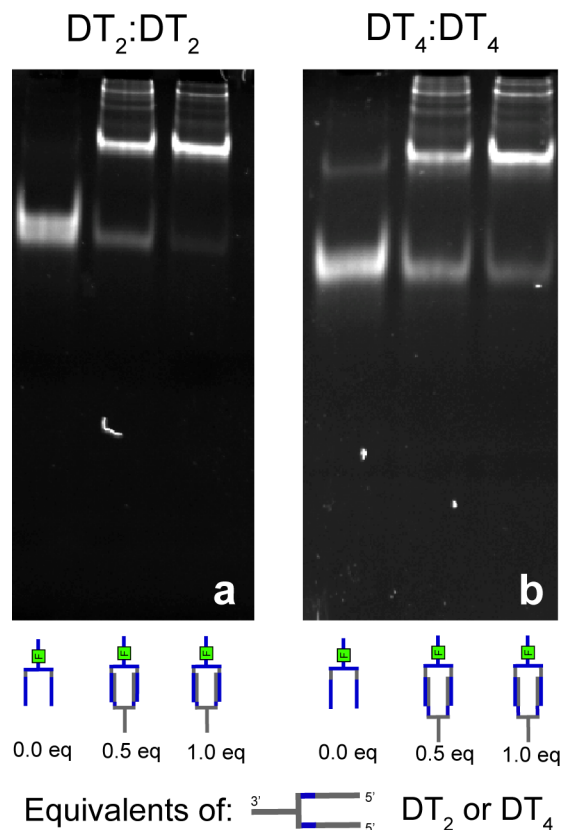


Figure 4.15 a) Titration of a fluorescein-labeled DT₂ with a complementary DT₂ strand by adding 0, 0.5 and 1 equivalents of the latter. The complex formation can be distinguished as the band corresponding to the Fln-doubler fades and a new higher band appears that corresponds to the caged dimer. b) Similar experiment using DT₄ doublers as also shown in Figure 4.5.

4.4.8 Melting analysis

The first derivative of the melting profiles based on the fluorescence experiments were obtained using Igor Pro (Wave Metrics, Inc. Version 6.2.2.2). A Gaussian function from Igor Pro was the fit to the first derivative (equation 1).

$$f'(T) = f'(0) + A \exp \left[- \left(\frac{T - T_m}{Width} \right)^2 \right] \quad (1)$$

where $f'(T)$ is the first derivative of the melting profile (fluorescence as a function of temperature), A is the amplitude, T is the temperature, T_m is the melting temperature and $Width$ is the width of the Gaussian peak, and $f'(0)$ is the value of the flat portions of the first derivative at low and high temperature, which correspond to the small linear change in fluorescein fluorescence as a function of temperature.

Similarly the sequential melting traces were fit with a two-peak Gaussian function (equation 2):

$$f'(T) = f'(0) + A_1 \exp \left[- \left(\frac{T - T_{m1}}{Width_1} \right)^2 \right] + A_2 \exp \left[- \left(\frac{T - T_{m2}}{Width_2} \right)^2 \right] \quad (2)$$

where $f'(T)$ is the normalized from zero to one first derivative of the melting profile A_1 is the amplitude of the first melting transition, T_{m1} is the first melting temperature, $Width_1$ is the width of the first peak, A_2 is the amplitude of the second melting, T_{m2} is the second melting temperature, $Width_2$ is the width of the second peak, and $f'(0)$ is the value corresponding to the flat portions of the first derivative at low and high temperature. For comparison, the plots shown in Figure 6B and Figure S1B were acquired by plotting equation 2 with the parameters obtained from the fit and a $f'(0)$ value of zero. The first derivatives exhibited in the figures were normalized from zero to one by dividing the values by the difference between the maximum value and the average minimum value measured in the flat region at high temperature. The T_m values were determined from the Gaussian fits, while the FWHM values were determined directly from the normalized Gaussian curves. Average values from at least three separate experiments are reported and the error

represents the standard deviation. The ΔT_m values were determined from the average T_m values and their corresponding standard deviations as error. The ΔT_m using the errors were obtained using error propagation. Degrees of freedom and t values were calculated using the t test for populations with different standard deviations,¹¹⁷ p-values were obtained using a web based p-value calculator.¹¹⁸

**Chapter 5 Tuning the thermal release of branched DNA
from GNPs by varying the extent of destabilization, DNA
length, and the number of branches.**

5.1 Introduction

In chapter 4 we demonstrated how the cooperative properties of branched DNA hybridized to DNA-GNPs could be used to sharpen the thermal release of the hybridized strands. This cooperative effect allowed us to illustrate a strategy for the stepwise release of strands from GNPs with minimum overlapping between the liberated species. Our outlook and perspectives of this method are mainly focused on applications in combination and sequential therapies,^{133, 135} in which several agents can be liberated at specific conditions and locations. As mentioned in previous chapters, these agents can be a combination of drugs liberated at different times, or the release of stability enhancers that are no longer required in an specific location, or a combination of imaging agents needed at different stages of the treatment. Another field in which release of several agents is required—especially nucleic acids—is in gene modulation. Recently, promising examples of gene regulation using gold nanostructures and nucleic acids have begun to appear in literature.^{139, 144, 148, 149, 172} One advantage of using these hybrid materials is that they offer the opportunity to control the cell machinery intracellularly, which in turn reduces the signal—the information inputted into the cell—distortion (i.e. degradation, diffusion, etc. of the input signal) observed when extracellular manipulation is attempted.¹³⁹ Nucleic acids or more specifically interfering oligonucleotides, are the first choice to control this internal machinery, however they not only need to be internalized using an appropriate vehicle, but also need to be released in a spatial and temporal controlled manner so that they can interact with the specific target.¹⁴⁸ Nucleic acids-gold nanostructures hybrids meet the requirements for these purposes, that is, the oligonucleotides can be loaded onto the nanostructure and the nanostructures' surface plasmon resonance properties (SPR) opens a route to the release of the cargo by the heat dissipated to the surroundings by the nanoparticle upon irradiation. In the last chapter we

highlighted the importance of releasing more than one agent, for example to control the expression of more than one protein in gene circuits. We already demonstrated that two branched DNA agents (i.e. DNA-doublers “DB”) can be released from GNPs in a thermally controlled fashion, In this chapter we explore ways to tune the melting temperature and sharpness of the dissociation to release more than two strands from GNPs over a narrow temperature range.

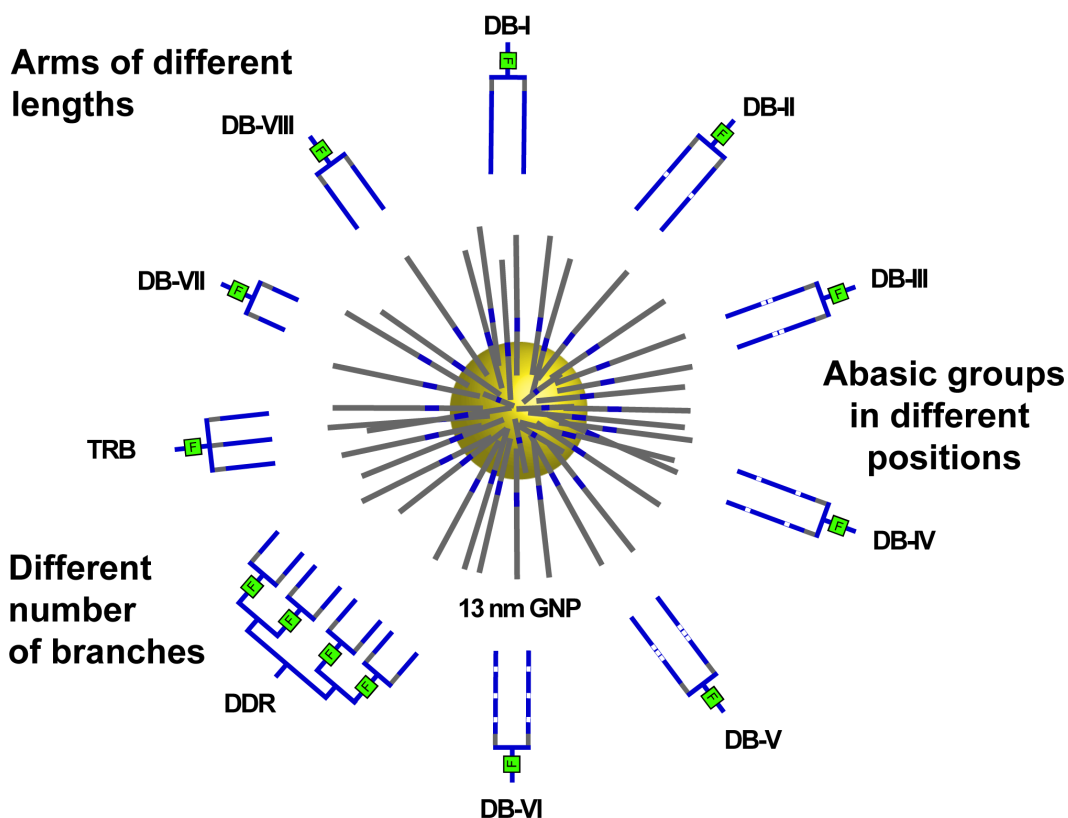


Figure 5.1 Branch DNA structures explored in this chapter. DNA–Doublers DB-I to DB-VI have 24 bases in each arm complementary to the GNP-DNA, white spaces represent the abasic groups. Doublers DB-VII and DB-VIII have 6 (short) and 12 (medium) complementary bases respectively. TRB are DNA-treblers (three arms or branches per molecule) with 10 complementary bases per arm. DDR are three-generation dendrimers with 7 complementary bases per arm. Gold nanoparticles (13nm) are functionalized with 34 bases DNA strands of which 24 bases are for hybridization.

Herein we present our efforts to extend the concepts discussed in the last section (Chapter 4), by increasing the number of strands liberated in a

narrow temperature window without overlapping. To do so, we studied several types of modified DNA strands to find ways to reduce the broadness of the thermal denaturing transitions as well as controlling the melting temperature. Figure 5.1 shows the different architectures we explored in this chapter to attain the proposed goals. It should be pointed out that the DNA on GNPs in this investigation had 24 bases available for hybridization compared with the 12 bases used on the GNPs of Chapter 4. First, we varied the number of abasic groups and their positions in the arms in long DNA-doublers containing 24 complementary bases. This length is twice the number of bases we used for the long DNA doublers in our previous chapter. Specifically, DB-I is an unmodified doubler with all 24 bases available for hybridization, DB-II has the same sequence as DB-I but one base at the center of each arm has been substituted by an abasic group; similarly, DB-III has two destabilizing units also located in the center of each arm instead of the corresponding bases. DB-IV also has two abasic groups but these are located at one fourth and three fourths of the length of the arms. We also tested constructs with three destabilizing groups; for example DB-V has three abasics in the middle of the arms and DB-VI has them at one fourth, two fourths, and three fourths of the length of the branch.

The next set of experiments consisted of doublers of different lengths; thus, we compared the melting behavior of doublers with 24 (DB-I), 12 (DB-VIII) and 6 (DB-VII) complementary bases in each arm (Figure 5.1). These strands were hybridized to ssDNA attached to the surface of 13 nm gold nanoparticles.

Finally, we varied the number of arms (or branches) that hybridized with the DNA on the nanoparticle. For these experiments, we synthesized a DNA-treble (TRB), which is similar to the doublers, but in this case three strands grow from the modifier. Also, we built a third-generation DNA dendrimer by coupling multiple doublers in a divergent approach obtaining

a total of eight arms as a result (Figure 5.1). The trebler's arms have 10 bases each and the dendrimer's seven. We compared these structures melting behavior with the doublers of 6 and 12 bases.

5.2 Results and discussion

5.2.1 Effect of abasic groups on the melting behavior

As stated in the introduction, we hybridized DNA-doublers with different numbers of abasic groups and in different positions with DNA-modified gold nanoparticles. Then we applied a temperature ramp from 20 °C to 86 °C while monitoring the fluorescence intensity increase. As explained in chapter 4, the doublers were modified with a fluorescein label that was quenched by the GNPs when the doublers were hybridized with the nanoparticle-bound strand. Upon dissociation of the duplex, quenching ceased and the fluorescent intensity increased. Figures 5.2a and 5.3a illustrate the melting behavior observed in these experiments. As expected the doubler with no destabilizing groups (DB-I) had the maximum melting temperature 76.3 ± 0.1 °C. The minimum T_m (49.7 ± 0.1 °C) was for DB-VI, which had three abasic groups distributed evenly over its arms. The doubler with only one abasic group located in the center of the arms (DB-II) had an intermediate melting transition of 65.8 ± 0.2 °C, compared to the minimum and the maximum obtained. Figures 5.2b and 5.3b illustrate the trends observed when two abasic groups are installed in the doublers. When the two destabilizing units are positioned separately, such as in DB-IV, the destabilizing power appears to be stronger than in the DB-III case. Comparing DB-III and DB-IV with the unmodified doubler we found that placing the two abasic groups in the center decreased the T_m by 12 °C, when the abasic groups are separated, the T_m was reduced by around 16 °C. Interestingly, when the two abasic groups are placed in the center of the strand (DB-III) only a very small difference in melting temperature (1.1 °C) was observed when compared to the doubler with only one abasic

group (DB-II). Regarding the doublers with three abasic units, we found again that when they are situated in the center of the arms, the destabilization was very close to that of the doubler with only one base removed at the same position. Specifically in this case, the melting values for one (DB-II), two (DB-III), and three (DB-V) abasic groups were 65.8 ± 0.2 °C, 64.7 ± 0.1 °C, and 62.2 ± 0.1 °C respectively. When the three destabilizing moieties were separated along the strand (DB-VI), we observed a more marked effect; this structure showed a T_m of 49.7 ± 0.1 °C, which is a reduction of 27 °C compared with the unmodified doubler (DB-I) and is almost 11 °C lower than the analogous diabasic doubler (DB-IV).

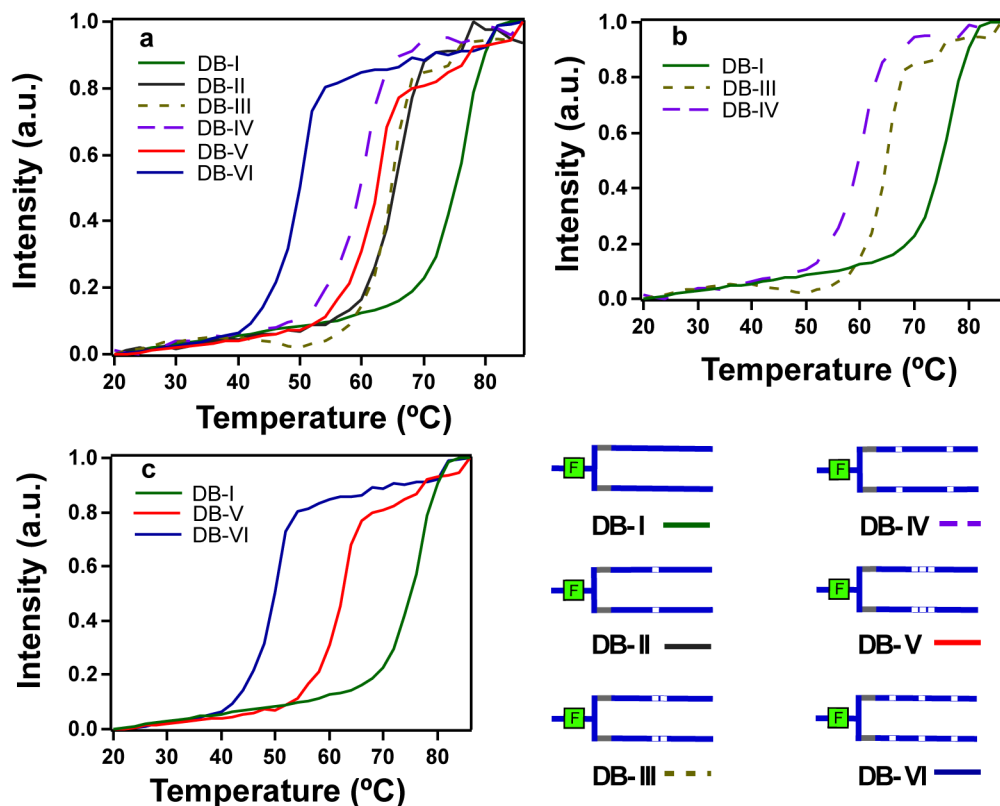


Figure 5.2 Melting profiles of DNA-doublers with abasic groups based on the change in fluorescent intensity with temperature. *Bottom right*

schematic: The doublers DB-I-VI explored. Each abasic group appears as a white box. a) Melting profiles of all experiments comparing the number of abasic groups and their positions. b) Profiles of the DNA-doublers with two abasic units (DB-III and IV) compared with a doubler that had no destabilizing groups (DB-I). c) Melting comparison of doublers with three abasic groups (DB-V and VI) and the doubler with no destabilizing modifications (DB-I).

Analysis of the broadness of the transitions showed that the unmodified doubler (DB-I) had the broadest melting manifested in the largest full width half maximum (FWHM of 7.8 ± 0.3 °C). Adding an abasic group to the center of the arms had a negligible effect on the broadness, decreasing the FWHM by just 0.2 °C. Interestingly, we found that a dramatic change was observed when another abasic group was added to the doubler systems. For example, two abasic modifiers in the middle of the arms, narrowed the melting transition by almost 2 °C from a FWHM of 7.8 ± 0.3 °C for DB-I to a FWHM of 5.9 ± 0.2 °C for DB-III (Figure 5.3b). The introduction of three destabilizing modifiers situated at the center of each arm yielded almost the same FWHM as the two-abasic system just discussed with a value of 6.2 ± 0.5 °C.

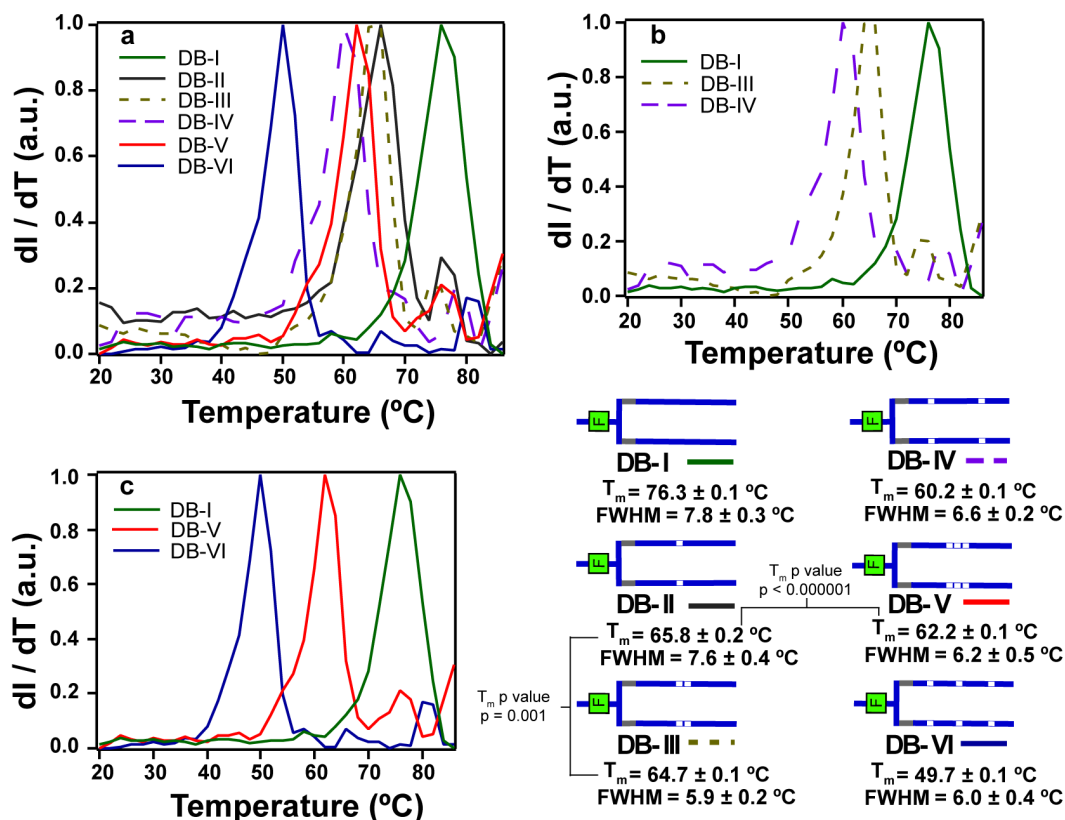


Figure 5.3 The normalized first derivatives of the melting profiles shown in Figure 5.2 and their respective full width half maximums (FWHM) and melting temperatures (T_m) a) for all the doublers explored; b) for DNA-doublers with only two abasic units (DB-III and IV) compared with a doubler with no destabilizing groups (DB-I); c) for DNA-doublers with three destabilizing groups (DB-V and VI) and the doubler with no destabilizing group (DB-I)

When the destabilizing groups were distributed evenly along the arms of the doublers, narrow transitions of similar magnitudes were measured. Specifically, the two-abasic doubler, DB-IV, showed a FWHM of 6.6(2) °C while, that with three abasic groups, DB-VI, had a FWHM of 6.0(4) °C. Thus far, these results follow some of the trends observed in Chapter 4; for example, long doublers with abasic groups as destabilizing moieties have narrow transitions. Surprisingly, we found in the present study, that the destabilized structures can even have significantly narrower transitions than that of the unmodified doublers. Also, we confirmed that using abasic modifiers is an excellent way to modulate the T_m 's of these constructs.

With the substitution of only a couple of bases, substantial changes in melting temperatures can be achieved without sacrificing the sharpness of the release. These experiments also show us that increasing the number of abasic groups in the center of the arms did not produce a significant effect in the T_m of the doublers. In contrast, separating the abasic groups throughout the branch had a more pronounced outcome.

5.2.2 Effect of the length of the arms on the melting behavior

In this section we decided to take a deeper look at the effect of the length of the doublers' arms on the T_m and FWHM of the transitions. Based on literature precedent, we predicted that longer arms should exhibit sharper transitions.¹⁷⁰ Our experiments in Chapter 4 (on particles and off particles) showed that long unmodified doublers of 12 bases per arm had the tendency towards narrower transitions than shorter doublers of 9 bases per arm (FWHM = 7.2 ± 0.1 long vs. FWHM = 7.7 ± 0.2 short). Since one aim of this chapter was to identify strategies to release as many strands as possible, we needed to evaluate the behavior of doublers with higher melting temperatures—with more bases for hybridization and therefore longer arms and further confirm the tendencies observed previously. With this in mind, we decided to test if the trend observed previously was conserved when variations in the length of the arms were greater than the removal of three bases. As a result, we synthesized three doublers with different arm lengths: a small doubler with only 6 hybridizable bases (DB-VII), a medium doubler with 12 bases (DB-VIII) the same as in Chapter 4, and a long doubler with 24 bases (DB-I). Figure 5.4 shows the melting profiles obtained for these structures. In the case of short doublers (DB-VII) the temperature ramp started at 12 °C, since the melting begins before the 20 °C used for the other experiments.

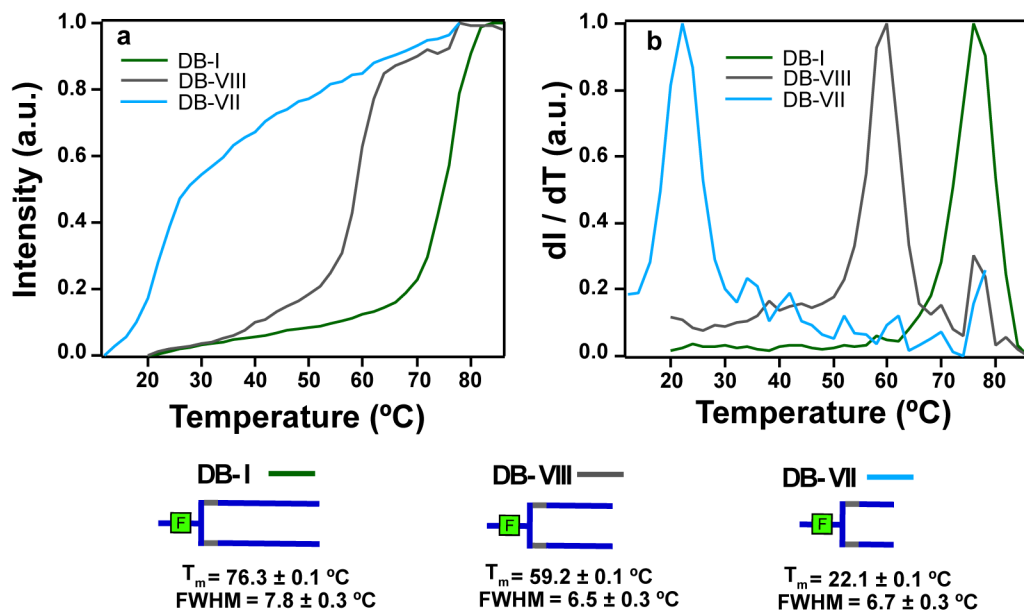


Figure 5.4 Melting properties of doublers with different lengths. a) Melting profiles of DNA-GNPs hybridized with: DB-I long doubler with 24 bases in each branch (green line); DB-VIII medium doubler with 12 bases in each arm (gray line); DB-VII short doubler with 6 bases in each branch (light blue). b) The normalized first derivatives of the corresponding melting profiles.

The broadness of these transitions showed an irregular trend (Figure 5.4). For example, the longest doubler (DB-I) had a FWHM of 7.8 ± 0.3 °C, which is greater than that of the medium doubler (DB-VIII) with a FWHM of 6.5 ± 0.3 °C, which is opposite of the predicted trend, in which doublers with longer arms have narrower transitions than doublers with shorter arms. When compared with the short doubler (DB-VII), the medium doubler (DB-VIII) tended to have a slightly sharper transition ($P = 0.4$). When comparing these results with those from the previous chapter, it should be borne in mind that the strands functionalized to nanoparticles in this section are longer than those in the former study, and this could be one of the causes of the discrepancies in the melting behavior of these constructs. We hypothesize that a dramatic change in the length of duplex formed may affect the flexibility of the complex, and as consequence perturbing the neighboring cooperativity.

Concerning the melting temperature, the trend was as expected, the longest doubler has the higher T_m and the shortest the lowest. It should be noted that increasing only six bases (4 G's, 1 T's, and 1 A's) from the short doubler to the medium one, caused an increase of 37 °C. On the other hand, increasing 12 bases (7 G's, 3 T's, and 2 A's) from the medium to the long doubler only increased the melting temperature by 17 °C. Similar behavior was observed in "off particle" experiments, in which free duplexes in solution exhibited a doubling of the melting temperature upon increasing from 10 to 20 bases, but only increased the temperature by one fourth going from 20 to 60 bases.¹⁷⁰

5.2.3 Effect of branching in the melting behavior

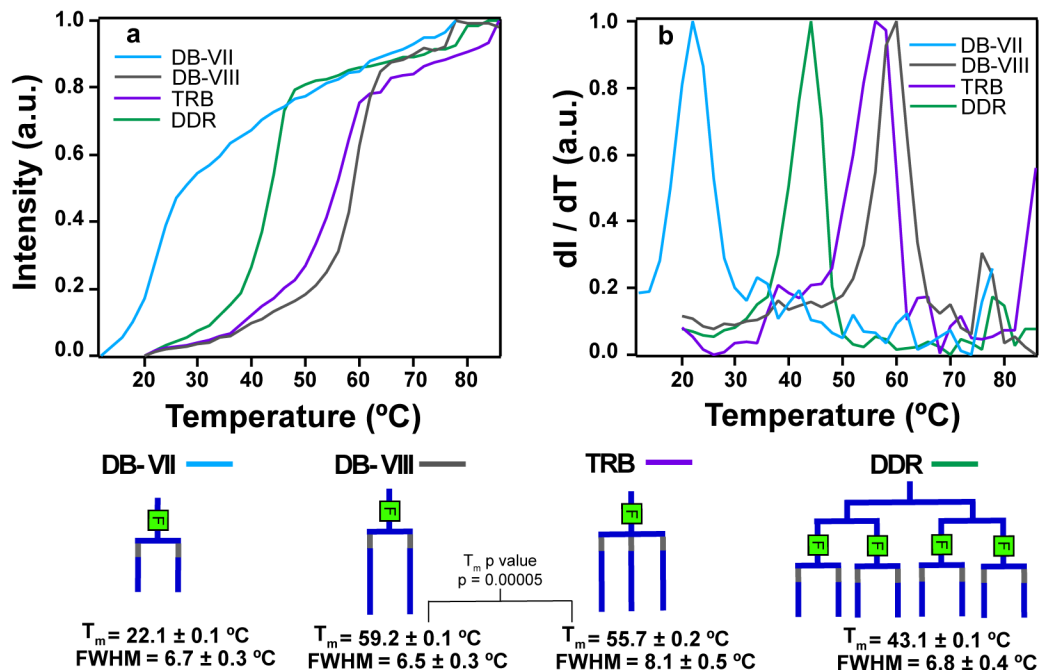


Figure 5.5 Melting properties of branched DNA with different number of arms. a) Melting profiles, DB-VII short doubler with 6 bases in each branch (light blue). DB-VIII medium doubler with 12 bases in each arm (gray line). TRB (Trebler-DNA) with 10 complementary bases (purple line). DDR (Dendrimer-DNA) with 7 complementary bases (light green). b) First derivative with respect to temperature of the same strands. Two distinct doublers have been displayed in order to make easier the comparison between the different numbers of bases of each strand.

We discussed in the previous chapter about the reasons behind the sharp melting transitions of DNA-GNPs aggregates. We mentioned that the crowded environment on the surface of the nanoparticle increases the local ion concentration and as consequence the strands end up sharing their respective ion clouds.^{72, 173, 174} This ion cloud sharing facilitates cooperative interactions among strands leading them to dissociate in a cascade manner. A related point that favors sharp dissociations is the number of strands hybridized close and parallel to each other. It is expected that a system that fulfills this condition should undergo narrower transitions as the number of interactions and crowdedness increases.^{150, 172, 173} In order to test the effect of the number of branches in our system,

we synthesized DNA strands with more than two arms. First, a fluorescently labeled DNA-treble (TRB) was prepared by using the corresponding modifier that allowed us to grow three strands in a single entity. Then, a fluorescent eight-branched DNA structure was prepared by coupling doublers together forming a third-generation dendrimer (DDR). These strands were loaded on the GNPs and their thermal dissociation was monitored in the same way as the doublers. We compared these experiments with the short and medium doublers based on their similar arm lengths with the dendrimer and trebler, respectively (Figure 5.5).

Surprisingly, these experiments showed us that the DNA-treble had a broader transition ($\text{FWHM} = 8.1 \pm 0.5 \text{ }^\circ\text{C}$) than both the small and medium doublers; however, the dissociation of the DNA-treble still appeared sharper than the linear DNA in Chapter 4 (ssDNA), which had a FWHM of $10.3 \pm 0.2 \text{ }^\circ\text{C}$. The DNA-treble, having 10 complementary bases, displayed a T_m of 55.7 ± 0.2 very close to that of the medium doubler with 12 bases ($T_m = 59.2 \pm 0.1 \text{ }^\circ\text{C}$) suggesting that the extra arm did not contribute significantly to the melting stabilization. In contrast, the dendrimer exhibited a melting transition in the range of the other constructs studied, with a FWHM of $6.8 \pm 0.4 \text{ }^\circ\text{C}$. Specifically, the melting temperature for DDR with 7 complementary bases was $43.1 \pm 0.1 \text{ }^\circ\text{C}$, which was much greater than that of the short doubler with only 6 bases that had a T_m of $22.1 \text{ }^\circ\text{C}$.

Over all, multi branched DNA appears to sharpen the melting transitions, however, with the branched systems studied thus far a clear trend cannot be envisaged. One possibility is that the curvature of the gold nanoparticles did not allow for the optimal geometry between all three arms of the treble (TBR) and the bound strands. For the DNA-dendrimers (DDR), an explanation for the sharper melting could be that the presence of many strands ensures that some of them hybridize, which is still sufficient to promote cooperative dissociation behavior and a sharper

release. As we will show later these findings can find applications in our desired system, which is releasing multiple strands from a single vehicle.

5.2.4 Release of multiple strands

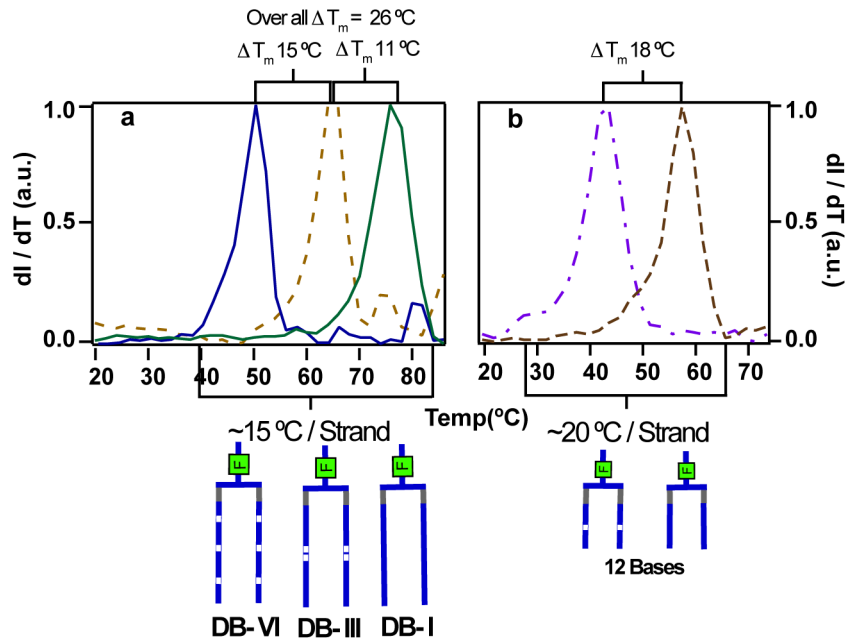


Figure 5.6 The normalized first derivatives of three DNA doublers of varying stability hybridized independently with GNP-DNA. a) The combination of doublers that could be used to release three strands above 36 °C. b) Experimental data from Figure 4.4d from the previous chapter as a comparison to the DNA-doublers in this investigation.

The purpose of these investigations is finding ways of narrowing the interval of thermal DNA dissociation and controlling its melting temperature. We have studied several architectures to accomplish this goal. In this section, we put these findings together and illustrate that using combinations of doublers or other structures, the release of multiple DNAs can be achieved.

Our first example, is regarding a reviewer’s comment on our last work (Chapter 4) that states the following:

“The work, although very interesting, might not be practical for the intended uses mentioned by the authors. The low temperature release

of DNA appears around physiological temperatures and the other melting transition is about 20 °C higher. The initial release would be initiated upon introduction of a sample into physiological conditions.

Tuning the temperature range will be a challenge... ..Although the system might not be realized for the mentioned applications *in vivo*, the authors should modify their statements to suggest..."

Even though, there are still other challenges to overcome before seeing the application of our systems *in vivo*, we used this as motivation and guidance to focus our research on strategies to release multiple strands above physiological temperatures. Figure 5.6 illustrates one possible combination of three doublers that can be released over a narrow temperature window above 36 °C. Significantly, the newly designed doublers DB-IV and DB-III both have FWHMs that are one degree less than the doublers studied in Chapter 4 (Figure 5.6b). As a consequence, the melting window for these two doublers is almost 10 °C smaller and the ΔT_m interval is 3 °C narrower than their counterparts from the previous chapter. As the unmodified long doubler DB-I also has a narrow transition and a distinct melting temperature from DB-VI and DB-III, with these constructs three strands should be liberated with little cross contamination in a window above physiological temperatures (40 °C to 84 °C) and still in a narrow range ~45 °C. The observed overlapping between these newer DNA-doublers appears to be comparable with the former system studied before (Figure 5.6b). This work demonstrates that varying the doubler's length and, the number and position of abasic groups, it is possible to release three strands starting at a temperature above physiological conditions (>36 °C).

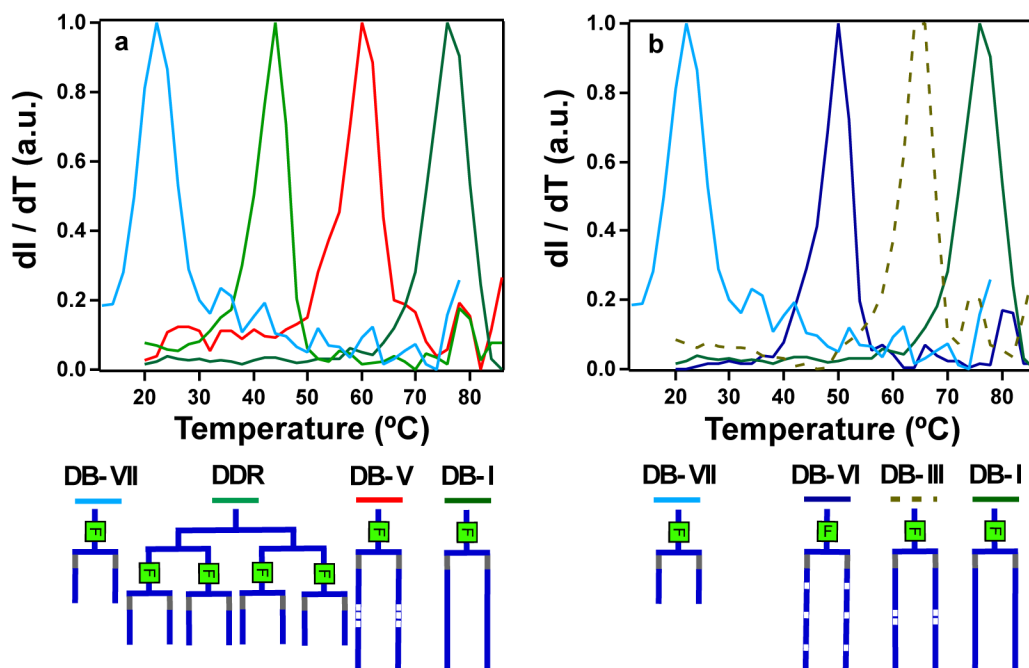


Figure 5.7 Combination of strands that could allow us to release four different strands in a temperature window from 14 to 84 $^{\circ}C$ with minimal overlapping.

Along the same lines, more than three strands could be released from the same structure, for applications where the temperature range is not limited to a minimum of 36 $^{\circ}C$. Figure 5.7b illustrates how using the shorter doubler DB-II with the combination shown in Figure 5.6a, four distinct strands can be accommodated with minimum cross contamination in a temperature window from 14 $^{\circ}C$ to 84 $^{\circ}C$. Interestingly, similar results can be achieved using different architectures; for example replacing the destabilized doublers DB-VI and DB-III with the DNA-dendrimer DDR and another destabilized doubler DB-V, four distinct transitions can be observed. This demonstrates the versatility of the method since the sharpness and melting temperatures required for the stepwise release can be achieved by a diverse type of approaches.

5.3 Conclusions

In the present chapter we explored different DNA architectures hybridized with DNA-GNPs to find ways to control the melting temperatures and narrow the broadness of their corresponding melting transitions. We varied the number of destabilizing abasic groups and their positions, changed the length of the hybridized branches (or arms), and increased the number of arms of these structures to analyze the effect on the melting behavior. We confirmed that abasic units provide a good strategy to reduce the melting temperature while still conserving sharp transitions. We also found that variations of the length of the arms of these constructs yielded an irregular trend that should be further confirmed by testing more doublers of different lengths and evaluating the influences of other variables; for example, the length of the DNA functionalized to the nanoparticle. Our next experiment on varying the number of arms also deserves a further exploration, even though it confirmed that multi branched DNA structures sharpen the melting transitions. More architectures should be tested in order to find the most critical variables that affect the melting behavior of branched DNA in our particular systems. Although not all of the variable led to definitive trends regarding the melting tendencies of our branched DNA, from the materials point of view, these approaches can be used to release multiple strands (>2) in a narrow temperature window with minimum to no overlapping. Furthermore, we revealed that up to three different strands could be liberated above physiological temperatures, overcoming one of the challenges that could face the application of our technology in sequential therapies or gene circuits using photothermal release.

5.4 Materials and methods

5.4.1 DNA sequences

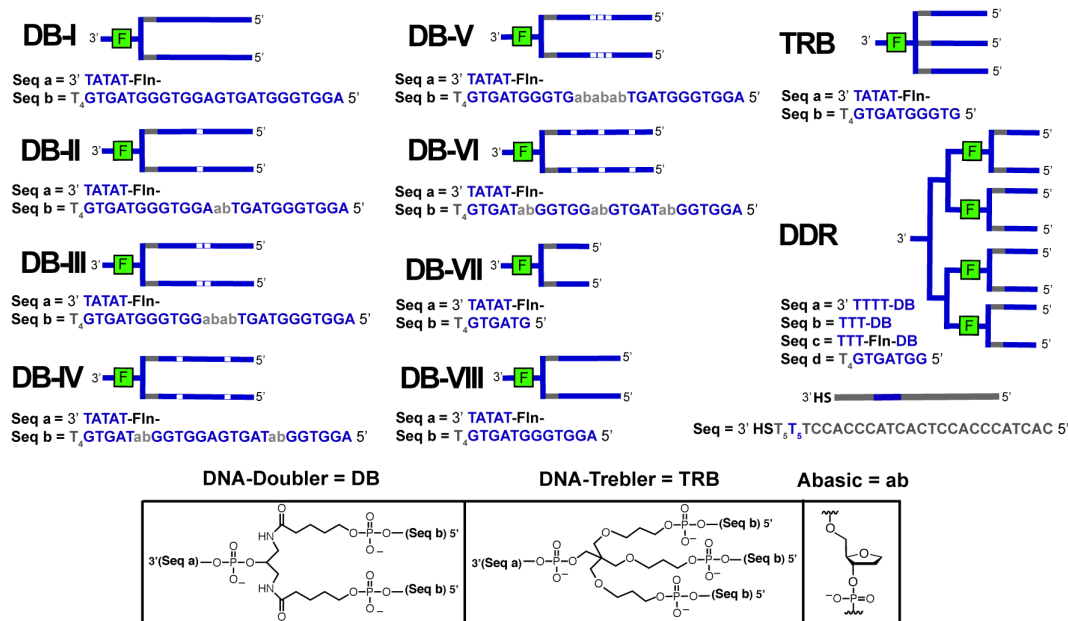


Figure 5.8 DNA sequences and structures used in this chapter.

5.4.2 Preparation of DNA strands and gold nanoparticles

See section (2.4.2). In addition to the standard nucleotide phosphoramidites, the following compounds were used: 6-Fluorescein Phosphoramidite (cat. 10-1964-95), Symmetric Doubler Phosphoramidite (cat. 10-1920-90), Trebler Phosphoramidite (cat. 10-1922-90), (abasic) dSpacer Phosphoramidite (cat. 10-1914-95). The DNA-Trebler were prepared using the standard protocol using DCI as the activator. Trebler was prepared using the same protocol for DNA-doubler, after attaching the corresponding doubler for each generation thymine spacer were inserted (Seq a, b, and c Figure 5.8).

5.4.3 DNA loading and hybridization

See section (4.4.3).

5.4.4 Melting experiments

The fluorescence intensity of the colloidal hybridization mixture was analyzed at 520 nm using an excitation wavelength of 480 nm, as it was heated from 20 °C to 86 °C, except for the short doubler (DB-VII) that was heated from 12 °C to 78 °C, at increments of 2 °C, allowing equilibration for 5 minutes between each measurement.

Chapter 6 Epilogue

6.1 General conclusions

Development of systems that allow better delivery of therapeutics is a priority in the pharmaceutical field. Nanotechnology offers several tools to achieve these goals; one of these most attractive approaches uses gold nanoparticles and DNA due to their unique properties. In particular, gold nanoparticles and their outstanding optical properties, and DNA and its programmability make hybrid materials from these components a promising choice in the field. Among the most critical properties to control for these materials to find real world applications are control of composition (i.e. functionalization) and controlled release of the payloads. In this thesis, we studied these properties in DNA-GNPs hybrids materials.

First we compared methods to control the DNA functionalization of the nanoparticles, the number of groups and the relative distribution. Using fluorescently labeled the DNA we found that DNA-directed (hybridization) approach is more effective to control the proportion of the groups on the surface of the GNPs. On the other hand, thiol directed assembly appears more useful to obtain high functionalization density, but this strategy has very poor performance on controlling the ratio among functionalities. Controlling the number (density) and proportion of functionalities on the vehicles surface is key to obtain the desired effects, modulating the specific number of drugs, tags, responsive agents, etc. Furthermore, control over these variables may enable the vehicle to be tuned for specific purposes for example, to have short or long circulations time.

Another aspect of surface modulation that is important to be addressed, especially for targeting strategies, is the spacing of groups on the periphery of the particle. We hypothesize that achieving control of the spacing of targeting ligands functionalized to the surface of a vehicle may lead to an increase in binding affinity for the cell. To provide a route to accomplish this objective, we used DNA as scaffold and constructed different architectures that have the ability to modulate the spacing

between their end groups. We called these constructs DNA clamps, they are made either of two semi complementary strands (“Y” shaped DNA) or a DNA-doubler to which an adjuster strand is added. Depending on the adjuster’s length the distance between the two ends of the “Y” complex or DNA-doubler can be tuned. We found indeed that the spacing can be controlled using this type of structures. The Y-shaped clamp exhibited spacing control in the nanometer-angstrom scale. The doubler also displayed similar properties; however, it appears unstable after a certain amount of adjuster strand is added. We also investigated the formation of these structures on the surface of gold nanoparticles. This experiments showed the apparent formation of these clamp structures, but due to the quenching properties of gold nanoparticles new experiment should be designed in order to obtain quantitative results.

The next objective in our investigations addressed the controlled release of payloads, specifically, the release of nucleic acids. We already mentioned in the previous chapter the importance of achieving spatio-temporal release of therapeutics agents; also we explain the promise of stepwise release of nucleic acids. Here, we studied a strategy to thermally release different nucleic acids stepwise over a narrow temperature range. Our method is based on the sharp melting transitions obtained when the hybridized DNA strands are parallel and close to each other in a crowded environment such as at the nanoparticle surface. To acquire this effect, we used DNA-doublers and hybridized them to DNA functionalized GNPs. We found that indeed sharper transitions result when DNA-doublers are employed. Also, introducing abasic groups (a “deoxyribonucleoside” without the base) or shortening the arms of these doublers, the melting temperature could be controlled. As a consequence, we were able to build a system in which two different strands are released from the same nanostructure stepwise, with minimum overlapping, and in narrow temperature window if compared to ssDNA hybridized to the same

structure. Further studies have demonstrated that not only doublers have sharper transitions but DNA-treblers and even DNA-dendrimers can also have a reduced melting interval when they are hybridized to DNA-GNPs. Additionally, we found that several abasic groups can be used to control the melting temperature maintaining or even increasing the sharpness of the transitions. For example, a marked effect was observed when the abasic units were located separated throughout the arms. Even though more studies are necessary to find a definitive trend or the effect of varying the length, the number of arms, and the number and position of destabilizing units in each arm, we demonstrated that is possible to release more than two strands from DNA-GNPs in a reduced temperature window. Specifically we showed that using a combination of the branched constructs, up to four strand could be released in an interval from 14 °C to 84 °C with expected negligible overlap.

Generally speaking, it is necessary to constantly revise strategies to build delivery vehicles from a basic-science point of view. From this perspective, unforeseen challenges can be approached systematically, perhaps saving costs at more advanced stages of the development. Another point, is evident the role of nucleic acids in the construction of more advanced nanostructured biomedical devices, from building block to therapeutic agent, they provide a extremely diverse platform, that combined with the powerful conjugation chemistries, offer innumerable opportunities in the field of nanomedicine. Gold nanoparticles by themselves also represent a group of structures that are already revolutionizing the field of detection and nanomedicine and further and investigations should be continued in the most promising applications.

6.2 Perspectives and future research

Future directions can be divided in to two parts: basic research and *in vitro* studies of the potential applications. In the first part, if the intention is

to accommodate different ligands (small molecules conjugated to DNA strands), studies regarding the charge, size, and other variables such as hydrophobicity and intercalation of DNA, should be addressed carefully to establish the effects of the moieties attached to the DNA-GNPs. Even though the literature suggests that length of the strands does not affect the relative proportions during the ligand exchange process, systematic studies varying length and sequence compositions should be investigated more carefully, especially when modifiers are included in the strand.

In our control of spacing experiments we observed that the doubler clamp appears unstable. We reasoned that one of the causes was that the sequence of the adjuster strands had to be reversed half way through the strand to match the sequence order of the doubler's arms. As consequence, distorting a proper geometry for the hybridization of the adjuster and causing ring strain. A closer look at the doubler hybridized to doubler experiments in chapter 4 reveals the similarities between both systems (doubler:adjuster and doubler:doubler). Gels experiments in the sequential release section demonstrated that indeed doubler:doubler complexes are formed. Therefore, we think that spacing control using doubler clamps could be achieved using another doubler as the adjuster strand, the doubler modifier would have the role of reversing the sequence without the need of reverse phosphoramidites and should prevent ring strain.

A way in which clamps can be tested on particles to overcome the quenching caused by GNPs could involve loading these devices on polymer particles. Also, it seems evident that the DNA density on nanoparticles should affect the formation of these clamps therefore this variable should also be studied.

Regarding, the stepwise release of DNA one basic question that still remains is how narrow the melting can be. Therefore, the study of different architectures that sharpen these transitions is key in the development of

more complex devices. Along the same lines, T_m control is very important to fine-tune the exact temperature range where overlapping among released strands is minimal. As consequence, any study in this direction should always bear in mind both variables. Also, depending on the specific application, sometimes it is necessary to have a fast release of the strand with slow rates of rehybridization (e.g. delivery of therapeutics that need long or permanent interaction with the targets), while for other applications, reversible systems that quickly return to their original state are needed (e.g. to examine the influence of a gene in a process; therefore the gene has to be turned off for a period and turned on again later). To do this, it is required to know the kinetics of hybridization and dehybridization at specific temperatures and find ways to tune these rates.

After solving some of the basic challenges still remaining, the next step is testing these systems *in vitro*. Therefore, experiments using different proportions of small molecule targeting agents, labels, and stabilizers should be performed. Something similar should be done with the DNA-clamps by attaching specific targeting groups and determining if the expected increased affinity can be observed.

We have discussed the potential use of the controlled release in the nanoplasmonic release of DNA. Therefore, it is necessary to incorporate our branched DNA to structure more suitable for these purposes for example silica-gold nanoparticles or gold nanorods. This is due to the NIR absorption properties of these nanostructures that allows them to operate in the water window. Another, challenge in this direction is whether it is possible to *gradually* heat the nanoparticle surroundings using laser irradiation.

Another opportunity to circumvent the photothermal release issues is using another source of heating; for example, magnetic hyperthermia or ultrasound. Using alternative heating sources, particles of different

materials might be used as a carrier, as a consequence diversifying the applications of these strategies.

Appendix Synthesis of a β -glycoside functionalized G \wedge C motif for self-assembly into rosette nanotubes with predefined length⁴

⁴ The research involving Synthesis of a β -glycoside functionalized G \wedge C motif for self-assembly into rosette nanotubes with predefined length described in this chapter was published R. L. Beingessner, J. A. Diaz, U. D. Hemraz and H. Fenniri, *Tetrahedron Lett.* 2011, **52**, 661–664

A.1 Introduction

G \wedge C base **1** (Figure A.1a) is a self-complementary guanine-cytosine hybrid molecule that was shown to self-assemble¹⁷⁵⁻¹⁹² in aqueous or organic solvents into six-membered supermacrocycles maintained by 18-hydrogen bonds. These assemblies further organize into linear stacks (termed rosette nanotubes, RNTs) with a central channel running the length of the stack. In principle, any functional group R covalently linked to the G \wedge C base **1** ends up being expressed on the outer surface of the RNTs, thereby providing a ‘built-in’ strategy to alter the RNTs’ chemical and physical properties and ultimately their applications.

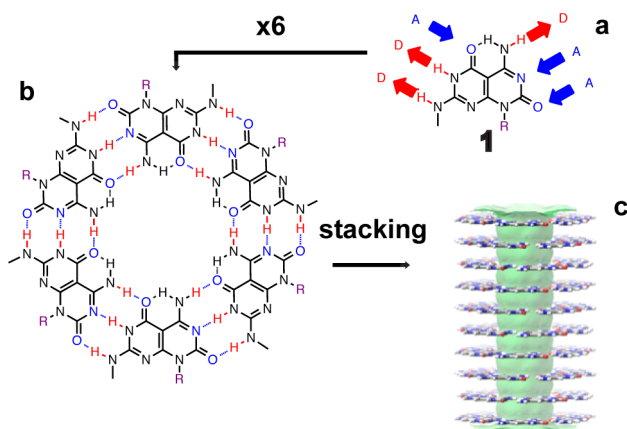


Figure A.1 G \wedge C motif. “D” and “A” refer to hydrogen bond donors and acceptors, respectively.

While we have reported several strategies to functionalize the G \wedge C motif,^{175, 177, 179, 193} they either relied on early functionalization via S_NAr, reductive amination or Suzuki cross-coupling late in the synthetic scheme. Here our aim was to develop a strategy that would allow us to streamline the synthesis of RNTs with predefined length by taking advantage of automated DNA synthesis methodology. A convergent approach illustrated in Figure A.2 was proposed, whereby the free amide nitrogen atom of intermediate **5** would be directly alkylated with the desired electrophile¹⁹⁴⁻¹⁹⁶ to provide **6**. Conversion to the corresponding phosphoramidite **7**¹⁹⁷ followed by oligomerization using automated DNA

synthesis,¹⁹⁸ then global deprotection, would furnish the corresponding G \wedge C oligomers. The latter are anticipated to undergo spontaneous self-assembly in water to generate discrete tubular architectures whose length is pre-determined by the length of the G \wedge C base oligomer.

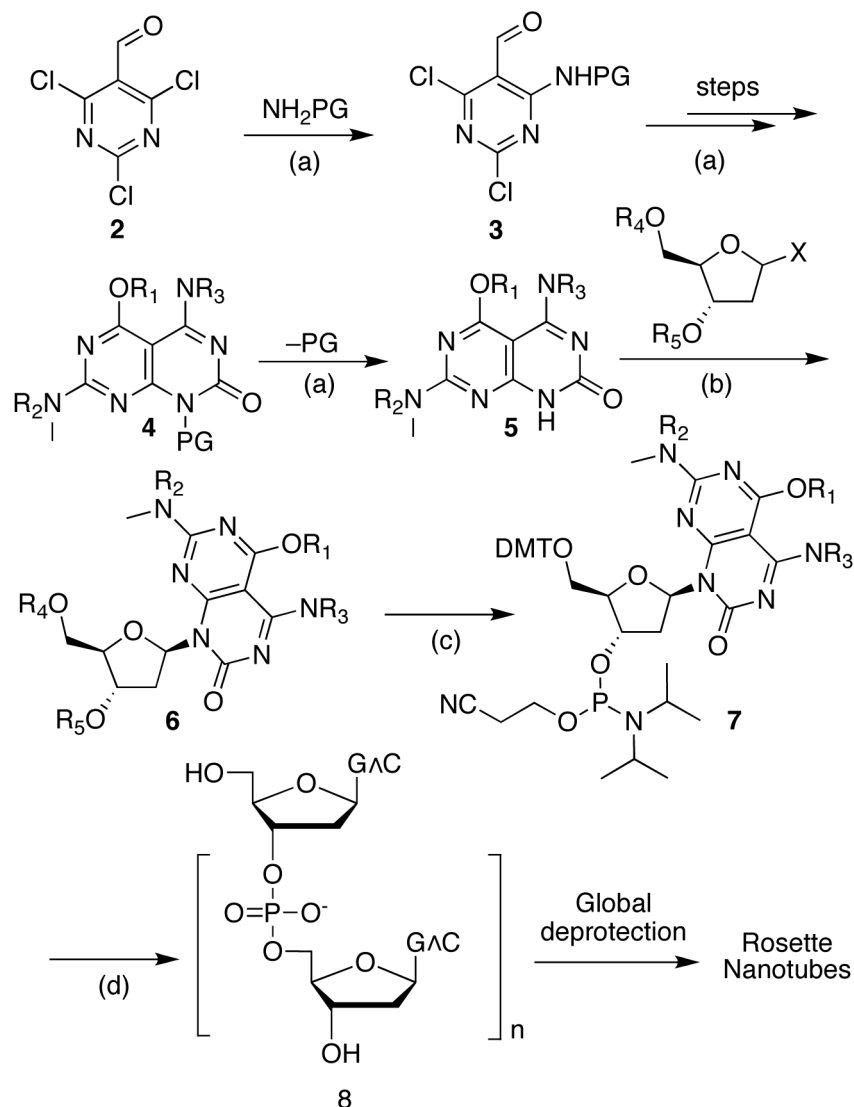


Figure A.2 Reagents and conditions scheme (a) According to the synthetic strategy detailed in this paper. (b) The ribose moiety would be prepared and coupled to the G \wedge C base according to previously reported procedures. (c) According to reported procedures. (d) Automated DNA synthesis.

A.2 Result and discussion

A.2.1 Protecting group strategies to access the free amide

The studies commenced by investigating protecting group strategies that would allow us to readily access the free amide **5** for the ensuing glycosylation reaction. We initially attempted a selective de-allylation reaction of an N-allylated G \wedge C base precursor **4** (PG = Allyl), the synthesis of which we have reported previously.^{175, 177-179, 193, 199} Despite using many different conditions, standard protocols such as Rh-catalyzed²⁰⁰ isomerization and Pd-catalyzed p-allyl methodologies^{201, 202} were unproductive in this deprotection reaction.

An alternative protecting group, trimethylsilyl ethane (TMSCH₂CH₂-) was next explored since its removal is known to be carried out under mild conditions (fluoride induced fragmentation).²⁰³ Furthermore, initial attempts at the S_NAr reaction between 2,4,6-trichloropyrimidine-5-carbaldehyde (**2**) and TMS-ethylamine proceeded in good yield (Figure A.3). Overall, compound **12** was synthesized from pyrimidine **2** in 9 steps in 82% average stepwise yield (18% overall). Unfortunately, treatment of **12** with fluoride sources such as TBAF, Et₃N•3HF, C₆H₅N•HF, CsF and KF under a variety of reaction conditions failed to unmask the amide. Basic (e.g. *n*BuLi) and acidic deprotection conditions (e.g. 4*N* HCl in dioxane at 45°C, 4 h) were also unsuccessful. The latter acidic conditions did remove the Bn and the Boc groups however, to provide G \wedge C base **13** in 80% yield (Figure A.3).

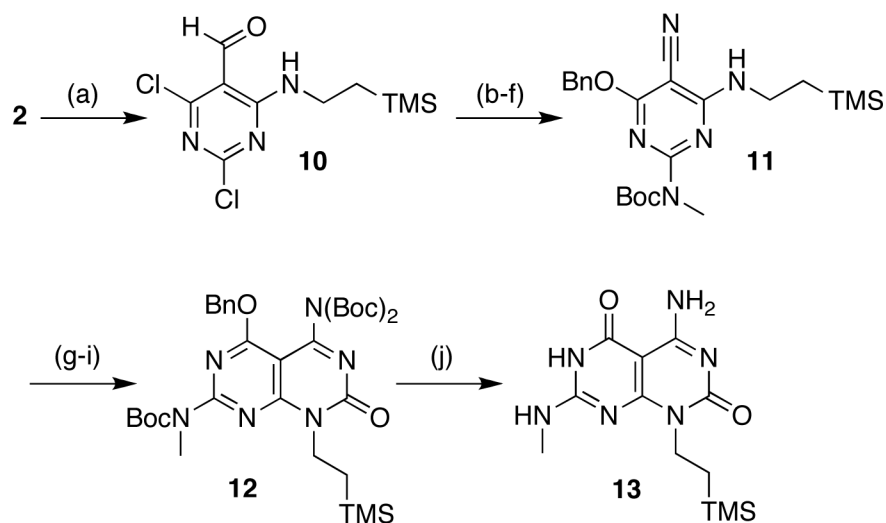


Figure A.3 Reagents and conditions (a) trimethylsilylethylamine hydrochloride,²⁰⁴ DIPEA, CH₂Cl₂, 60% (b) MeNH₂, THF, 88% (c) BnOH, NaH, THF, 77% (d) (Boc)₂O, DMAP, Et₃N, THF, 94% (e) NH₂OH·HCl, pyridine (f) TFAA, Et₃N, THF, 79%, 2 steps (g) *N*-(chlorocarbonyl) isocyanate, CH₂Cl₂, 78% (h) 7*N* NH₃ in MeOH, 97% (i) (Boc)₂O, DMAP, Et₃N, THF, 79% (j) 4*N* HCl in dioxane, 80%.

Given the unusual stability of the silyl derivative **12**, we decided to develop a fragmentation strategy that would yield the desired compound according to Figure A.4. We reasoned that the fragmentation could be triggered thermally via the cyclic transition state **22** (Path 1), or promoted with a primary or secondary amine (Path 2). In the latter case, imine **17** obtained from aldehyde **16** could tautomerize to the corresponding intermediate enamine **19**, which can then eliminate imine **20** to furnish the target compound **5** (tautomer of **21**). To test this strategy compound **16** was synthesized in 12 steps according to Scheme 4 and then treated with a variety of amines (Table A.1)

A.2.2 Deprotection of the G \wedge C base amide

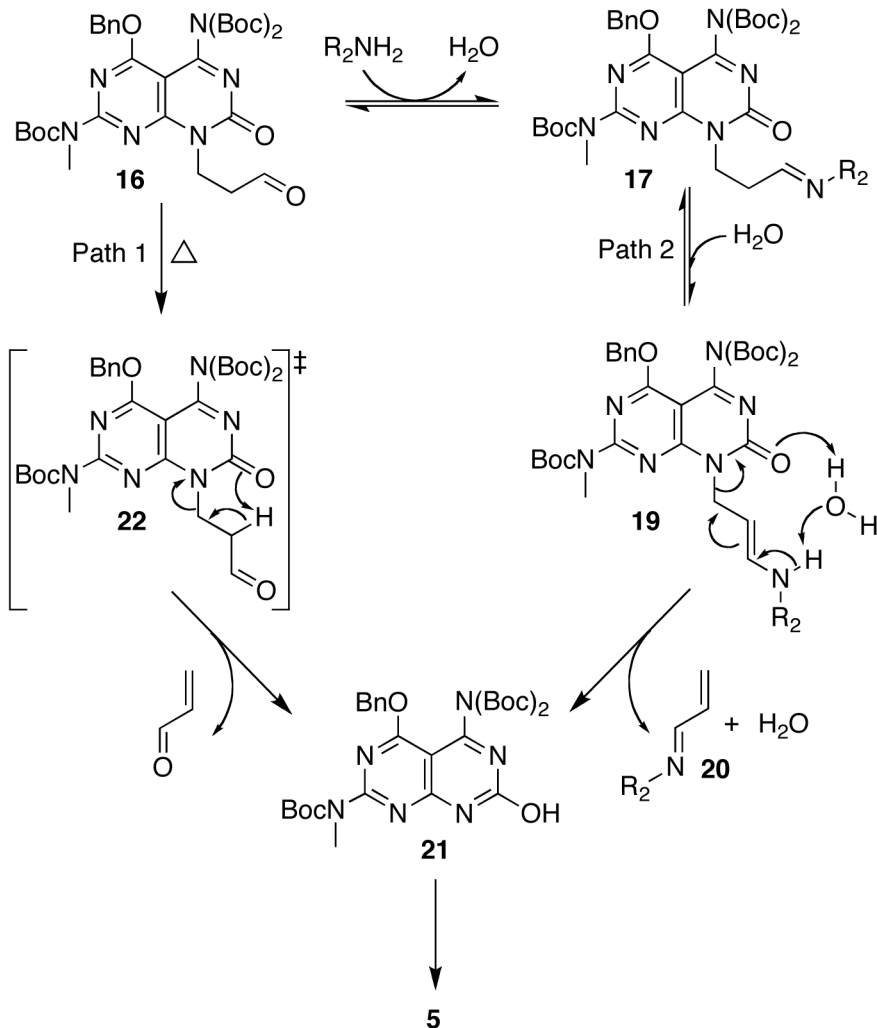


Figure A.4 Proposed mechanism for the deprotection of **16**.

While the thermal fragmentation gave several unidentified by-products along with target compound **5**, activation with primary amines gave **5** in good yields as shown in Table A.1. Secondary amines such as diethylamine were unproductive and only starting material was recovered after 24 h. Aromatic amines such as aniline were also ineffective, giving a mixture of products. Interestingly, performing the reaction for longer periods of time (>36 h) or heating (>40°C) with 0.25–2.0 equivalents of benzylamine led to a decline in the yield caused by the formation of the substituted product **18** (Figure A.5).

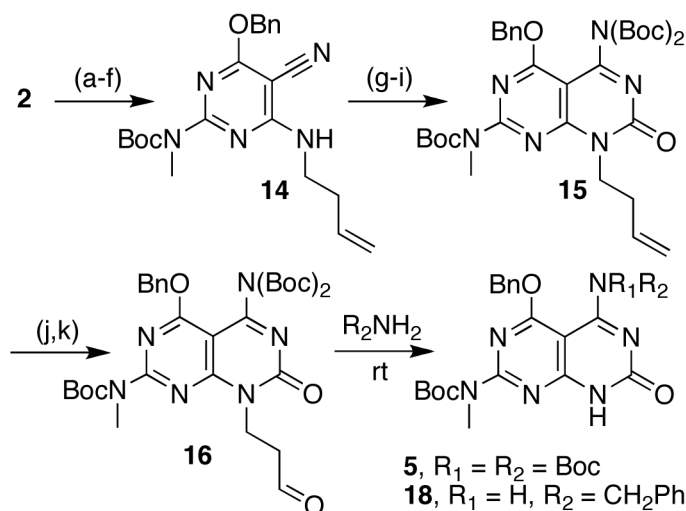


Figure A.5 Reagents and conditions (a) but-3-en-1-amine, CH_2Cl_2 , quant. (b) MeNH_2 , 4h, 92% (c) BnOH , NaH , THF, 74% (d) $(\text{Boc})_2\text{O}$, DMAP, Et_3N , THF, 98% (e) $\text{NH}_2\text{OH}\cdot\text{HCl}$, KHCO_3 , MeOH, 53% (f) TFAA, Et_3N , THF, 70% (g) *N*-(chlorocarbonyl) isocyanate, Et_3N , CH_2Cl_2 (h) 7*N* NH_3 in MeOH, 95%, 2 steps (i) $(\text{Boc})_2\text{O}$, DMAP, Et_3N , THF, 62% (j) OsO_4 , NMO, acetone/ H_2O , 77% (k) NaIO_4 , $\text{CH}_2\text{Cl}_2/\text{H}_2\text{O}$, 89%

While the thermal fragmentation gave several unidentified by-products along with target compound **5**, activation with primary amines gave **5** in good yields as shown in Table A.1. Secondary amines such as diethylamine were unproductive and only starting material was recovered after 24 h. Aromatic amines such as aniline were also ineffective, giving a mixture of products. Interestingly, performing the reaction for longer periods of time (>36 h) or heating (>40°C) with 0.25–2.0 equivalents of benzylamine led to a decline in the yield caused by the formation of the substituted product **18** (Figure A.5).

Table A.1 Deprotection of 16 in the presence of primary amines (in 1,2-dichloroethane, at room temperature for 24 h).

Entry	Amine	Yield %
1	L-lysine	56
2	methylamine	64
3	<i>n</i> -butylamine	67
4	benzylamine	92

A.2.3 Glycosylation

Finally, with compound **5** in hand, we proceeded to test the glycosylation reaction. As shown in Scheme 5, reaction of **5** with the toluyl-protected deoxyribose **23**¹⁹⁴⁻¹⁹⁶ was successfully performed in THF using NaH as a base.²⁰⁵ The resulting alkylated G \wedge C motif **24** was very unstable however, at both room temperature and -20°C due to the elimination of the sugar moiety which led to further decomposition. In order to improve its stability, the Boc groups of **24** were removed by adsorbing over silica gel under high vacuum. Subsequent purification using silica gel chromatography and reverse phase HPLC afforded the desired β anomer **25** in 22% yield (2 steps). The corresponding α anomer **26**, was also isolated in 10% yield (dr b/a, 96/4). Structural elucidation of both the β and α -adducts were unambiguously established using 1D and 2D NMR techniques (ROESY, COSY, HSQC, HMBC). In both cases, the presence of two conformational states²⁰⁶⁻²⁰⁸ were evident in the ^1H NMR taken at 25°C in $\text{DMSO}-d_6$.

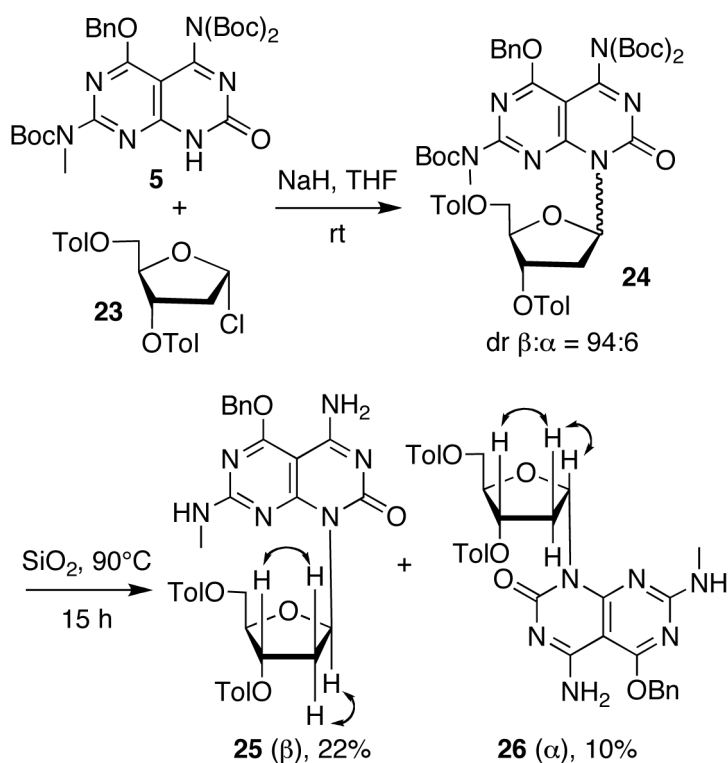


Figure A.6 Glycosylation and deprotection reaction of **5**.

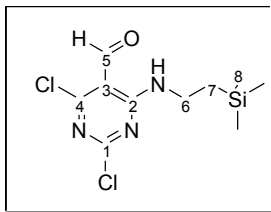
A.3 Conclusion

In this paper, we have described the synthesis of the β -glycoside compound **25**. This is an important key step for the synthesis of G \wedge C oligonucleotides, which we anticipate will readily self-assemble into RNTs with predefined length. During the course of these studies, we have also optimized a protecting group strategy for the urea nitrogen^{203, 209-212} of the G \wedge C base. More specifically, it was determined that oxidative cleavage of alkene **15** followed by treatment of aldehyde **16** with a primary amine (benzylamine) at room temperature in 1,2-dichloroethane for 24 h, generated the corresponding deprotected **5** in good yield. Current efforts will be focused on the synthesis of the phosphoramidite **7** from **25** as well as exploring alternative protecting group strategies for R² and R³ such as Bz, that are more traditionally used for the automated DNA synthesis technology.

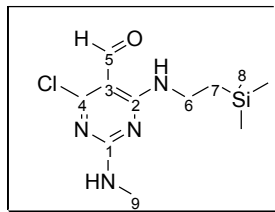
A.4 Materials and methods

All the reagents and solvent are commercially available from Aldrich, Fluka, or Fisher Scientific and were used without further purification. Chromatographic supports were silica flash Merck 60 (0.040–0.063 mm) or silica gel Merck 60 (0.063–0.2) for gravity chromatography. Silica-coated TLC plates (Merck F60254) were used for monitoring reactions.

^1H and ^{13}C -NMR spectra were recorded on Varian Inova spectrometers (400, 500, or 600 MHz). NMR data is presented as follows: chemical shift, peak assignment, multiplicity, coupling constant, and integration. Assignments were made from 2D-NMR techniques (ROESY, COSY, HSQC, HMBC). Mass Spectra were obtained at the Mass Spectrometry Facility at the Department of Chemistry, University of Alberta.

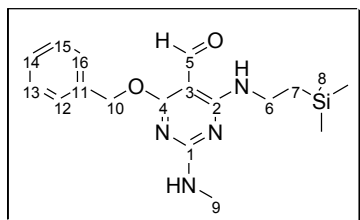


2,4-Dichloro-6-(2-(trimethylsilyl)ethylamino)pyrimidine-5-carbaldehyde (10). A solution of 2,4,6-trichloropyrimidine-5-carbaldehyde (300 mg, 1.42 mmol) in CH_2Cl_2 (2 mL) at -78°C was treated with DIPEA (0.30 mL, 1.7 mmol) followed by a solution of trimethylsilyl ethylamine hydrochloride (260 mg, 1.69 mmol) in CH_2Cl_2 (2 mL). After stirring for 2 h, the reaction was warmed to room temperature and stirred for an additional 12 h. The solvents were then removed under reduced pressure and the product was purified by flash chromatography on silica gel (5-8% EtOAc in hexanes) to provide 250 mg of **10** as a white solid ($\text{C}_{10}\text{H}_{15}\text{Cl}_2\text{N}_3\text{OSi}$, 60%). $R_f = 0.61$ (15% EtOAc in hexane), $\text{Mp} = 159^\circ\text{C} - 161^\circ\text{C}$. $^1\text{H-NMR}$ (300 MHz, CDCl_3) d (ppm) 10.25 (C_5H , s, 1H), 9.22 (NH, bs, 1H), 3.61 – 3.53 (C_6H , m, 2H), 0.96 – 0.88 (C_7H , m, 2H), 0.06 (C_8H , s, 9H); $^{13}\text{C-NMR}$ (125 MHz, CDCl_3) d (ppm) 188.1 (C_5), 165.4, 161.8, 160.5 (C_1 , C_2 , C_4), 101.5 (C_3), 37.8 (C_6), 17.7 (C_7), -1.68 (C_8); **CI-HRMS**: Calcd mass for $[\text{M}+\text{H}^+]/z$, 292.0434; Observed, 292.0432.

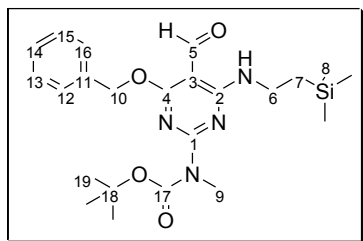


4-Chloro-2-(methylamino)-6-(2

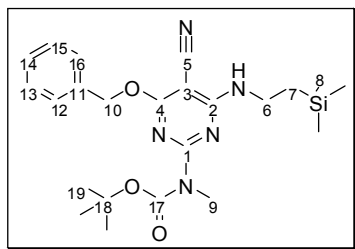
(trimethylsilyl)ethylamino)pyrimidine-5-carbaldehyde. A solution of **10** (750 mg, 2.57 mmol) in THF (10 mL) was treated with methylamine (2.86 mL, 2M in THF, 5.72 mmol) at 0 °C and then warmed to room temperature. After stirring for 2 h, the reaction was quenched with a saturated aqueous solution of NH₄Cl (1 mL) and the product was extracted with CH₂Cl₂ (3x). The combined organic phases were washed with water and brine, dried over anhydrous Na₂SO₄, filtered and concentrated. Purification by flash chromatography on silica gel (10-20% EtOAc in hexanes) provided 650 mg of 4-chloro-2-(methylamino)-6-(2-(trimethylsilyl)ethylamino)pyrimidine-5-carbaldehyde as a white solid (C₁₁H₁₉ClN₄OSi, 88%). R_f = 0.38 (10% EtOAc in hexanes), Mp = 178 °C - 180 °C. **¹H-NMR** (400 MHz, CDCl₃) δ (ppm) 10.03 (C₅H, s, 1H), 9.30 (NH, brs, 1H), 5.50 (NH, brs, 1H), 3.65 – 3.52 (C₆H, m, 2H), 3.01 (C₉H, d, J = 4.8 Hz, 3H), 1.04 – 0.91 (C₇H, m, 2H), 0.06 (C₈H, s, 9H); **¹³C-NMR** (100 MHz, CDCl₃) δ (ppm) 188.2 (C₅), 165.3, 161.7, 161.4 (C₁, C₂, C₄), 101.4 (C₃), 36.9 (C₆), 28.1 (C₉), 17.4 (C₇) -1.7 (C₈); **ES-HRMS:** Calcd mass for [M+H⁺]/z, 287.1095; Observed, 287.1090



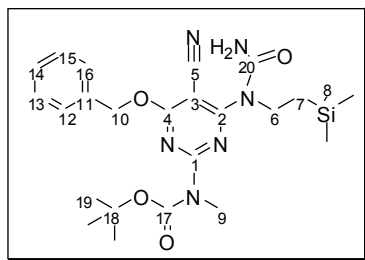
4-(Benzyloxy)-2-(methylamino)-6-(2-(trimethylsilyl)ethylamino)pyrimidine-5-carbaldehyde. Benzyl alcohol (0.046 mL, 0.45 mmol) was added to a suspension of NaH (13 mg, 0.52 mmol) in THF (1 mL) at room temperature. After stirring for 15 min, a solution of 4-chloro-2-(methylamino)-6-(2-(trimethylsilyl)ethylamino) pyrimidine-5-carbaldehyde (130 mg, 0.456 mmol) in THF (1 mL) was added and the mixture was refluxed for 24 h. After cooling down to 0 °C, the reaction was quenched with a saturated aqueous solution of NH₄Cl and the product was extracted with EtOAc (3x). The combined organic layers were washed with water and brine, dried over anhydrous Na₂SO₄, filtered and concentrated. Purification by flash chromatography on silica gel (3-5% EtOAc in hexanes) provided 125 mg of 4-(benzyloxy)-2-(methylamino)-6-(2-(trimethylsilyl)ethylamino)pyrimidine-5-carbaldehyde (C₁₈H₂₆N₄O₂Si, 77%) as an oil. R_f = 0.60 (5% MeCN in benzene). **¹H-NMR** (400 MHz, CDCl₃) δ (ppm) 9.99 (C₅H, s, 1H), 9.29 (NH, brs, 1H), 7.40 – 7.29 (C₁₂H – C₁₆H, m, 5H), 5.46 (NH, brs, 1H), 5.34 (C₁₀H, s, 2H), 3.59 – 3.46 (C₆H, m, 2H), 2.96 (C₉H d, *J* = 5.2 Hz, 3H), 0.99 – 0.92 (C₇H, m, 2H), 0.06 (C₈H, s, 9H); **¹³C-NMR** (100 MHz, CDCl₃) δ (ppm) 185.5 (C₅), 171.3 (C₄) 162.8, 162.5 (C₁, C₂), 136.5 (C₁₁), 128.2, 127.7 (C₁₂ – C₁₆), 92.4 (C₃), 67.1 (C₁₀), 36.4 (C₆), 27.9 (C₉), 17.6 (C₇) -1.8 (C₈); **EI-HRMS:** Calcd mass for [M+H⁺]/z, 359.1903; Observed, 359.1895.



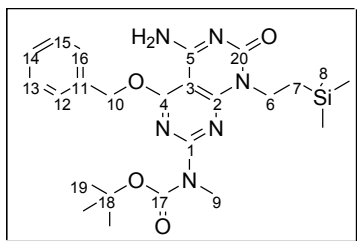
tert-Butyl 4-(benzyloxy)-5-formyl-6-(2-(trimethylsilyl)ethylamino)pyrimidin-2-yl(methyl) carbamate. Boc₂O (288 mg, 1.32 mmol) was added to a solution of 4-(benzyloxy)-2-(methylamino)-6-(2-(trimethylsilyl)ethylamino)pyrimidine-5-carbaldehyde (400 mg, 1.11 mmol), DMAP (13 mg, 0.11 mmol) and Et₃N (0.46 mL, 3.3 mmol) in THF (4 mL) at room temperature. After stirring for 24 h, the reaction was quenched with water and the product was extracted with EtOAc (3x). The combined organic layers were washed with water and brine, dried over anhydrous Na₂SO₄, filtered and concentrated. Purification by flash chromatography on silica gel (2-3% EtOAc in hexanes) provided 480 mg of *tert*-butyl 4-(benzyloxy)-5-formyl-6-(2-(trimethylsilyl)ethylamino)pyrimidin-2-yl(methyl) carbamate as a foam (C₂₃H₃₄N₄O₄Si, 94%). R_f = 0.62 (15% EtOAc in hexanes). **¹H-NMR** (400 MHz, CDCl₃) δ (ppm) 10.12 (C₅H, s, 1H), 9.09 (NH, brs, 1H), 7.44 – 7.33 (C₁₂H – C₁₆H, m, 5H), 5.47 (C₁₀H, s, 2H), 3.60 – 3.54 (C₆H, m, 2H), 3.39 (C₉, s, 3H), 1.55 (C₁₉H, s, 9H), 0.97 – 0.93 (C₇H, m, 2H), 0.05 (C₈H, s, 9H); **¹³C-NMR** (100 MHz, CDCl₃) δ (ppm) 187.2 (C₅), 171.3 (C₄) 162.1, 161.7 (C₁, C₂), 153.6 (C₁₇), 136.2 (C₁₁), 128.3, 128.0, 127.8 (C₁₂ – C₁₆), 93.9 (C₃), 81.5 (C₁₈), 68.0 (C₁₀), 36.9 (C₆), 34.4 (C₉), 28.0 (C₁₉), 17.6 (C₇), -1.8 (C₈); **ES-HRMS:** Calcd mass for [M+H⁺]/z, 459.2422; Observed, 459.2420.



tert-Butyl 4-(benzyloxy)-5-cyano-6-(2-(trimethylsilyl)ethylamino)pyrimidin-2-yl(methyl) carbamate (11). $\text{NH}_2\text{OH}\cdot\text{HCl}$ (243 mg, 3.50 mmol) was added to a solution of *tert*-butyl 4-(benzyloxy)-5-formyl-6-(2-(trimethylsilyl)ethylamino)pyrimidin-2-yl(methyl) carbamate (800 mg, 1.75 mmol) in pyridine (5 mL) at room temperature. After stirring for 3 h, the pyridine was removed under reduced pressure and the product was extracted with EtOAc (3x). The combined organic layers were washed with saturated aqueous solution of NaHCO_3 , followed by water and brine, dried over anhydrous Na_2SO_4 , filtered and concentrated. The crude product (735 mg, 1.55 mmol) was then dissolved in THF (5 mL), cooled to 0°C and treated with Et_3N (0.65 mL, 4.7 mmol). TFAA (0.33 mL, 2.3 mmol) was then added and the mixture was stirred for 15 min at 0°C , followed by 5 h at 80°C . After cooling to room temperature, EtOAc (60 mL) was added and the organic layer was washed with water and brine, dried over anhydrous Na_2SO_4 , filtered and concentrated. Purification by flash chromatography on silica gel (5-8% EtOAc in hexanes) afforded 530 mg of **11** as a paste ($\text{C}_{23}\text{H}_{33}\text{N}_5\text{O}_3\text{Si}$, 79%). $R_f = 0.53$ (15% EtOAc in hexanes). **$^1\text{H-NMR}$** (400 MHz, CDCl_3) d (ppm) 7.39 – 7.27 ($\text{C}_{12}\text{H} - \text{C}_{16}\text{H}$, m, 5H), 5.42 (C_{10}H , s, 2H), 5.34 (C_6NH , m, 1H), 3.53 – 3.48 (C_6H , m, 2H), 3.32 (C_9H , s, 3H), 1.50 (C_{19}H , s, 9H), 0.90 – 0.86 (C_7H , m, 2H), 0.02 (C_8H , s, 9H); **$^{13}\text{C-NMR}$** (100 MHz, CDCl_3) d (ppm) 170.2 (C_4), 163.7, 160.8 (C_1, C_2), 153.5 (C_{17}), 135.9 (C_{11}), 128.4, 128.1, 127.9 ($\text{C}_{12} - \text{C}_{16}$), 114.8 (C_5), 81.8 (C_{18}), 68.7, 68.4 ($\text{C}_{10}, \text{C}_3$), 38.0 (C_6), 34.5 (C_9), 28.1 (C_{19}), 17.8 (C_7), -1.7 (C_8); **ES-HRMS**: Calcd mass for $[\text{M}+\text{H}^+]/z$, 456.2426; Observed, 456.2425.

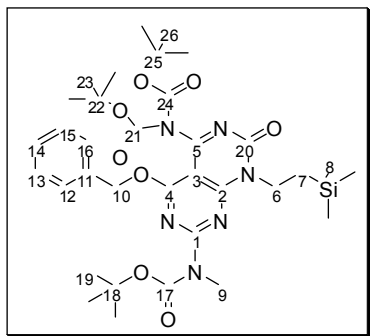


tert-Butyl 4-(benzyloxy)-5-cyano-6-(1-(2-(trimethylsilyl)ethyl)ureido)pyrimidin-2-yl(methyl)carbamate. *N*-chlorocarbonylisocyanate (0.025 mL, 0.30 mmol) was added dropwise to a solution of **11** (70 mg, 0.15 mmol) in CH₂Cl₂ (3 mL) at 0 °C. After stirring for 2 h, the reaction was warmed to room temperature and stirred for an additional 3 h. The mixture was then cooled to 0 °C and quenched with water. The product was extracted with CHCl₃ (3x) and the combined organic layers were washed with saturated aqueous NaHCO₃ and brine, dried over anhydrous Na₂SO₄, filtered and concentrated to provide 60 mg of *tert*-butyl 4-(benzyloxy)-5-cyano-6-(1-(2-(trimethylsilyl)ethyl)ureido)pyrimidin-2-yl(methyl)carbamate (C₂₄H₃₄N₆O₄Si, 78%) as a white solid. The product was used in the next step without further purification. R_f = 0.27 (5% MeOH/CH₂Cl₂). Mp = 165 °C – 166 °C. ¹H-NMR (400 MHz, CDCl₃) d (ppm) 7.46 – 7.32 (C₁₂H – C₁₆H, m, 5H), 5.51 (C₁₀H, s, 2H), 4.30 – 4.26 (C₆H, m, 2H), 3.41 (C₉H, s, 3H), 1.53 (C₁₉H, s, 9H), 1.04 – 1.01 (C₇H, m, 2H), 0.06 (C₈H, s, 9H); ¹³C-NMR (100 MHz, CDCl₃) d (ppm) 172.3 (C₄), 163.3, 158.7, 155.6, 152.6 (C₁, C₂, C₂₀, C₁₇), 135.4 (C₁₁), 128.8, 128.6, 127.8 (C₁₂ – C₁₆), 113.8 (C₅), 83.5 (C₁₈), 69.8 (C₁₀, C₃), 43.9 (C₆), 34.6 (C₉), 28.2 (C₁₉), 17.6 (C₇), -1.4 (C₈); **ES-HRMS:** Calcd mass for [M+Na⁺]/z, 521.2303; Observed, 521.2303.

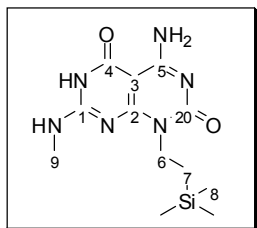


***tert*-Butyl 4-amino-5-(benzyloxy)-1,2-dihydro-1-(2-(trimethylsilyl)ethyl)-2-oxopyrimido[4,5-*d*]pyrimidin-7-**

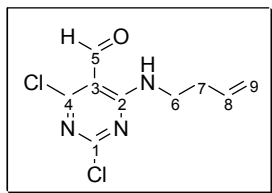
ylmethylcarbamate. A solution of *tert*-butyl 4-(benzyloxy)-5-cyano-6-(1-(2-(trimethylsilyl)ethyl)ureido)pyrimidin-2-yl(methyl)carbamate (60 mg, 0.12 mmol) in MeOH (2 mL) and treated with 7N NH₃ in methanol (1 mL) at room temperature. After stirring for 3 h, the solution was concentrated and the yellow solid was washed with Et₂O, centrifuged, collected and dried under high vacuum to furnish 60 mg of *tert*-butyl 4-amino-5-(benzyloxy)-1,2-dihydro-1-(2-(trimethylsilyl)ethyl)-2-oxopyrimido[4,5-*d*]pyrimidin-7-ylmethylcarbamate as a solid (C₂₅H₃₈N₆O₄Si, 97%). R_f = 0.55 (5% MeOH in CHCl₃), Mp = decomposes > 315 °C. **¹H-NMR** (600 MHz, CDCl₃) d (ppm) 7.71 (NH, brs, 1H), 7.46 – 7.35 (C₁₂H – C₁₆H, m, 5H), 7.00 (NH, brs, 1H), 5.62 (C₁₀H, s, 2H), 4.26 – 4.23 (C₆H, m, 2H), 3.44 (C₉H, s, 3H), 1.57 (C₁₉H, s, 9H), 1.04 – 1.01 (C₇H, m, 2H), 0.07 (C₈H, s, 9H); **¹³C-NMR** (150 MHz, CDCl₃) d (ppm) 166.4 (C₄), 160.8, 160.7, 160.2 (C₁, C₂, C₅), 155.8, 152.9 (C₂₀, C₁₇), 135.1 (C₁₁), 128.82, 128.80, 128.6 (C₁₂ – C₁₆), 86.1 (C₃), 82.3 (C₁₈), 69.8 (C₁₀), 39.4 (C₆), 34.8 (C₉), 28.2 (C₁₉), 16.2 (C₇), -1.7 (C₈); **ES-HRMS:** Calcd mass for [M+H⁺]/z, 499.2489; Observed, 499.2484.



***tert*-Butyl 4-(benzyloxy)-5-(*di-tert*-butylaminodicarbonate)-7-oxo-8-(2-(trimethylsilyl)ethyl)-7,8-dihydropyrimido[4,5-*d*]pyrimidin-2-yl(methyl)carbamate (12).** (Boc)₂O (210 mg, 0.96 mmol) was added to a solution of *tert*-butyl 4-amino-5-(benzyloxy)-1,2-dihydro-1-(2-(trimethylsilyl)ethyl)-2-oxopyrimido[4,5-*d*]pyrimidin-7-ylmethylcarbamate (120 mg, 0.240 mmol), Et₃N (0.10 mL, 0.72 mmol) and DMAP (30 mg, 0.24 mmol) in THF (4 mL). After stirring for 12 h, the reaction was quenched with water and the product was extracted with EtOAc (3x). The combined organic layers were washed successively with saturated aqueous NaHCO₃ solution, water and brine, dried over anhydrous Na₂SO₄, filtered and concentrated. Purification by flash chromatography on silica gel (15-20% EtOAc in hexanes) provided 135 mg of **12** (C₃₅H₅₄N₆O₈Si, 79%) as a white foam. R_f = 0.67 (50% EtOAc in hexanes). **¹H-NMR** (300 MHz, CDCl₃) d (ppm) 7.44 – 7.32 (C₁₂H – C₁₆H, m, 5H), 5.57 (C₁₀H, s, 2H), 4.37 – 4.34 (C₆H, m, 2H), 3.47 (C₉H, s, 3H), 1.59 (C₁₉H, s, 9H), 1.32 (C₂₃H, C₂₆H, s, 18H), 1.09 – 1.06 (C₇H, m, 2H), 0.09 (C₈H, s, 9H); **¹³C-NMR** (150 MHz, CDCl₃) d (ppm) 165.7 (C₄), 161.1, 160.5, 159.9 (C₁, C₂, C₅), 155.4, 152.5 (C₂₀, C₁₇), 149.2 (C₂₁, C₂₄), 134.9 (C₁₁), 128.5, 128.43, 128.39 (C₁₂ – C₁₆), 93.0 (C₃), 83.5 (C₂₂, C₂₅), 82.8 (C₁₈), 69.9 (C₁₀), 40.5 (C₆), 34.8 (C₉), 28.1 (C₁₉), 27.8 (C₂₃, C₂₆), 15.8 (C₇), -1.7 (C₈); **ES-HRMS**: Calcd mass for [M+Na⁺]/z, 721.3357; Observed, 721.3351



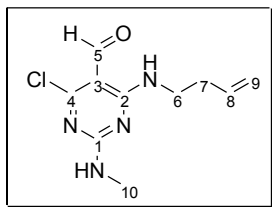
4-Amino-7-(methylamino)-1-(2-(trimethylsilyl)ethyl)pyrimido[4,5-d]pyrimidine-2,5(1H,6H)-dione (13). A solution of **12** (200 mg, 0.286 mmol) in 4*N* HCl in dioxane (1.5 mL) was stirred for 4 h at 45°C. The solution was then concentrated and Et₂O was added. The resulting mixture was centrifuged and the solid was collected, washed with Et₂O and centrifuged again. After repeating the process 3 times, the white solid was dried under high vacuum to provide 88 mg of **13** (C₁₂H₂₀N₆O₂Si + 1/3H₂O + 1/3Et₂O + 4/3HCl, 80%). Mp = decomposes > 300°C. **¹H-NMR** (400 MHz, DMSO-*d*₆) δ (ppm) 12.23 (NH, brs, 1H), 9.14 (NH, s, 1H), 8.55 (NH, s, 1H), 8.01 (NH, s, 1H), 4.08 (C₆H, m, 2H), 2.93 (C₉H, s, 3H), 0.94 (C₇H, m, 2H), 0.04 (C₈H, s, 9H); **¹³C-NMR** (100 MHz, DMSO-*d*₆) δ (ppm) 161.6, 159.7, 156.0, 155.8 (C₄, C₂, C₅, C₁), 147.7 (C₂₀), 82.4 (C₃), 69.9 (C₆), 27.9 (C₉), 15.6 (C₇), -1.9 (C₈); **ES-HRMS**: Calcd mass for [M+H⁺]⁺/z, 309.1490; Observed, 309.1493; **Elemental Analysis**: Calcd for C₁₂H₂₀N₆O₂Si + 1/3H₂O + 1/3Et₂O + 4/3HCl, C = 41.30%, H = 6.59%, N = 21.67%; Observed, C = 41.27 %, H = 6.25%, N = 21.44%.



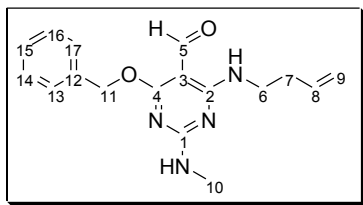
4-(But-3-enylamino)-2,6-dichloropyrimidine-5-carbaldehyde.

A

solution of 2,4,6-trichloropyrimidine-5-carbaldehyde (**2**) (13 g, 62 mmol) in CH_2Cl_2 at -78°C was treated with but-3-en-1-amine (8.7 g, 81 mmol). After stirring for 6 h at -78°C , the solution was warmed to -20°C over a period of 2 h. The reaction was then quenched with dH_2O (20 mL) and the product was extracted with CH_2Cl_2 (3x). The combined organic layers were washed with dH_2O , brine, dried over anhydrous sodium sulfate, filtered and concentrated *in vacuo*. Purification by flash chromatography on silica gel (100% hexanes – 2% EtOAc in hexanes) provided 15.2 g of 4-(but-3-enylamino)-2,6-dichloropyrimidine-5-carbaldehyde ($\text{C}_9\text{H}_9\text{Cl}_2\text{N}_3\text{O}$, quant.) as a yellow oil. $R_f = 0.55$ (10% EtOAc in hexanes). **$^1\text{H-NMR}$** (200 MHz, CDCl_3) d (ppm) 10.32 (C_5H , s, 1H), 9.33 (NH s, 1H), 5.84 – 5.76 (C_8H , m, 1H), 5.20 – 5.15 (C_9H , m, 2H), 3.67 (C_6H , m, 2H), 2.43 – 2.38 (C_7H , q, $J = 6.8$ Hz, 2H); **$^{13}\text{C-NMR}$** (125 MHz, CDCl_3) d (ppm) 189.8 (C_5), 165.4, 162.1, 161.1 ($\text{C}_1, \text{C}_2, \text{C}_4$), 133.9 (C_8), 117.5 (C_9), 106.0 (C_3), 40.1 (C_6), 32.6 (C_7); **EI-HRMS**: Calcd mass for $[\text{M}+\text{H}^+]/z$, 245.0115; Observed, 245.0108.

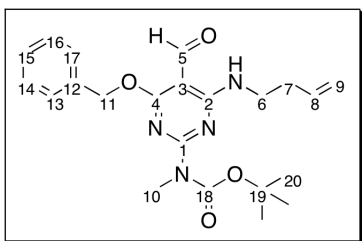


4-(But-3-enylamino)-6-chloro-2-(methylamino)pyrimidine-5-carbaldehyde. A solution of 4-(but-3-enylamino)-2,6-dichloropyrimidine-5-carbaldehyde (9.6 g, 39 mmol) in THF (250 mL) at 0 °C was treated with methylamine (39 mL, 2M in THF, 78 mmol). After stirring for 2 h at 0 °C, the mixture was warmed to room temperature and stirred for an additional 2 h. The reaction was then quenched with a saturated aqueous solution of NH₄Cl and the solvent was removed *in vacuo*. The product was extracted with CH₂Cl₂ (3x) and the combined organic phases were washed successively with dH₂O and brine, dried over anhydrous Na₂SO₄, filtered and concentrated. Purification by flash chromatography on silica gel (100% hexanes – 8% EtOAc in hexanes) afforded 8.7 g of 4-(but-3-enylamino)-6-chloro-2-(methylamino)pyrimidine-5-carbaldehyde (C₁₀H₁₃ClN₄O, 92%) as a white foam. R_f = 0.29 (10% EtOAc in hexanes). **¹H-NMR** (200 MHz, CDCl₃) d (ppm) 10.03 (C₅H, s, 1H), 9.31 (NH, brs, 1H), 7.43 (NH, d, *J* = 4.5 Hz, 1H), 5.91 – 5.71 (C₈H, m, 1H), 5.16 – 5.04 (C₉H, m, 2H), 3.58 (C₆H, m, 2H), 3.00 (C₁₀H, d, *J* = 6.0 Hz, 3H), 2.37 (C₇H, q, *J* = 6.1 Hz, 2H); **¹³C-NMR** (50 MHz, CDCl₃) d (ppm) 188.0 (C₅), 165.0, 162.0, 161.2 (C₁, C₂, C₄), 135.0 (C₈), 117.1 (C₉), 101.3 (C₃), 39.8 (C₆), 33.2 (C₇), 28.0 (C₁₀); **EI-HRMS:** Calcd mass for [M+H⁺]/z, 241.0801; Observed, 241.0799.

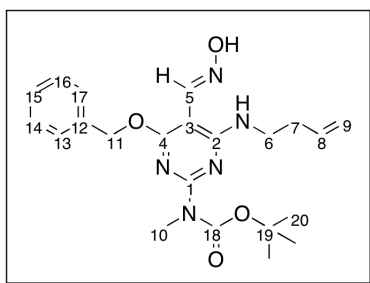


4-(Benzyloxy)-6-(but-3-enylamino)-2-(methylamino)pyrimidine-5-carbaldehyde

A mixture of NaH (3.61 g, 95%, 143 mmol) in THF (300 mL) at 0 °C was slowly treated with benzyl alcohol (3.7 mL, 36 mmol). After stirring for 30 min, 4-(but-3-enylamino)-6-chloro-2-(methylamino)pyrimidine-5-carbaldehyde (8.6 g, 36 mmol) was added and the mixture was refluxed overnight. After cooling to 0 °C, the reaction was carefully quenched with an aqueous 10% citric acid solution. The solvent was then removed *in vacuo* and the product was extracted with EtOAc (3x). The combined organic layers were washed successively with 5% aqueous Na₂CO₃, dH₂O, brine, dried over anhydrous Na₂SO₄, filtered and concentrated. Purification by flash chromatography on silica gel (100% hexanes – 4% EtOAc in hexanes) afforded 8.2 g of 4-(benzyloxy)-6-(but-3-enylamino)-2-(methylamino)pyrimidine-5-carbaldehyde (C₁₇H₂₀N₄O₂, 74%) as a viscous yellow oil. R_f = 0.62 (5% acetonitrile in benzene). **¹H-NMR** (300 MHz, CDCl₃) d (ppm) 9.98 (C₅H, s, 1H), 9.28 (NH, brs, 1H), 9.12 (NH, brs, 1H), 7.38 – 7.31 (C₁₃H – C₁₇H, m, 5H), 5.83 (C₈H, m, 1H), 5.36 (C₁₁H, s, 2H), 5.17 – 5.07 (C₉H, m, 2H), 3.62 – 3.49 (C₆H, m, 2H), 2.99 (C₁₀H, d, *J* = 5.1 Hz, 3H), 2.40 – 2.26 (C₇H, m, 2H); **¹³C-NMR** (125 MHz, CDCl₃) d (ppm) 185.3 (C₅), 170.9 (C₄), 163.1, 162.5 (C₁, C₂), 136.4 (C₁₂), 135.1 (C₈), 128.0 – 126.5 (C₁₃ – C₁₇), 116.5 (C₉), 92.4 (C₃), 67.0 (C₁₁), 39.5 (C₆), 33.4 (C₇), 27.7 (C₁₀); **EI-HRMS**: Calcd mass for M⁺/*z*, 312.1586; Observed, 312.1593.

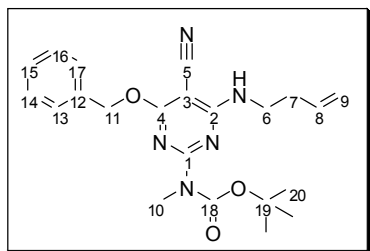


tert-Butyl 4-(benzyloxy)-6-(but-3-enylamino)-5-formylpyrimidin-2-ylmethylcarbamate. (Boc)₂O (5.6 g, 26 mmol) was added to a solution of 4-(benzyloxy)-6-(but-3-enylamino)-2-(methylamino)pyrimidine-5-carbaldehyde (5.4 g, 17 mmol), Et₃N (7.3 mL, 52 mmol) and DMAP (1.1 g, 8.6 mmol) in THF (200 mL) at room temperature. After stirring overnight, the reaction was quenched with dH₂O and the solution was concentrated under reduced pressure. The product was extracted with Et₂O (3x) and the combined organic layers were washed successively with 10% aqueous citric acid, 5% aqueous Na₂CO₃, dH₂O and brine, dried over anhydrous Na₂SO₄, filtered and concentrated *in vacuo*. Purification by flash chromatography on silica gel (100% hexanes – 2% EtOAc in hexanes) provided 7 g of *tert*-butyl 4-(benzyloxy)-6-(but-3-enylamino)-5-formylpyrimidin-2-ylmethylcarbamate (C₂₂H₂₈N₄O₄, 98%) as a white foam. R_f = 0.35 (10% EtOAc in hexanes). **¹H-NMR** (500 MHz, CDCl₃) d (ppm) 9.17 (C₅H, s, 1H), 7.44 – 7.33 (C₁₃H – C₁₇H, m, 5H), 5.85 – 5.80 (C₈H, m, 1H), 5.48 (C₁₁H, s, 2H), 5.17 – 5.09 (C₉H, m, 2H), 3.63 – 3.59 (C₆H, dt, *J* = 7.0 Hz, 7.0 Hz, 2H), 3.40 (C₁₀H, s, 3H), 2.40 – 2.36 (C₇H, q, *J* = 7.0 Hz, 2H), 1.56 (C₂₀H, s, 9H); **¹³C-NMR** (50 MHz, CDCl₃) d (ppm) 187.2 (C₅), 171.1 (C₄), 162.4, 161.5 (C₁, C₂), 153.5 (C₁₈), 136.1 (C₁₂), 134.8 (C₈), 128.2, 128.0, 127.7 (C₁₃ – C₁₇), 116.9 (C₉), 93.9 (C₃), 81.5 (C₁₉), 67.9 (C₁₁), 49.8 (C₆), 34.4 (C₇), 33.5 (C₁₀), 27.9 (C₂₀); **ESI-HRMS:** Calcd mass for [M+H⁺]/*z*, 413.2183; Observed, 413.2186.

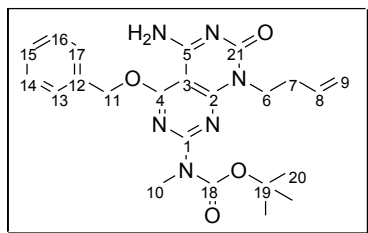


***tert*-Butyl 4-(benzyloxy)-6-(but-3-enylamino)-5-((hydroxyimino)methyl)**

pyrimidin-2-yl(methyl)carbamate. KHCO_3 (17.0 g, 170 mmol) and hydroxylamine hydrochloride (6.9 g, 97 mmol) were added to a solution of *tert*-butyl 4-(benzyloxy)-6-(but-3-enylamino)-5-formylpyrimidin-2-ylmethylcarbamate (10 g, 24 mmol) in MeOH (150 mL) at 0 °C. After refluxing for 6 h, the mixture was cooled to 0 °C and quenched with dH_2O . The solvent was removed *in vacuo* and the product was extracted with EtOAc (3x). The combined organic layers were washed with dH_2O and brine, dried over anhydrous Na_2SO_4 , filtered and concentrated. Purification by flash chromatography on silica gel (100% hexanes – 3% EtOAc in hexanes) provided 5.5 g of *tert*-butyl 4-(benzyloxy)-6-(but-3-enylamino)-5-((hydroxyimino)methyl)pyrimidin-2-yl(methyl)carbamate ($\text{C}_{22}\text{H}_{29}\text{N}_5\text{O}_4$, 53%) as a yellow oil. $R_f = 0.35$ (20% EtOAc/hexanes). **$^1\text{H-NMR}$** (300 MHz, CDCl_3) d (ppm) 9.04 (C_5NOH , s, 1H), 8.59 (C_5H , s, 1H), 8.15 (C_6NH , t, $J = 5.3$ Hz, 1H), 7.45 – 7.29 ($\text{C}_{13}\text{H} - \text{C}_{17}\text{H}$, m, 5H), 5.87 – 5.78 (C_8H , m, 1H), 5.46 (C_{11}H , s, 2H), 5.15 – 5.05 (C_9H , m, 2H), 3.66 – 3.59 (C_6H , dt, $J = 6.6$ Hz, 6.0 Hz, 2H), 3.43 (C_{10}H , s, 3H), 2.40 – 2.33 (C_7H , q, $J = 6.9$ Hz, 2H), 1.59 (C_{20}H , s, 9H); **$^{13}\text{C-NMR}$** (75 MHz, CDCl_3) d (ppm) 166.9, 160.6, 158.8 ($\text{C}_1, \text{C}_2, \text{C}_4$), 154.3 (C_{18}), 145.5 (C_5), 136.6 (C_{12}), 135.2 (C_8), 128.2, 127.7 ($\text{C}_{13} - \text{C}_{17}$), 116.6 (C_9), 87.8 (C_3), 81.2 (C_{19}), 67.9 (C_{11}), 40.3 (C_6), 34.6 (C_7), 33.7 (C_{10}), 28.1 (C_{20}); **ESI-HRMS:** Calcd mass for $[\text{M}+\text{H}^+]/z$, 428.2292; Observed, 428.2294.



tert-Butyl 4-(benzyloxy)-6-(but-3-enylamino)-5-cyanopyrimidin-2-yl(methyl)carbamate (14). Trifluoroacetic anhydride (3.5 mL, 25 mmol) was slowly added to a solution of *tert*-butyl 4-(benzyloxy)-6-(but-3-enylamino)-5-((hydroxyimino)methyl)pyrimidin-2-yl(methyl)carbamate (9.8 g, 23 mmol), Et₃N (9.5 mL, 68 mmol) and THF (200 mL) at 0 °C. After refluxing for 4 h, the reaction was cooled to 0 °C and quenched with dH₂O. The solvent was removed under reduced pressure and the product was extracted with Et₂O (3x). The combined organic phases were washed successively with 10% aqueous citric acid, 5% aqueous Na₂CO₃, dH₂O and brine, dried over anhydrous Na₂SO₄, filtered and concentrated *in vacuo*. Purification by flash chromatography on silica gel (100% hexanes – 2% EtOAc in hexanes) provided 6.5 g of **14** (C₂₂H₂₇N₅O₃, 70%) as a yellow foam. R_f = 0.25 (10% EtOAc in hexanes). ¹H-NMR (400 MHz, CDCl₃) d (ppm) 7.45 – 7.32 (C₁₃H – C₁₇H, m, 5H), 5.82 – 5.76 (C₈H, m, 1H), 5.47 (C₁₁H, s, 2H), 5.39 (NH, 1H), 5.17 – 5.10 (C₉H, m, 2H), 3.61 – 3.58 (C₆H, m, 2H), 3.37 (C₁₀H, s, 3H), 2.39 – 2.36 (C₇H, m, 2H), 1.55 (C₂₀H, s, 9H); ¹³C-NMR (75 MHz, CDCl₃) d (ppm) 170.1 (C₄), 163.9, 160.6 (C₁, C₂), 153.3 (C₁₈), 135.8 (C₁₂), 134.6 (C₈), 128.2, 127.9, 127.7 (C₁₃ – C₁₇), 117.3 (C₉), 114.5 (C₅), 81.7 (C₁₉), 68.7 (C₃), 68.3 (C₁₁), 40.2 (C₆), 34.4 (C₇), 33.4 (C₁₀), 28.0 (C₂₀); **ESI-HRMS:** Calcd mass for [M+H⁺]/z, 410.2187; Observed, 410.2191.



tert-Butyl 4-amino-5-(benzyloxy)-1-(but-3-enyl)-1,2-dihydro-2-oxypyrimido[4,5-d]pyrimidin-7-ylmethylcarbamate.

N-chlorocarbonylisocyanate (0.36 mL, 4.9 mmol) was slowly added to a solution of *tert*-butyl 4-(benzyloxy)-6-(but-3-enylamino)-5-cyanopyrimidin-2-yl(methyl)carbamate (1.0 g, 2.4 mmol) and Et₃N (0.68 mL, 4.9 mmol) in CH₂Cl₂ at 0 °C. After stirring for 2 h, the reaction was quenched with dH₂O and the organic layer was separated, dried over anhydrous Na₂SO₄, filtered and concentrated *in vacuo*. The resulting solid was dissolved in MeOH (30 mL), cooled to 0 °C and then treated with 7 *N* NH₃ in MeOH (12 mL). After stirring for 2 h, the reaction was concentrated and the product was extracted with CH₂Cl₂ (3x). The combined organic layers were washed with dH₂O and brine, dried over anhydrous Na₂SO₄, filtered and concentrated. Purification by flash chromatography on silica gel (100% CH₂Cl₂ followed by 2% MeOH in CH₂Cl₂) provided 1.05 g of *tert*-butyl 4-amino-5-(benzyloxy)-1-(but-3-enyl)-1,2-dihydro-2-oxypyrimido[4,5-d]pyrimidin-7-ylmethylcarbamate (C₂₃H₂₈N₆O₄, 95%) as a white foam. R_f = 0.34 (10% MeOH in CH₂Cl₂). ¹H-NMR (500 MHz, CDCl₃) δ (ppm) 7.47 – 7.35 (C₁₃H – C₁₇H, m, 5H), 7.09 (NH, brs, 1H), 5.88 – 5.62 (C₈H, m, 1H), 5.62 (C₁₁H, s, 2H), 5.09 – 5.05 (C₉H, dd, J_{AX} = 17.0 Hz, J_{AB} = 0.5 Hz, 1H), 5.01 – 4.98 (C₉H, dd, J_{BX} = 10.0 Hz, J_{AB} = 0.5 Hz, 1H), 4.28 (C₆H, t, J = 4.5 Hz, 2H), 3.45 (C₁₀H, s, 3H), 2.45 (C₇H, q, J = 7.2 Hz, 2H), 1.57 (C₂₀H, s, 9H); ¹³C-NMR (75 MHz, CDCl₃) δ (ppm) 166.4 (C₄), 161.0, 160.5, 160.4, 155.9, 153.0 (C₁, C₂, C₅, C₂₁, C₁₈), 135.02 (C₁₂), 134.96 (C₈), 128.7, 128.5 (C₁₃ – C₁₇), 116.7 (C₉), 86.0 (C₃), 82.4 (C₁₉), 69.7 (C₁₁), 41.7 (C₆), 34.6, 32.2 (C₁₀, C₇), 28.1 (C₂₀); **EI-HRMS**: Calcd mass for M⁺/z, 452.2172; Observed, 452.2174.

Bibliography

1. K. Strebhardt and A. Ullrich, *Nat. Rev. Cancer*, 2008, **8**, 473–480.
2. M. Ferrari, *Trends Biotechnol.*, 2010, **28**, 181–188.
3. A. E. Nel, L. Mädler, D. Velegol, T. Xia, E. M. V. Hoek, P. Somasundaran, F. Klaessig, V. Castranova and M. Thompson, *Nature Mater.*, 2009, **8**, 543–557.
4. L. Zhang, F. Gu, J. Chan, A. Wang, R. Langer and O. Farokhzad, *Clin. Pharmacol. Ther.*, 2008, **83**, 761–769.
5. S. Nie, Y. Xing, G. J. Kim and J. W. Simons, *Annu. Rev. Biomed. Eng.*, 2007, **9**, 257–288.
6. T. Harper, *Market Opportunities in Nanotechnology Drug Delivery* Scientifica, 2012.
7. K. E. Drexler, *Proc. Natl. Acad. Sci. USA*, 1981, **78**, 3275–5278.
8. K. E. Drexler, *Engines of Creation: The Coming Era of Nanotechnology*, Anchor Books Editions, USA, 1986.
9. V. Wagner, A. Dullaart, A.-K. Bock and A. Zweck, *Nature Biotechnol.*, 2006, **24**, 1211–1217.
10. R. A. Freitas, *Nanomedicine*, 2005, **1**, 2–9.
11. R. A. Petros and J. M. DeSimone, *Net. Rev. Drug Discov.*, 2010, **9**, 615–627.
12. S. K. Vashist, A. G. Venkatesh, K. Mitsakakis, G. Czilwik, G. n. Roth, F. v. Stetten and R. Zengerle, *BioNanoSci.*, 2012, **2**, 115–126.
13. V. Gubala, L. F. Harris, A. J. Ricco, M. X. Tan and D. E. Williams, *Anal. Chem.*, 2012, **84**, 487–515.
14. O. M. Koo, I. Rubinstein and H. Onyuksel, *Nanomedicine*, 2005, **1**, 193–212.
15. J. Funkhouser, *Curr. Drug. Discovery.*, 2002, **2**.
16. S. S. Kelkar and T. M. Reineke, *Bioconjugate Chem.* , 2011, **22**, 1879–1903.
17. N. C. Seeman, *J. Theor. Biol.*, 1982, **99**, 237–247.
18. A. Chworos, I. Severcan, A. Y. Koyfman, P. Weinkam, E. Oroudjev, H. G. Hansma and L. Jaeger, *Science*, 2004, **306**, 2068–2072.

19. F. A. Aldaye, A. L. Palmer and H. F. Sleiman, *Science*, 2008, **321**, 1795–1799.
20. A. V. Pinheiro, D. Han, W. M. Shih and H. Yan, *Nature Nanotechnol.*, 2011, **6**, 763–772.
21. S. M. Douglas, J. J. Chou and W. M. Shih, *Proc. Natl. Acad. Sci. USA*, 2007, **104**, 6644–6648.
22. B. Giese, *Acc. Chem. Res.*, 2000, **33**, 631–636.
23. E. S. Andersen, M. Dong, M. M. Nielsen, K. Jahn, R. Subramani, W. Mamdouh, M. M. Golas, B. Sander, H. Stark, C. L. P. Oliveira, J. S. Pedersen, V. Birkedal, F. Besenbacher, K. V. Gothelf and J. Kjems, *Nature*, 2009, **459**, 73–76.
24. S. Dhar, W. L. Daniel, D. A. Giljohann, C. A. Mirkin and S. J. Lippard, *J. Am. Chem. Soc.*, 2009, **131**, 14652–14653.
25. M. Faraday, *Phil. Trans. R. Soc. Lond.*, 1857, **147**, 145–181.
26. S. Nayak and L. A. Lyon, *Angew. Chem. Int. Ed.*, 2005, **44**, 7686–7708.
27. s. Yella, H.-W. Lee, H. N. Tsao, C. Yi, A. K. Chandiran, M. K. Nazeeruddin, E. W.-G. Diao, C.-Y. Yeh, S. M. Zakeeruddin and M. Grätzel, *Science*, 2011, **334**, 629–634.
28. S.-W. Kim, M. Kim, W. Y. Lee and T. Hyeon, *J. Am. Chem. Soc.*, 2002, **124**, 7642–7643.
29. W. H. D. Jong and P. J. Borm, *Int. J. Nanomedicine*, 2008, **2**, 133–149.
30. J. Conde, G. Doria and P. Baptista, *Journal of Drug Delivery*, 2012, **2012**, 1–12.
31. P. Schwerdtfeger, *Heteroat. Chem.*, 2002, **13**, 578–584.
32. D. J. Gorin and F. D. Toste, *Nature*, 2007, **446**, 395–403.
33. E. C. Dreaden, A. M. Alkilany, X. Huang, C. J. Murphy and M. A. El-Sayed, *Chem. Soc. Rev.*, 2012, **41**, 2740–2779.
34. S. Eustis and M. A. El-Sayed, *Chem. Soc. Rev.*, 2006, **35**, 209–217.
35. K. Saha, S. S. Agasti, C. Kim, X. Li and V. M. Rotello, *Chem. Rev.*, 2012, **112**, 2739–2779.
36. N. R. Jana, L. Gearheart and C. J. Murphy, *Adv. Mater.*, 2001, **13**, 1389–1393.
37. B. Nikoobakht and M. A. El-Sayed, *Chem. Mater.*, 2003, **15**, 1957–1962.

38. F. Kim, S. Connor, H. Song, T. Kuykendall and P. Yang, *Angew. Chem. Int. Ed.*, 2004, **43**, 3673–3677.
39. T. K. Sau and C. J. Murphy, *J. Am. Chem. Soc.*, 2004, **126**, 8648–8649.
40. J. Zhang, M. R. Langille, M. L. Personick, K. Zhang, S. Li and C. A. Mirkin, *J. Am. Chem. Soc.*, 2010, **132**, 14012–14014.
41. J. C. Love, L. A. Estroff, J. K. Kriebel, R. G. Nuzzo and G. M. Whitesides, *Chem. Rev.*, 2005, **105**, 1103–1169.
42. D. A. Giljohann, D. S. Seferos, W. L. Daniel, M. D. Massich, P. C. Patel and C. A. Mirkin, *Angew. Chem. Int. Ed.*, 2010, **49**, 3280–3294.
43. C. Sanchez, K. J. Shea and S. Kitagawa, *Chem. Soc. Rev.*, 2011, **40**, 471–472.
44. C. Sanchez, P. Belleville, M. Popalld and L. Nicole, *Chem. Soc. Rev.*, 2010, **40**, 696–753.
45. E. Ruoslahti, S. N. Bhatia and M. J. Sailor, *J. Cell. Biol.*, 2010, **188**, 759–768.
46. E. Jin, B. Zhang, X. Sun, Z. Zhou, X. Ma, Q. Sun, J. Tang, o. Shen, E. V. Kirk, W. J. Murdoch and M. Radosz, *J. Am. Chem. Soc.*, 2013, **135**, 933–940.
47. L. Maus, O. Dick, H. Bading, J. P. Spatz and R. Fiammengo, *ACS Nano*, 2010, **4**, 6617–6628.
48. R. Levy, N. T. K. Thanh, R. C. Doty, I. Hussain, R. J. Nichols, D. J. Schiffrin, M. Brust and D. G. Fernig, *J. Am. Chem. Soc.*, 2004, **126**, 10076–10084.
49. I. Olmedo, Eyleen Araya, F. Sanz, Elias Medina, J. Arbiol, P. Toledo, A. Alvarez-Lueje, E. Giralt and M. J. Kogan, *Bioconjugate Chem.*, 2008, **19**, 1154–1163.
50. H. Xie, A. G. Tkachenko, W. R. Glomm, J. A. Ryan, M. K. Brennaman, J. M. Papanikolas, S. Franzen and D. L. Feldheim, *Anal. Chem.*, 2003, **75**, 5797–5805.
51. Y. Liu and S. Franzen, *Bioconjugate Chem.*, 2008, **19**, 1009–1016.
52. L. B. Paolo Pengo, Lucia Pasquato,* and Paolo Scrimin, *Angew. Chem. Int. Ed.*, 2007, **46**, 400–404.
53. Y. N. Tan, J. Y. Lee and D. I. C. Wang, *J. Am. Chem. Soc.*, 2010, **132**, 5677–5686.
54. W. Eck, G. Craig, A. Sigdel, G. Ritter, L. J. Old, L. Tang, M. F. Brennan, P. J. Allen and M. D. Mason, *ACS Nano*, 2008, **2**, 2263–2272.

55. K. Zhu, Y. Zhang, S. He, W. Chen, J. Shen, Z. Wang and X. Jiang, *Anal. Chem.*, 2012, **84**, 4267–4270.
56. M. A. Dobrovolskaia, A. K. Patri, J. Zheng, J. D. Clogston, N. Ayub, P. Aggarwal, B. W. Neun, J. B. Hall and S. E. McNeil, *Nanomed. Nanotechnol. Biol. Med.*, 2009, **5**, 106–117.
57. A. Salvati, A. S. Pitek, M. P. Monopoli, K. Prapainop, F. B. Bombelli, D. R. Hristov, P. M. Kelly, C. Åberg, E. Mahon and K. A. Dawson, *Nat. Nanotechnol.*, 2013, **8**, 137–143.
58. C. M. Niemeyer, *Angew. Chem. Int. Ed.*, 2001, **40**, 4128–4158.
59. D.-H. Tsai, F. W. DelRio, A. M. Keene, K. M. Tyner, R. I. MacCuspie, T. J. Cho, M. R. Zachariah and V. A. Hackley, *Langmuir*, 2011, **27**, 2464–2477.
60. W.-T. Chien, C.-C. Yu, C.-F. Liang, C.-H. Lai, P.-C. Lin and C.-C. Len, in *ACS symposium Series*, ed. ACS, 2011.
61. K. M. Halkes, A. C. d. Souza, C. E. P. Maljaars, G. J. Gerwig and J. P. Kamerling, *Eur. J. Org. Chem.*, 2005, **2005**, 3650–3659.
62. M. Ahmed, Z. Deng, S. Liu, R. Lafrenie, A. Kumar and R. Narain, *Bioconjugate Chem.*, 2009, **20**, 2169–2176.
63. C.-C. Lin, Y.-C. Yeh, C.-Y. Yang, C.-L. Chen, G.-F. Chen, C.-C. Chen and Y.-C. Wu, *J. Am. Chem. Soc.*, 2002, **124**, 3508–3509.
64. M. S. Eom, W. Jang, Y. S. Lee, G. Choi, Y.-U. Kwon and M. S. Han, *Chem. Commun.*, 2012, **48**, 5566–5568.
65. P. He and M. W. Urban, *Biomacromolecules*, 2005, **6**, 1224–1225.
66. N. C. M. Tam, B. M. T. Scott, D. Voicu, B. C. Wilson and G. Zheng, *Bioconjugate Chem.*, 2010, **21**, 2178–2182.
67. C. J. Orendorff, T. M. Alam, D. Y. Sasaki, B. C. Bunker and J. A. Voigt, *ACS Nano*, 2009, **3**, 971–983.
68. D. P. Cormode, T. Skajaa, M. M. v. Schooneveld, R. Koole, P. Jarzyna, M. E. Lobatto, C. Calcagno, A. Barazza, R. E. Gordon, P. Zanzonico, E. A. Fisher, Z. A. Fayad and W. J. M. Mulder, *Nano Lett.*, 2008, **8**, 3715–3723.
69. C. A. Mirkin, R. L. Letsinger, R. C. Mucic and J. J. Storhoff, *Nature*, 1996, **382**, 607–609.
70. S. J. Hurst, A. K. R. Lytton-Jean and C. A. Mirkin, *Anal. Chem.*, 2006, **78**, 8313–8318.
71. R. Jin, G. Wu, Z. Li, C. A. Mirkin and G. C. Schatz, *J. Am. Chem. Soc.*, 2003, **125**, 1643–1654.

72. B. R. Stepp, J. M. Gibbs-Davis, D. L. F. Koh and S. T. Nguyen, *J. Am. Chem. Soc.*, 2008, **130**, 9628–9629.
73. J. M. Gibbs-Davis, G. C. Schatz and S. T. Nguyen, *J. Am. Chem. Soc.*, 2007, **129**, 15535–15540.
74. D. A. Giljohann, D. S. Seferos, P. C. Patel, J. E. Millstone, N. L. Rosi and C. A. Mirkin, *Nano Lett.*, 2007, **7**, 3818–3821.
75. P. C. Patel, D. A. Giljohann, W. L. Daniel, D. Zheng, A. E. Prigodich and C. A. Mirkin, *Bioconjugate Chem.*, 2010, **21**, 2250–2256.
76. T. Niidome and L. Huang, *Gene Ther.*, 2002, **9**, 1647–1652.
77. N. L. Rosi, D. A. Giljohann, C. S. Thaxton, A. K. R. Lytton-Jean, M. S. Han and C. A. Mirkin, *Science*, 2006, **312**, 1027–1030.
78. D. S. Seferos, D. A. Giljohann, N. L. Rosi and C. A. Mirkin, *ChemBioChem*, 2007, **8**, 1230–1232.
79. J.-S. Lee, M. S. Han and C. A. Mirkin, *Angew. Chem. Int. Ed.*, 2007, **46**, 4093–4096.
80. J. Liu and Y. Lu, *Angew. Chem. Int. Ed.*, 2006, **45**, 90–94.
81. C. Yang, Y. Wanga, J.-L. Marty and X. Yang, *Biosens. Bioelectron.*, 2010, **26**, 2724–2727.
82. B. Dubertret, M. Calame and A. J. Libchaber, *Nat. Biotechnol.*, 2001, **19**, 365–370.
83. S.-J. Park, T. A. Taton and C. A. Mirkin, *Science*, 2002, **295**, 1503–1505.
84. X. Yao, X. Li, F. Toledo, C. Zurita-Lopez, M. Gutova, J. Momand and F. Zhou, *Anal. Biochem.*, 2006, **354**, 220–228.
85. D. S. Seferos, D. A. Giljohann, H. D. Hill, A. E. Prigodich and C. A. Mirkin, *J. Am. Chem. Soc.*, 2007, **129**, 15477–15479.
86. W. A. Kibbe, *Nucl. Acids Res.*, 2007, **35**, W43-W46.
87. M. Ferrari, *Nat. Rev. Cancer*, 2005, **5**, 161-171.
88. M. Mammen, S.-K. Choi and G. M. Whitesides, *Angew. Chem. Int. Ed.*, 1998, **37**, 2754–2794.
89. P. I. Kitov and D. R. Bundle, *J. Am. Chem. Soc.*, 2003, **125**, 16271–16284.
90. A. C. R. Grayson, I. S. Choi, B. M. Tyler, P. P. Wang, H. Brem, M. J. Cima and R. Langer, *Nat. Mater.*, 2003, **2**, 767–772.
91. A. Wijaya, S. B. Schaffer, I. G. Pallares and K. Hamad-Schifferli, *ACS Nano*, 2009, **3**, 80–86.

92. X. Li, J. Guo, J. Asong, M. A. Wolfert and G.-J. Boons, *J. Am. Chem. Soc.*, 2011, **133**, 11147–11153.
93. V. P. Torchilin, *Nat. Rev. Drug Discov.*, 2005, **4**, 145–160.
94. R. K. Jain and T. Stylianopoulos, *Nat. Rev. Clin. Oncol.*, 2010, **7**, 653–664.
95. S. J. Tan, P. Kiatwuthinon, Y. H. Roh, J. S. Kahn and D. Luo, *Small*, 2011, **7**, 841–856.
96. R. Duncan, *Nat. Rev. Cancer*, 2006, **6**, 688–701.
97. O. Nakagawa, X. Ming, L. Huang and R. L. Juliano, *J. Am. Chem. Soc.*, 2010, **132**, 8848–8849.
98. J. Kim, Y. Piao and T. Hyeon, *Chem. Soc. Rev.*, 2008, **38**, 372–390.
99. P. C. Patel, D. A. Giljohann, D. S. Seferos and C. A. Mirkin, *Proc. Natl. Acad. Sci. USA*, 2008, **105**, 17222–17226.
100. R. S. Ingram, M. J. Hostetler and R. W. Murray, *J. Am. Chem. Soc.*, 1997, **119**, 9175–9178.
101. A. C. Templeton, W. P. Wuelfing and R. W. Murray, *Acc. Chem. Res.*, 1999, **33**, 27–36.
102. A. C. Templeton, M. J. Hostetler, E. K. Warmoth, S. Chen, C. M. Hartshorn, V. M. Krishnamurthy, M. D. E. Forbes and R. W. Murray, *J. Am. Chem. Soc.*, 1998, **120**, 4845–4849.
103. C. M. Niemeyer, B. I. Ceyhan and P. Hazarika, *Angew. Chem. Int. Ed.*, 2003, **42**, 5766–5770.
104. L. Maus, J. P. Spatz and R. Fiammengo, *Langmuir*, 2009, **25**, 7910–7917.
105. M. S. Azam, S. L. Fenwick and J. M. Gibbs-Davis, *Langmuir*, 2010, **27**, 741–750.
106. C. D. Bain and G. M. Whitesides, *J. Am. Chem. Soc.*, 1988, **110**, 6560–6561.
107. J. F. Kang, S. Liao, R. Jordan and A. Ulman, *J. Am. Chem. Soc.*, 1998, **120**, 9662–9667.
108. L. M. Demers, C. A. Mirkin, R. C. Mucic, R. A. Reynolds, R. L. Letsinger, R. Elghanian and G. Viswanadham, *Anal. Chem.*, 2000, **72**, 5535–5541.
109. Y.-H. Sun, R.-M. Kong, D.-Q. Lu, X.-B. Zhang, H.-M. Meng, W. Tan, G.-L. Shena and R.-Q. Yu, *Chem. Comm.*, 2011, **47**, 3840–3842.

110. F. Abendroth, A. Bujotzek, M. Shan, R. Haag, M. Weber and O. Seitz, *Angew. Chem. Int. Ed.*, 2011, **50**, 8592–8596.
111. Z. Cao, R. Tong, A. Mishra, W. Xu, G. C. L. Wong, J. Cheng and Y. Lu, *Angew. Chem. Int. Ed.*, 2009, **48**, 6494–6498.
112. Y.-H. M. Chan, B. v. Lengerich and S. G. Boxer, *Proc. Natl. Acad. Sci. USA*, 2009, **106**, 979–984.
113. M. Kwak and A. Herrmann, *Angew. Chem. Int. Ed.*, 2010, 8574–8587.
114. E. Ruiz-Hernández, A. Baeza and M. Vallet-Regí, *ACS Nano*, 2011, **5**, 1259–1266.
115. K. C. Grabar, R. G. Freeman, M. B. Hommer and M. Natan, *Anal. Chem.*, 1995, **67**, 735–743.
116. W. Zhao, M. M. Ali, S. D. Aguirre, M. A. Brook and Y. Li, *Anal. Chem.*, 2008, **80**, 8434–8437.
117. D. C. Harris, *Quantitative chemical analysis*, 5th edn., New York, 1998.
118. *Probability (P) Value T test Calculator*, <http://easycalculation.com/statistics/p-value-t-test.php>, Accessed May 25, 2013, 2013.
119. D. Yang, M. J. Campolongo, T. N. N. Tran, R. C. H. Ruiz, J. S. Kahn and D. Luo, *WIREs Nanomedicine and Nanotechnology*, 2010, **2**, 648–669.
120. J. Bath and A. J. Turberfield, *Nature Nanotechnol.*, 2007, **2**, 275–284.
121. P. K. Dutta, R. Varghese, J. Nangreave, S. Lin, H. Yan and Y. Liu, *J. Am. Chem. Soc.*, 2011, **133**, 11985–11993.
122. P. I. Kitov, J. M. Sadowska, G. Mulvey, G. D. Armstrong, H. Ling, N. S. Pannu, R. J. Read and D. R. Bundle, *Nature*, 2000, 669–672.
123. E. Fan, Z. Zhang, W. E. Minke, Z. Hou, C. L. M. J. Verlinde and W. G. J. Ho, *J. Am. Chem. Soc.*, 1999, **122**, 2663–2664.
124. P. Rai, C. Padala, V. Poon, A. Saraph, S. Basha, S. Kate, K. Tao, J. Mogridge and R. S. Kane, *Nat. Biotechnol.*, 2006, **24**, 582–586.
125. A. J. Golumbfskie, V. S. Pande and A. K. Chakraborty, *Proc. Natl. Acad. Sci. USA*, 1999, **96**, 11707–11712.
126. Z. Zhang, E. A. Merritt, M. Ahn, C. Roach, Z. Hou, C. L. M. J. Verlinde, W. G. J. Ho and E. Fan, *J. Am. Chem. Soc.*, 2002, **124**, 12991–12998.

127. A. J. Torres, M. Wu, D. Holowka and B. Baird, *Annu. Rev. Biophys.*, 2008, **37**, 265–288.
128. S. Menon, K. Rosenberg, S. A. Graham, E. M. Ward, M. E. Taylor, K. Drickamer and D. E. Leckband, *Proc. Natl. Acad. Sci. USA*, 2009, **106**, 11524–11529.
129. M. F. Bachmann and G. T. Jennings, *Nat. Rev. Immunol.*, 2010, **10**, 787–796.
130. J. S. Josan, H. L. Handl, R. Sankaranarayanan, L. Xu, R. M. Lynch, J. Vagner, E. A. Mash, V. J. Hruby and R. J. Gillies, *Bioconjugate Chem.*, 2011, **22**, 1270–1278.
131. A. Iqbal, S. Arslan, B. Okumus, T. J. Wilson, G. Giraud, D. G. Norman, T. Ha and D. M. J. Lilley, *Proc. Natl. Acad. Sci. USA*, 2008, **105**, 11176–11181.
132. F. Yuan, L. Griffin, L. Phelps, V. Buschmann, K. Weston and N. L. Greenbaum, *Nucl. Acids Res.*, 2007, **35**, 2833–2845.
133. D. Miles, G. V. Minckwitz and A. D. Seidman, *Oncologist*, 2002, **7**, 13–19.
134. D. Lane, *Nat. Biotechnol.*, 2006, **24**, 163–164.
135. S. Fulda and K.-M. Debatin, *Oncogene*, 2004, **23**, 6702–6711.
136. D. Hanahan, G. Bergers and E. Bergsland, *J. Clin. Invest.*, 2000, **105**, 1045–1047.
137. S. Sengupta, D. Eavarone, I. Capila, G. Zhao, N. Watson, T. Kiziltepe and R. Sasisekharan¹, *Nature*, 2005, **436**, 568–572.
138. A. Barhoumi, R. Huschka, R. Bardhan, M. W. Knight and N. J. Halas, *Chem. Phys. Lett.*, 2009, **482**, 171–179.
139. S. E. Lee and L. P. Lee, *Curr. Opin. Chem. Biol.*, 2010, **14**, 623–633.
140. N. L. Rosi, D. A. Giljohann, C. S. Thaxton, A. K. R. Lytton-Jean, M. S. Han and C. A. Mirkin, *Science*, 2006, **312**, 1027–1030.
141. E. Crew, S. Rahman, A. Razzak-Jaffar, D. Mott, M. Kamundi, G. Yu, N. Tchah, J. Lee, M. Bellavia and C.-J. Zhong, *Anal. Chem.*, 2012, **84**, 26–29.
142. C. K. McLaughlin, G. D. Hamblin and H. F. Sleiman, *Chem. Soc. Rev.*, 2011, **40**, 5647–5656.
143. A. E. Prigodich, D. S. Seferos, M. D. Massich, D. A. Giljohann, B. C. Lane and C. A. Mirkin, *ACS Nano*, 2009, **3**, 2147.
144. S. E. Lee, G. L. Liu, F. Kim and L. P. Lee, *Nano Lett.*, 2009, **9**, 562–570.

145. R. Huschka, J. Zuloaga, M. W. Knight, L. V. Brown, P. Nordlander and N. J. Halas, *J. Am. Chem. Soc.*, 2011, **133**, 12247–12255.
146. L. Poon, W. Zandberg, D. Hsiao, Z. Erno, D. Sen, B. D. Gates and N. R. Branda, *ACS Nano*, 2010, **11**, 6395–6403.
147. M. R. Jones, J. E. Millstone, D. A. Giljohann, D. S. Seferos, K. L. Young and C. A. Mirkin, *ChemPhysChem*, 2009, **10**, 1461–1465.
148. S. E. Lee, D. Y. Sasaki, Y. Park, R. Xu, J. S. Brennan, M. J. Bissell and L. P. Lee, *ACS Nano*, 2012, **6**, 7770–7780.
149. P. Anikeeva and K. Deisseroth, *ACS Nano*, 2012, **9**, 7548.
150. O.-S. Lee, T. R. Prytkova and G. C. Schatz, *J. Phys. Chem. Lett.*, 2010, **1**, 1781–1788.
151. M. R. Jones, R. J. Macfarlane, A. E. Prigodich, P. C. Patel and C. A. Mirkin, *J. Am. Chem. Soc.*, 2011, **133**, 18865–18869.
152. A. K. R. Lytton-Jean, J. M. Gibbs-Davis, H. Long, G. C. Schatz, C. A. Mirkin and S. T. Nguyen, *Adv. Mater.*, 2009, **21**, 706–709.
153. J. M. Gibbs-Davis, G. C. Schatz and S. T. Nguyen, *J. Am. Chem. Soc.*, 2007, **129**, 15535–15540.
154. J. M. Gibbs, S.-J. Park, D. R. Anderson, K. J. Watson, C. A. Mirkin and S. T. Nguyen, *J. Am. Chem. Soc.*, 2005, **127**, 1170–1178.
155. J. I. Cutler, E. Auyeung and C. A. Mirkin, *J. Am. Chem. Soc.*, 2012, **134**, 1376–1391.
156. I. Eryazici, T. R. Prytkova, George C. Schatz and S. T. Nguyen, *J. Am. Chem. Soc.*, 2010, **132**, 17068–17070.
157. I. Eryazici, I. Yildirim, G. C. Schatz and S. T. Nguyen, *J. Am. Chem. Soc.*, 2012, **134**, 7450–7458.
158. A. A. Greschner, V. Toader and H. F. Sleiman, *J. Am. Chem. Soc.*, 2012, **134**, 14382–14389.
159. G. Baffou, R. Quidant and F. J. G. d. Abajo, *ACS Nano*, 2010, **4**, 709–716.
160. J. Croissant and J. I. Zink, *J. Am. Chem. Soc.*, 2012, **134**, 7628–7631.
161. S. L. Wong, P. B. Mangu, M. A. Choti, T. S. Crocenzi, G. D. D. III, G. S. Dorfman, C. Eng, Y. Fong, A. F. Giusti, D. Lu, T. A. Marsland, R. Michelson, G. J. Poston, D. Schrag, J. Seidenfeld and A. B. B. III, *J. Clin. Oncol.*, 2010, **28**, 493–508.
162. M. Hiraoka, S. Jo, Y. Dodo, K. Ono, M. Takahashi, H. Nishida and M. Abe, *Cancer*, 1984, **54**, 2898–2904.
163. R. Hergt and S. Dutz, *J. Magn. Magn. Mater.*, 2007, **311**, 187–192.

164. J. Carrey, B. Mehdaoui and M. Respaud, *J. Appl. Phys.*, 2011, **109**, 083921-083921-083921-083917.
165. K. W. Ferrara, M. A. Borden and H. Zhang, *Acc. Chem. Res.*, 2009, **42**, 881-892.
166. B. E. O'Neill, H. Vo, M. Angstadt, K. P. C. Li, T. Quinn and V. Frenkel, *Ultrasound in Med. & Biol.*, 2009, **35**, 416-424.
167. S. Dromi, V. Frenkel, A. Luk, BryanTraughber, MaryAngstadt, M. Bur, J. Poff, J. Xie, S. K. Libutti, K. C. P. Li and BradfordJ.Wood, *Clin. Cancer. Res.*, 2007, **13**, 2722-2727.
168. V. Frenkel, *Adv. Drug Deliv. Rev.*, 2008, **60**, 1193-1208.
169. A. K. R. Lytton-Jean and C. A. Mirkin, *J. Am. Chem. Soc.*, 2005, **127**, 12754-12755.
170. R. Owczarzy, Y. You, B. G. Moreira, J. A. Manthey, L. Huang, M. A. Behlke and J. A. Walder, *Biochemistry*, 2004, **43**, 3537-3554.
171. T. J. Matray and E. T. Kool, *J. Am. Chem. Soc.*, **120**, 6191-6192.
172. W. Lu, G. Zhang, R. Zhang, L. G. F. II, Q. Huang, J. G. Gelovani and C. Li, *Cancer Res.*, 2010, **70**, 3177-3188.
173. A. Kudlay, J. M. Gibbs, G. C. Schatz, S. T. Nguyen and M. O. d. I. Cruz, *J. Phys. Chem. B*, 2007, **111**, 1610-1619.
174. H. Long, A. Kudlay and G. C. Schatz, *J. Phys. Chem. B*, 2006, **110**, 2918-2926.
175. H. Fenniri, P. Mathivanan, K. L. Vidale, D. M. Sherman, K. Hallenga, K. V. Wood and J. G. Stowell, *J. Am. Chem. Soc.*, 2001, **123**, 3854-3855.
176. H. Fenniri, B.-L. Deng and A. E. Ribbe, *J. Am. Chem. Soc.*, 2004, **124**, 11064-11072.
177. H. Fenniri, B.-L. Deng, A. E. Ribbe, K. Hallenga, J. Jacob and P. Thiyagarajan, *Proc. Natl. Acad. Sci. USA*, 2002, **99**, 6487-6492.
178. J. G. Moralez, J. Raez, T. Yamazaki, R. K. Motkuri, A. Kovalenko and H. Fenniri, *J. Am. Chem. Soc.*, 2005, **127**, 8307-8309.
179. G. Tikhomirov, T. Yamazaki, A. Kovalenko and H. Fenniri, *Langmuir*, 2008, **24**, 4447-4450.
180. M. Mascal, N. M. Hext, R. Warmuth, M. H. Moore and J. P. Turkenburg, *Angew. Chem. Int. Ed. Engl.*, 1996, **35**, 2204-2206.
181. A. Marsh, M. Silvestri and J.-M. Lehn, *Chem. Commun.*, 1996, 1527-1528.
182. G. M. Whitesides, S. Eric E, J. P. Mathias, C. T. Seto, D. N. Chin, M. Mammen and D. M. Gordon, *Acc. Chem. Res.*, 1995, **28**, 37-44.

183. S. V. Kolotuchin and S. C. Zimmerman, *J. Am. Chem. Soc.*, 1998, **120**, 9092–9093.
184. L. J. Prins, D. N. Reinhoudt and P. Timmerman, *Angew. Chem. Int. Ed.*, 2001, **40**, 2382–2426.
185. J. F. Stoddart and H.-R. Tseng, *Proc. Natl. Acad. Sci. USA*, 2002, **99**, 4797–4800.
186. L. R. MacGillivray and J. L. Atwood, *Angew. Chem. Int. Ed.*, 1999, **38**, 1018–1033.
187. F. Hof, S. L. Craig, C. Nuckolls and J. Julius Rebek, *Angew. Chem. Int. Ed.*, 2002, **41**, 1488–1508.
188. J. J. L. M. Cornelissen, A. E. Rowan, R. J. M. Nolte and N. A. J. M. Sommerdijk, *Chem. Rev.*, 2001, **101**, 4039–4070.
189. A. Müller, H. Reuter and S. Dillinger, *Angew. Chem. Int. Ed.*, 1995, **34**, 2328–2361.
190. D. J. Hill, M. J. Mio, R. B. Prince, T. S. Hughes and J. S. Moore, *Chem. Rev.*, 2001, **101**, 3893–4011.
191. D. S. Lawrence, T. Jiang and M. Levett, *Chem. Rev.*, 1995, **95**, 2229–2260.
192. L. Brunsveld, B. J. B. Folmer, E. W. Meijer and R. P. Sijbesma, *Chem. Rev.*, 2001, **101**, 4071–4097.
193. R. L. Beingessner, B.-L. Deng, P. E. Fanwick and H. Fenniri, *J. Org. Chem.*, 2008, **73**, 931–939.
194. V. r. Rolland, M. Kotera and J. Lhomme, *Synth. Commun.*, 1997, **27**, 3505–3511.
195. M. Hoffer, *Chem. Ber.*, 1960, **93**, 2777–2781.
196. B. M. Domínguez and P. M. Cullis, *Tetrahedron Lett.*, 1999, **40**, 5783–5786.
197. M. Ober, H. Müller, C. Pieck, J. Gierlich and T. Carell, *J. Am. Chem. Soc.*, 2005, **127**, 18143–18149.
198. M.A.Dorman, S. A. Noble, L. J. McBride and M.H.Caruthers, *Tetrahedron*, 1984, **40**, 95–102.
199. H. Fenniri, B.-L. Deng and A. E. Ribbe, *J. Am. Chem. Soc.*, 2002, **124**, 11064–11072.
200. B. C. Laguzza and B. Ganem, *Tetrahedron Lett.*, 1981, **22**, 1483–1486.
201. S. Lemaire-Audoire, M. Savignac and J. P. Genet, *Tetrahedron Lett.*, 1995, **36**, 1267–1270.

202. M. Honda, H. Morita and I. Nagakura, *J. Org. Chem.*, 1997, **62**, 8932–8936.
203. T. W. Greene and P. G. M. Wute, *Protective Groups in Organic Synthesis*, John Wiley & Sons, Inc, New York, 1999.
204. V. Fialova, V. Bazant and V. Chvalovsky, *Collect. Czech. Chem. Commun.*, 1973, **38**, 3837–3840.
205. R.-W. Wang and B. Gold, *Org. Lett.*, 2009, **11**, 2465–2468.
206. W. Saenger, *Angew. Chem. Int. Ed. Engl.*, 1973, **12**, 591–682.
207. C. Altona and M. Sundaralingam, *J. Am. Chem. Soc.*, 1972, **94**, 8205–8212.
208. J. Plavec, W. Tong and J. Chattopadhyaya, *J. Am. Chem. Soc.*, 1993, **115**, 9734–9746.
209. D. R. Reddy, M. A. Iqbal, R. L. Hudkins, P. A. Messina-McLaughlin and J. P. Mallamo, *Tetrahedron Lett.*, 2002, **43**, 8063–8066.
210. S. Knapp, J. J. Hale, Margarita Bastos and F. S. Gibson, *Tetrahedron Lett.*, 1990, **15**, 2109–2112.
211. R. W. Hungate, J. L. Chen, K. E. Starbuck, S. A. Macaluso and R. S. Rubino, *Tetrahedron Lett*, 1996, **37**, 4113–4116.
212. D. L. Flynn, R. E. Zelle and P. A. Grieco, *J. Org. Chem.*, 1983, **48**, 2424–2426.

